Effect of Domain Wall Motion and Phase Transformations on Nonlinear Hysteretic Constitutive Behavior in Ferroelectric Materials

A Dissertation
Presented to
The Academic Faculty

By

Kyle Grant Webber

In Partial Fulfillment
Of the Requirements for the Degree
Doctor of Philosophy in Mechanical Engineering

Georgia Institute of Technology
April 2008

Effect of Domain Wall Motion and Phase Transformations on Nonlinear Hysteretic Constitutive Behavior in Ferroelectric Materials

Reading Committee:

Dr. Christopher S. Lynch, Chairman
School of Mechanical and Aerospace Engineering
University of California Los Angeles

Dr. Arash Yavari
School of Civil and Environmental Engineering
The Georgia Institute of Technology

Dr. Richard W. Neu
School of Mechanical Engineering
The Georgia Institute of Technology

Dr. Nazanin Bassiri-Gharb
School of Mechanical Engineering
The Georgia Institute of Technology

Dr. Jianmin Qu
School of Mechanical Engineering
The Georgia Institute of Technology

Dr. Rosario A. Gerhardt
School of Materials Science and Engineering
The Georgia Institute of Technology

Date Accepted: 29 February 2008

In Loving Memory

of

My Dad

ACKNOWLEDGEMENTS

There are many people that I want to extend thanks to for their help and support. Firstly, I sincerely thank Prof. Christopher Lynch. Without his knowledge, patience and unwavering optimism this work would not have been possible. Working with and learning from him has been an incredible experience that will influence my career forever. I am also very appreciative to Profs. Arash Yavari, Richard Neu, Nazanin Bassiri-Gharb, Jianmin Qu and Rosario Gerhardt for serving on my thesis committee and giving me their valuable insight and advice. Thanks are due to Dr. Harold Robinson and his team at NUWC for the providing the experimental measurements presented in Chapter 4. I also acknowledge Prof. William Oates and Dr. Tieqi Liu for answering my questions with serenity.

Thank you to all the friends that I have met during my time here, especially those who frequented The Golden Pheasant, for ruining any chance I had to run for public office.

Lastly, but most importantly, I would like to thank my family and especially my wife, Britta. Her love and unbelievable patience are why I am here.

TABLE OF CONTENTS

LIST OF TABLES

LIST OF FIGURES

LIST OF SYMBOLS

E_c – Coercive field

ε_{ij} – Total strain

ε_{ij}^{L} – Elastic component of total strain

ε_{ij}^{s} – Spontaneous strain

ε_{ij}^{R} – Remanent strain

D_i – Electric displacement

P_i – Total polarization

P_i^{L} – Elastic component of total polarization

P_i^{s} – Spontaneous polarization

P_i^{R} – Remanent polarization

σ_{ij} – Stress

E_i – Electric field

ΔT – Temperature change

s_{ijkl} – Compliance

d_{kij} – Piezoelectric coefficients

κ_{ik} – Dielectric permittivity

α_{ij} – Coefficient of thermal expansion

q_i – Pyroelectric coefficients

ε_o – Permittivity of free space

PMN-*x*PT – Lead magnesium niobate-lead titanate - (1-*x*)$Pb(Mg_{1/3}Nb_{2/3})O_3$-*x*$PbTiO_3$

PZN-*x*PT – Lead zinc niobate-lead titanate - (1-*x*)$Pb(Zn_{1/3}Nb_{2/3})O_3$-*x*$PbTiO_3$

PZT – Lead zirconate titanate - $Pb(Zr,Ti)O_3$

PLZT – Lead lanthanum zirconate titanate - $(Pb,La)(Zr,Ti)O_3$

MPB – Morphotropic phase boundary

T – Tetragonal phase

R – Rhombohedral phase

O – Orthorhombic phase

M_A, M_B, M_C – Monoclinic phases

m^{α} – Modulus of α phase material response

m^{β} – Modulus of β phase material response

R_r^{α} – Remanent material response value of α phase

R_r^{β} – Remanent material response value of β phase

F_1^c – Forward phase transformation value to applied fields

F_2^c – Reverse phase transformation value to applied fields

w – Work per unit volume

$\Delta w^{\alpha\to\beta}$ – Total increment in work per unit volume done to transform from phase α to β

$\Delta\varepsilon_{ij}^{\alpha\to\beta}$ – Change in strain from phase α to β

$\Delta D_m^{\alpha\to\beta}$ – Change in electric displacement from phase α to β

SDECS – Stress-dependent electromechanical characterization system

NUWC – Naval Undersea Warfare Center Division Newport

a_{ij} – Transformation matrix

f^{α} – Variant volume fraction of variant α

$G^{\alpha\to\beta}$ – Driving force for volume fraction evolution

$G_{mech}^{\alpha\to\beta}$ – Mechanical component of driving force for volume fraction evolution

$G_{elec}^{\alpha\to\beta}$ – Electrical component of driving force for volume fraction evolution

$G_{B}^{\alpha\to\beta}$ – Back field

$G_{0}^{\alpha\to\beta}$ – Threshold for volume fraction evolution

A, *B*, *C* and *D* – Material constants in back field expression

Y – Young's Modulus

ν – Poisson's ratio

δ_{ij} – Kronecker delta

α – Angle of poling direction between the [001] and [111] crystallographic orientations

n_1 – Relative switching threshold ratio between 180^{o} and 70.53^{o} switches

n_2 – Relative switching threshold ratio between 180^{o} and 109.47^{o} switches

SUMMARY

The primary focus of this research is to investigate the non-linear behavior of single crystal and polycrystalline relaxor ferroelectric PMN-*x*PT and PZN-*x*PT through experimentation and modeling.

Characterization of single crystal and polycrystalline specimens with similar compositions was performed. These data give experimental insight into the differences that may arise in a polycrystal due to local interaction with inhomogeneities. Single crystal specimens were characterized with a novel experimental technique that reduced clamping effects at the boundary and gave repeatable results. The measured experimental data was used in conjunction with electromechanical characterizations of other compositions of single crystal specimens with the same crystallographic orientation to study the compositional effects on material properties and phase transition behavior.

Experimental characterization provided the basis for the development of a model of the continuous phase transformation behavior seen in PMN-*x*PT single crystals. In the modeling it is assumed that a spatial chemical and structural heterogeneity is primarily responsible for the gradual phase transformation behavior observed in relaxor ferroelectric materials. The results are used to simulate the effects of combined electrical and mechanical loading.

An improved rate-independent micromechanical constitutive model based on the experimental observations of single crystal and polycrystalline specimens under large field loading is also presented. This model accounts for the non-linear evolution of variant volume fractions. The micromechanical model was calibrated using single crystal

data. Simulations of the electromechanical behavior of polycrystalline ferroelectric materials are presented. These results illustrate the effects of non-linear single crystal behavior on the macroscopic constitutive behavior of polycrystals.

CHAPTER 1

INTRODUCTION

Piezoelectric materials are a class of materials that exhibit a thermo-electromechanical coupling. These materials are widely used in engineered devices and systems that either convert mechanical energy into electrical signals such as sonar, ultrasound and charge generators or convert electrical energy into mechanical displacement such as actuators and micro-positioning systems. This chapter presents a review of the basics of piezoelectricity and ferroelectricity, relaxor ferroelectric materials and gives an overview of the contents of this thesis.

1.1 Piezoelectric Materials

The Discovery of the Piezoelectric Effect

The piezoelectric effect (surface charge from mechanical pressure) was discovered in 1880 by the Curie brothers, Pierre and Jacques. Since then, piezoelectricity has been found in many naturally occurring materials such as tourmaline, quartz, topaz, cane sugar and Rochelle salt. The brothers experimentally discovered that a surface charge could be measured when a mechanical stress was applied to certain crystals that had been given a surface treatment. The brothers also discovered that there was a relationship between temperature and surface charge intensity. The Curie brothers, however, did not predict the converse piezoelectric effect (electricity from a mechanical stress). It was not until 1881 when Gabriel Lippmann, Marie Curie's thesis advisor,

proved mathematically that the converse piezoelectric effect was possible that the Curie brothers quickly completed experiments to show that it was indeed present.

Perovskites and the Discovery of Ferroelectricity

Perovskite is the name for the general class of crystals that take on the basic chemical formula ABO_3. These crystals have the ability to reorient their polarization direction through the application of external loads over a range of temperatures (ferroelectricity), something that is not seen in all piezoelectric materials. Although ferroelectricity was previously proposed, it was not until 1921 that this phenomenon was experimentally discovered in single crystal Rochelle salt specimens [1]. Water-soluble rochelle salt (sodium potassium tartrate tetrahydrate) and potassium dihydrogen phosphate (KDP) were the only two ferroelectric materials known until barium titanate ($BaTiO_3$). The exact history of the discovery of barium titanate is unclear because much of the initial research began in secrecy in the early 1940s during World War II for use in high dielectric-constant capacitors. After the conclusion of the War, much of the research that was accomplished in secrecy was published and the source of the high dielectric constant was determined to be due to the ferroelectric behavior [2, 3].

The discovery of lead zirconate titanate (PZT, $Pb(Ti,Zr)O_3$) came about in the early 1950s [4] and offered increased properties over barium titanate including lower dielectric loss and higher Curie points [5]. PZT is a solid solution of lead zirconate (PZ, $PbZrO_3$) and lead titanate (PT, $PbTiO_3$) where the ratio between the components can be varied, changing material properties. In addition, additives such as lanthanum can be included in the solid solution to affect the constitutive behavior. The variability in PZT

material properties due to mixture ratios led to the discovery of the morphotropic phase boundary (MPB) where exceptional piezoelectric coefficients were discovered [6]. Efforts to grow single crystal PZT failed [7], stalling major single crystal research until the early 1990s.

Relaxor Ferroelectrics

It was not until the early 1950s that lead based relaxor ferroelectric materials with the chemical formula of $Pb(B',B'')O_3$, where B' is a low valence cation and B" is a high valence cation, were discovered by Soviet researchers [8, 9]. Materials with this chemical structure were shown to not display Curie-Weiss behavior, instead having a diffuse dielectric permittivity around the Curie point. Of the many interesting relaxor materials discovered, lead magnesium niobate (PMN, $Pb(Mg_{1/3}Nb_{2/3})O_3$) proved to be the most promising [10]. PMN was shown to have reduced electrical conduction [11] and an anhysteretic electrostrictive effect [12, 13], making it useful for many applications, such as micro-positioning systems.

In the late 1970s, it was discovered that by creating a solid solution of PMN and PT the phase transformation temperature and the anhysteretic quadratic strains increased [14]. This finding was quickly followed by the discovery that with increased compositional levels of PT, the electrostrictive behavior of PMN-PT ($(1-x)Pb(Mg_{1/3}Nb_{2/3})O_3$-$xPbTiO_3$) was replaced by a more normal ferroelectric behavior seen in other materials [15]. This led to the creation of the phase diagram which showed a MPB separating the room temperature stable rhombohedral and tetragonal phases [16].

Although single crystal PMN was initially reported in the early 1960s [9, 17], it was not until the late 1960s that solid solution single crystal relaxor ferroelectrics emerged for another relaxor ferroelectric material, lead zinc niobate (PZN, $Pb(Zn_{1/3}Nb_{2/3})O_3$) [18, 19]. It was found that single crystal PZN-PT ((1-*x*)$Pb(Zn_{1/3}Nb_{2/3})O_3$-*x*$PbTiO_3$) behavior was phase [20] and orientation [21, 22] dependent, with some compositions and crystallographic directions exhibiting extremely large piezoelectric behavior. This work was followed by the studies of single crystal PMN-PT in the early 1990s [22, 23] and renewed the interest in ferroelectric materials. Today single crystal and ceramic ferroelectrics continues to be an exciting research area that promises even further discoveries.

1.1.1 Piezoelectricity

The piezoelectric effect is associated with a lack of charge symmetry about the center of a unit cell. A unit cell is the smallest three-dimensional atomic structure periodically repeated throughout the crystalline structure that still shows the crystal symmetry [6]. There are 21 classes of crystals that do not have a center of symmetry, with 20 of those classes being piezoelectric. The remaining non-piezoelectric class, *432* point group, does not show a piezoelectric effect because of the combination of other symmetry elements. Each piezoelectric crystal class has a symmetry which is reflected in the material properties such as compliance, piezoelectric constants and dielectric permittivity [24]. The piezoelectric effect is not found exclusively in crystalline materials. Certain kinds of polymers have been found that exhibit electromechanical behavior including rubber, wood fiber and silk. Figure 1-1 shows a schematic of a cubic

(a) and tetragonal (b) unit cell for lead titanate, PT. The non-piezoelectric cubic unit cell is referred to as the paraelectric phase and is found above the material specific Curie point. As the material is cooled past the Curie point a spontaneous polarization, P^s, is formed by a phase transformation into the tetragonal phase. The tetragonal phase has transverse isotropic symmetry and six possible spontaneous polarization directions along the principal axes. The spontaneous polarization is shown schematically in Figure 1-1 as the displacement of the central titanium ion. Accompanying the spontaneous polarization is an elongation parallel to the polarization direction and a contraction perpendicular to it.

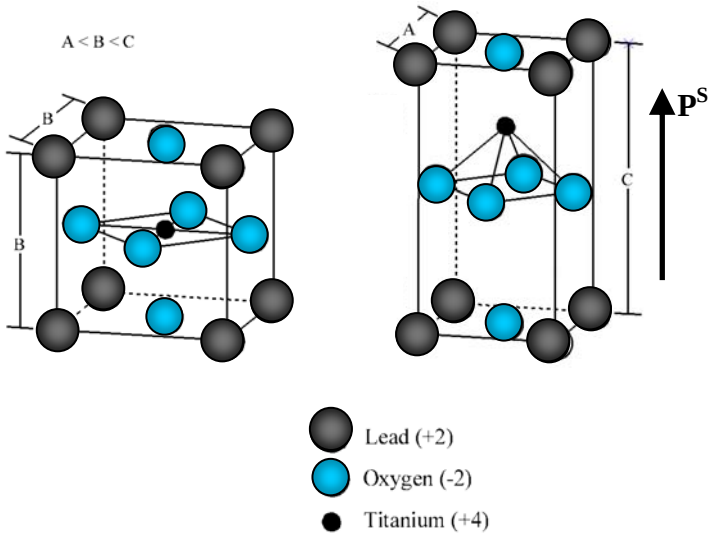

Figure 1-1. Schematic of the high temperature cubic crystal structure (a) and the lower temperature ferroelectric tetragonal phase (b) of PT.

1.1.2 Ferroelectricity

Ferroelectric materials are a subgroup of piezoelectric materials. Materials which fall into this category have a spontaneous polarization within a defined temperature range and the ability to reorient their spontaneous polarization through the application of an

external field [25]. A net remanent polarization may be produced in a multidomain ferroelectric material by applying a dc electric field greater than the coercive field [25]. This is defined as poling.

The reorientation of spontaneous polarization in ferroelectric materials is principally controlled by the motion of domain walls. Domains are regions of a ferroelectric material which share the same spontaneous polarization direction. The boundary between neighboring domains is called a domain wall. Reorientation of the polarization of unit cells in an unconstrained ferroelectric single crystal due to an applied field results in translation of domain walls. Polarization reorientation within one phase can be induced by either applied stress (ferroelastic switching) or electric field (ferroelectric switching). Ferroelectric polycrystalline material behavior is more complicated as each of the randomly oriented grains is a constrained single crystal subjected to local stress and electric field due to grain boundaries and local inhomogeneities. Figure 1-2 shows the experimentally measured electric displacement behavior of a soft (donor doped) PZT polycrystal (3195HD) manufactured by the CTS Communications Corporation, Inc. This composition is comparable to the Naval standard PZT-5A.

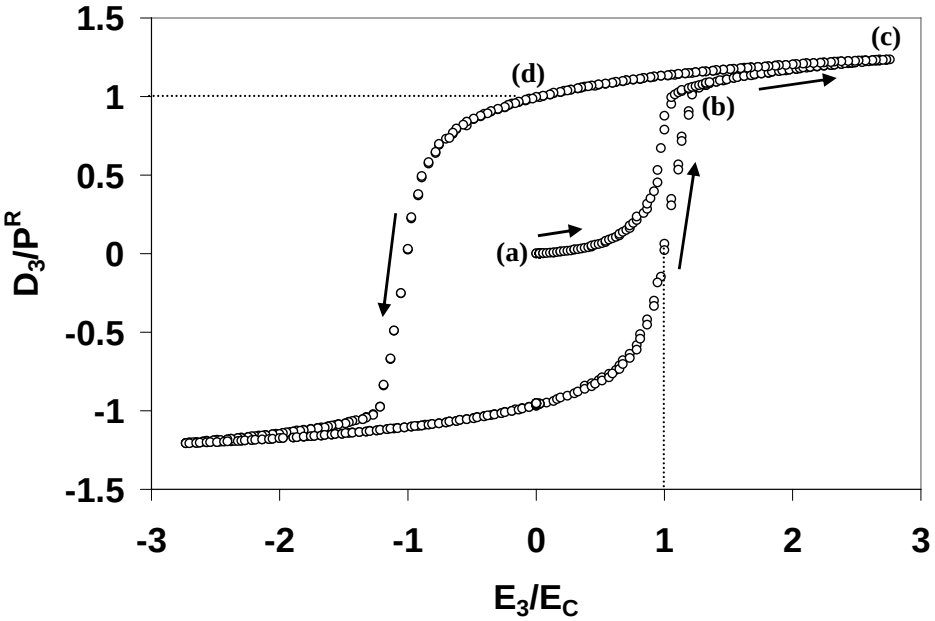

Figure 1-2. Experimentally measured dielectric behavior of polycrystalline PZT.

An unpoled polycrystalline ferroelectric material initially has no remanent strain or electric displacement. This is shown in Figure 1-2 as point (a). With the application of an electric field the spontaneous polarization direction of each grain begins to switch to the most favorable orientation. This results in increased polarization indicated by the arrow leading from Point (a) to Point (b). Point (b) denotes the saturation point when the domains are as closely aligned parallel to the electric field as possible. Point (c) represents the maximum electric displacement occurring at the maximum applied electric field. As the electric field is reduced the electric displacement will also decrease, but will not return to the initially zero value. This is because some domains will not return to their original orientations. Inhomogeneities can cause ferroelastic or ferroelectric switching to unstable, or unfavorable, domain states because of locally generated fields. Point (d) represents the remanent polarization, or the residual electric displacement. This value is smaller than the spontaneous polarization of the unit cell because the measured

polycrystalline behavior is the volume average of all grains. At this point the polycrystal is said to be poled. Further reduction of the electric field causes domains to reorient 180^o from their poled polarization direction when the coercive field is reached. The coercive field is defined as the electric field required to reduce the polarization to zero. Again increasing the electric field will cause the polarization to again switch 180^o and will complete the electric displacement hysteresis loop.

1.1.3 Relaxor Ferroelectrics

Relaxor ferroelectric materials are distinguished by their dispersive dielectric response and diffuse phase transformations about the temperature at which maximum dielectric permittivity is measured, T_{max} [26]. Relaxor ferroelectrics also show a decrease in hysteresis and remanent polarization as the temperature is increased to T_{max}, frequency-dependent ferroelectric properties and the optical isotropy at temperatures below the dielectric maximum when there is no external field.

Recently solid solutions of PMN-*x*PT [12, 27], $(1-x)Pb(Mg_{1/3}Nb_{2/3})O_3$-$xPbTiO_3$, and PZN-*x*PT [28], $(1-x)Pb(Zn_{1/3}Nb_{2/3})O_3$-$xPbTiO_3$, have been developed for use in engineered structures. The addition of the ferroelectric PT to relaxor PMN or PZN forms a complex solid solution system with enhanced electromechanical properties [29]. The addition of PT was also shown to increase the temperature at which maximum dielectric permittivity was found [30]. In non-relaxor ferroelectrics this is called the Curie point. Extensive work has been done on the growth of relaxor PMN-*x*PT and PZN-*x*PT single crystals by the flux growth, top-cooled solution growth, bottom-cooled solution and the Bridgman growth techniques [31-36]. Presently it remains difficult and expensive to

manufacture large single crystals with minimal fluctuations in piezoelectric properties [37, 38] for academic research or industrial applications [39]. Figure 1-3 shows the strain behavior of various compositions of PMN- and PZN-based single crystal and polycrystalline specimens due to unipolar electric field loading [29].

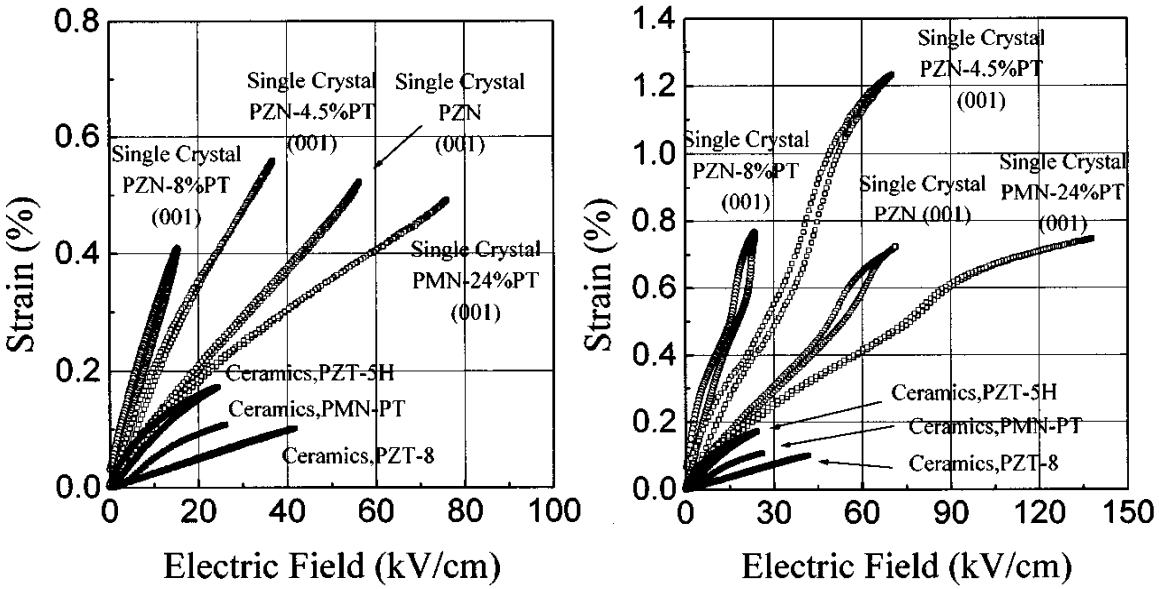

Figure 1-3. Electric field induced strain for various compositions of relaxor single crystals and ferroelectric polycrystals. Low electric field loads (a) produce nearly linear material response while at elevated electric fields (b) the initiation of phase transformations are apparent from the presence of hysteresis and nonlinear change in the electromechanical response [29].

Because of the symmetry in single crystals certain crystallographic orientations exhibit larger electromechanical couplings and reduced non-linearity and hysteresis. Experimental investigations have principally focused on the $\langle 001 \rangle$ due to the large electromechanical coupling factor ($k_{33} > 90\%$), piezoelectric constant ($d_{333} > 2500$ *p*C/N), dielectric permittivity ($\kappa_{33} \geq 5000$) and low dielectric loss ($\leq 1\%$) [29]. Park and Shrout

[29] have experimentally measured longitudinal strains as high as 1.7% in single crystal PZN-0.08PT applied with a ~120kV/cm electric field. As the crystallographic orientation is changed to the $\langle 111 \rangle$ crystal cut the measured longitudinal strain decreases. The exceptional material properties have been related to the domain and phase states [39].

Implementation of relaxor single crystals in applications can be challenging. Their constitutive behavior is rate-dependent as well as sensitive to temperature, electric field and stress [6]. They generally have a low coercive field, when compared to polycrystalline materials, which limits their usable loading range unless a bias field is applied [6]. Further understanding of the nonlinear electromechanical response, domain evolution, phase evolution and effects of composition on this behavior are important components of the implementation of these materials into new applications.

1.2 Contents of Dissertation

Chapter 2 presents a more detailed description of the primary length scales under consideration in a ferroelectric material and their effects on measurable behavior as well as the macroscopic constitutive relations of ferroelectric materials. In addition, previous experimental characterization of polarization reorientation and phase transformations and the nonlinear modeling of ferroelectric single crystal and polycrystalline materials are reviewed.

An experimental characterization and comparison of the measured large field constitutive behavior of $\langle 001 \rangle$ oriented single crystal PMN-0.26PT and polycrystalline PMN-0.32PT specimens is presented in Chapter 3. Electric displacement and strain were measured along the poling axis as a function of combined unipolar stress and bipolar and

electric field loading. Also presented is a comparison of measured single crystal behavior with previously published results for $\langle 001 \rangle$ oriented single crystal PMN-0.32PT. This gives a direct indication of the effect of composition (proximity to the MPB) on the single crystal behavior. The results are discussed in terms of the effects of domain wall and phase boundary motion. Chapter 3 also introduces an improved characterization technique for measuring the electromechanical properties of smaller specimens.

The constitutive behaviors of relaxor $\langle 001 \rangle$ oriented single crystal PMN-0.27PT and PMN-0.29PT were characterized at the Naval Undersea Warfare Center in Newport, Rhode Island at various temperatures in response to stress and electric field loading. The raw data was forwarded for graphical representation and interpretation. The experimental results are presented in Chapter 4 as three-dimensional surface plots that show the effects of applied fields. A comparison of results to those of earlier studies on different compositions of PMN-*x*PT single crystals near the morphotropic phase boundary is made illustrating the effects of composition on the phase transformation behavior and the linear material properties.

In Chapter 5, a model of the continuous field driven phase transformations observed in PMN-*x*PT relaxor ferroelectric single crystals is presented along with a comparison to experimentally measured material response. In developing the model it was assumed that the field induced diffuse phase transformations in relaxor ferroelectrics are the result of property fluctuations at the nanometer length scale. An energy analysis was utilized in simulating the effect of the orientation of the applied load with respect to the crystallographic axes.

Chapter 6 presents a micromechanical model of the constitutive behavior of polycrystalline PMN-0.32PT in terms of the measured constitutive behavior of single crystals of similar composition. The non-linear and hysteretic constitutive behavior of ferroelectric polycrystalline materials is governed by mechanisms that are associated with several smaller length scales and over multiple time scales. These include the length scales of grains, domains, defect structures and unit cells. The variant volume fractions evolve in response to local stress and electric fields. The effects of the form of the evolution law on the predicted polycrystalline behavior are explored and compared with measured single crystal and polycrystalline behavior.

The final Chapter of this dissertation provides major conclusions and recommendations for further research. These results are utilized to draw comparisons between single crystal and polycrystalline behavior as well as develop energy-based micromechanical and phase transformation models.

CHAPTER 2

BACKGROUND

Relaxor ferroelectric single crystals have been shown to have exceptional electromechanical properties [29] and in recent years refined crystal growth techniques [32] have provided both larger and less expensive single crystals. This has led to their utilization in many high-performance engineered structures such as sensors, receivers and actuators. Polycrystalline ferroelectric materials, although exhibiting decreased electromechanical properties from single crystals, are a useful lower cost alternative in many applications. The subsequent review will consider (i) the primary length scales under consideration and their effects on measurable behavior, (ii) experimental characterization of polarization reorientation and phase transformations, (iii) the macroscopic constitutive relations of ferroelectric materials and (iv) the nonlinear modeling of ferroelectric single crystal and polycrystalline materials.

2.1 Length Scales in Ferroelectric Materials

The behavior of ferroelectric materials is governed by complex multiscale phenomena, where nonlinearities at each length scale affect the macroscopic constitutive behavior. The primary length scales under consideration are shown in Figure 2-1.

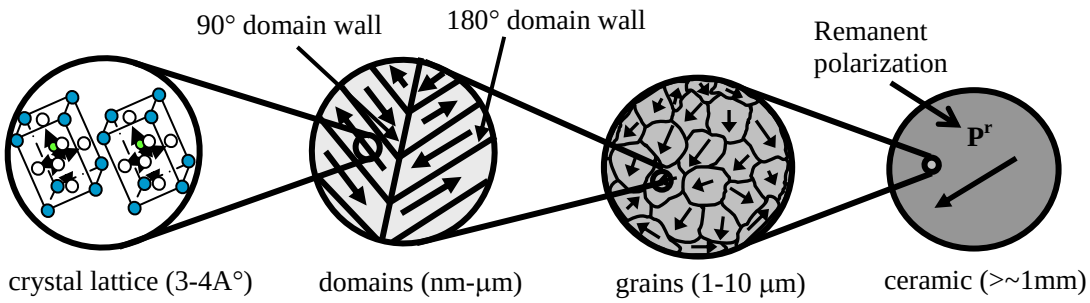

Figure 2-1. Primary length scales of ferroelectric materials [40].

2.1.1 Unit Cell Length Scale

The piezoelectric effect is associated with a lack of charge symmetry about the center of a unit cell [6]. The separation of the positive and negative charge centers in a unit cell is directly related to the spontaneous strain and electric displacement. Change in the equilibrium distance between charge centers is called the linear piezoelectric effect. In ferroelectric materials the spontaneous polarization direction can be switched to another energetically equivalent direction through externally applied loads. Volume averaging the responses of all unit cells provides the intrinsic response of a ferroelectric material.

A simplified model of ferroelectric unit cell switching is presented in Figure 2-2. This model considers the tetragonal perovskite crystal phase which has six possible distinct spontaneous polarization directions, called variants. Above a material specific temperature, called the Curie point, the unit cell has a non-ferroelectric (paraelectric) cubic symmetry (the unit cell does not have a spontaneous polarization direction). The spontaneous polarization forms in the unit cell when the temperature is reduced below the Curie point. Figure 2-2b shows a unit cell with spontaneous polarization. In this state the unit cell has a particular polarization direction that can be reoriented through the

application of an electrical (Figure 2-2c) or mechanical load (Figure 2-2d). This is referred to as switching, or polarization reorientation. It is possible for an electrical load to reorient the polarization direction to any of the other five possible variants; however a mechanical load can only induce 90^o switching as 180^o switches cause no change in strain.

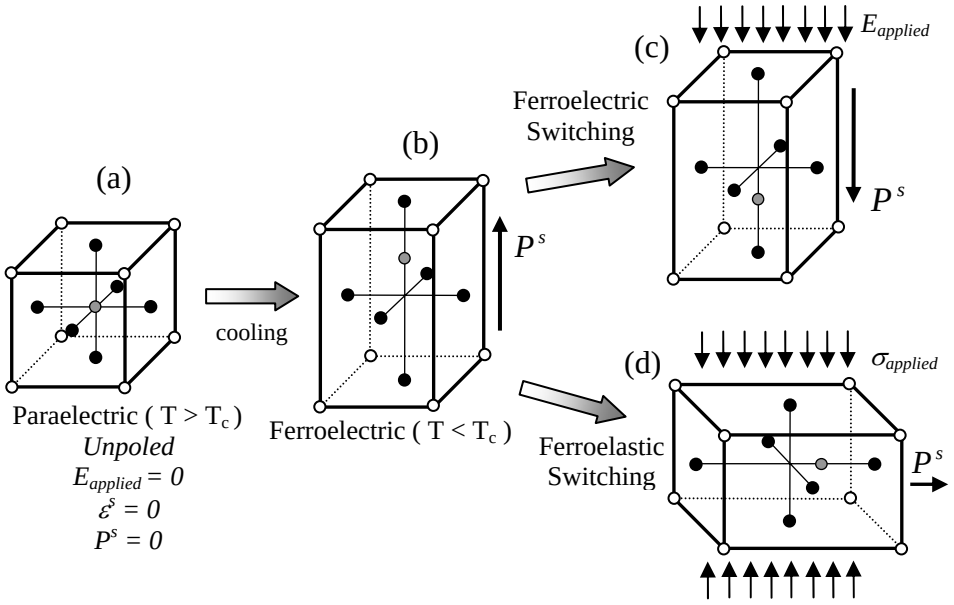

Figure 2-2. Idealized tetragonal ferroelectric unit cell undergoing a phase transformation from the paraelectric phase (a) at high temperature to the ferroelectric phase (b) due to cooling below the Curie point (T_c). Below the Curie point the ferroelectric unit cell can undergo ferroelectric switching (c) due to applied electric field or ferroelastic switching (c) due to mechanical load.

In addition to reorienting the polarization, the application of external fields can also initiate phase transformations in relaxor PMN-*x*PT ($0 \le x \le 0.33$), and PZN-*x*PT ($0 \le x \le 0.08$), materials [28, 41-43]. Common crystal phases for PMN-PT and PZN-PT are tetragonal, rhombohedral, orthorhombic and the monoclinic phase. Each phase has a crystal symmetry with associated symmetries of the elastic, dielectric and piezoelectric tensors unique to that phase [24]. The spontaneous polarization directions of the

tetragonal, rhombohedral and orthorhombic phases are oriented in the $\langle 001 \rangle$, $\langle 111 \rangle$ and $\langle 011 \rangle$ cubic referenced directions, respectively, which creates 6 possible polarization directions for tetragonal, 8 possible polarization directions for rhombohedral and 12 possible polarization directions for orthorhombic. There are also three monoclinic phases (M_A, M_B, M_C) which are the result of a continuous polarization rotation between phases [44]. Figure 2-3 shows the three phases possible below the Curie point with the possible spontaneous polarization direction for each phase defined.

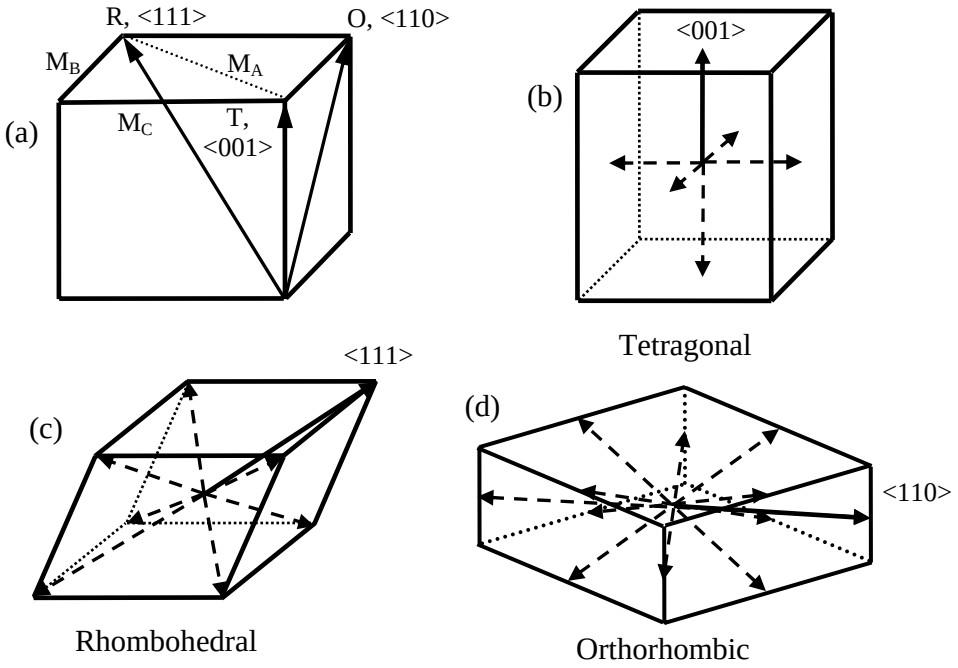

Figure 2-3. Unit cell illustrating the polarization direction and relationships of the different phases (a) [45]. Tetragonal (b), rhombohedral (c) and orthorhombic (d) crystal structures [46].

The symmetry of the compliance, piezoelectric and dielectric material tensors is dependent on the symmetry of crystal phase present. Each of the phases has different

crystal symmetry [24]. The tetragonal phase has 4*mm* symmetry which results in non-zero piezoelectric components $d_{31}=d_{32}$, d_{33} and $d_{15}=d_{24}$ and non-zero compliance components of $s_{11}=s_{22}$, s_{12}, $s_{13}=s_{23}$, s_{33}, $s_{44}=s_{55}$ and s_{66}. The rhombohedral phase has 3*m* symmetry which has non-zero piezoelectric components $d_{31}=d_{32}$, d_{33}, $d_{15}=d_{24}$ and $-2d_{22}=2d_{21}=d_{16}$ and non-zero compliance components $s_{11}=s_{22}$, s_{12}, $s_{13}=s_{23}$, s_{33}, $s_{44}=s_{55}$, $s_{56}=-2s_{24}=2s_{14}$ and $s_{66}=2(s_{11}-s_{12})$. The orthorhombic phase has *mm*2 symmetry which results in non-zero piezoelectric components $d_{31,}$ d_{32}, d_{33}, d_{15} and d_{24} and non-zero compliance components s_{11}, s_{12}, s_{13}, s_{22}, s_{23}, s_{33}, s_{44}, s_{55} and s_{66}.

The phase state of a relaxor single crystal is dependent on the composition and applied fields such as stress, electric field and temperature. Recent x-ray diffraction studies have shown that PMN-*x*PT single crystals at room temperature have a rhombohedral phase structure when $x < 0.3$, and a tetragonal phase when $x > 0.35$ to 0.37 [47, 48]. The region which separates the rhombohedral and tetragonal phase is called the morphotropic phase boundary (MPB). Similar behavior is seen in PZN-*x*PT single crystals which display a MPB for $x \approx 0.08$. Studies have shown that PMN-*x*PT and PZN-*x*PT specimens near the MPB are in a multiphase state and have speculated that this may be the cause of the increased electromechanical properties [39, 47, 49]. A number of researchers have shown experimental evidence of monoclinic phases for various compositions of PMN-*x*PT and PZN-*x*PT specimens near the MPB [47, 50-53]. Figure 2-4 shows phase diagrams for PMN-*x*PT and PZN-*x*PT as a function of temperature and composition [47, 54].

Previous experimental work on the compositional dependence of single crystal relaxor ferroelectrics has focused on determining the electromechanical coefficients at

various compositions, primarily around the MPB [29, 55, 56]. However, little work has focused on understanding the effect of composition on field induced phase transitions. Increased understanding of phase transformation behavior is imperative for increasing modeling capabilities and successful implementation of these materials into new applications. Chapter 4 presents a study on the compositional dependence of PMN-*x*PT single crystals.

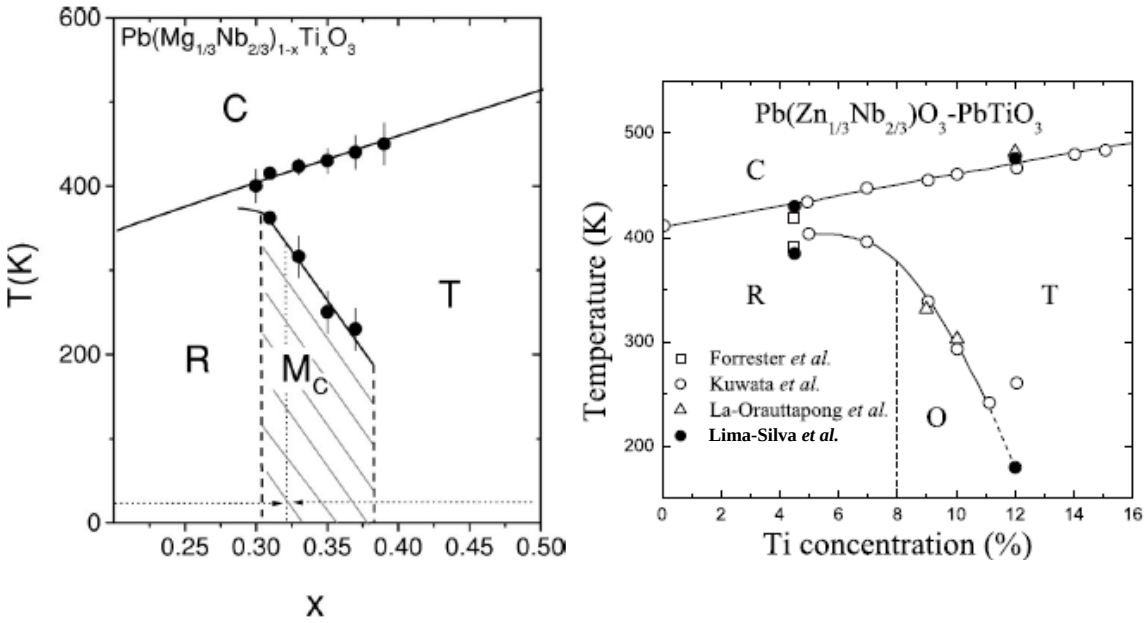

(a) (b)

Figure 2-4. Phase diagrams of PMN-PT (a) [47] and PZN-PT (b) [54].

2.1.2 Domain Length Scale

Clusters of unit cells with like spontaneous polarization are called domains. Domains form in ferroelectric polycrystals as "energy minimizers" during cooling from the sintering temperature to reduce the elastic energy associated with mechanical constraints between grain boundaries, and the electrostatic energy of the depolarizing electric field within the crystal [44]. Numerous domains tend to form in a single

specimen, with the boundary between two different domains referred to as a domain wall. Reorientation of the spontaneous polarization and spontaneous strain of the unit cells within each domain occurs when an applied electrical or mechanical field is in excess of the coercive field, i.e. the field required to cause domain reversal [6]. However, the entire domain will not simultaneously reorient. Domain switching will nucleate, most likely near areas of increased driving force such as a surface or a field concentration, followed by the growth of the switched area. This effect will "sweep" through the material eventually switching the polarity of each unit cell until there is no longer a driving force for switching [57]. This process is referred to as domain wall motion and is in some ways analogous to the dislocation motion in plasticity [58, 59]. Domain wall motion is rate dependent. At low applied field levels domain walls can bend. At higher applied fields the local barriers to domain wall motion, such as vacancies, interstitials and inclusions are unable to stop further motion. The assumption that the translation of domain walls past lattice defects represents a system of irreversibility and in conjunction with the sweeping effect causes domain wall motion to be a hysteretic effect is consistent with macroscopic observations [60]. The domain wall motion effect is seen in single crystal ferroelectric materials in addition to the single crystal grains of ferroelectric polycrystalline materials. Attempts have been made to experimentally witness domain wall motion in polycrystalline ferroelectrics [61, 62]. Li *et al*. [62] presented evidence that polarization switching of PZT polycrystals near the morphotropic phase boundary is primarily controlled by 90^{o} switching. Figure 2-5 shows domain patterns seen in PZN-0.045PT single crystal specimens with a polarizing microscope. PZN-0.045PT is on the rhombohedral side of the MPB.

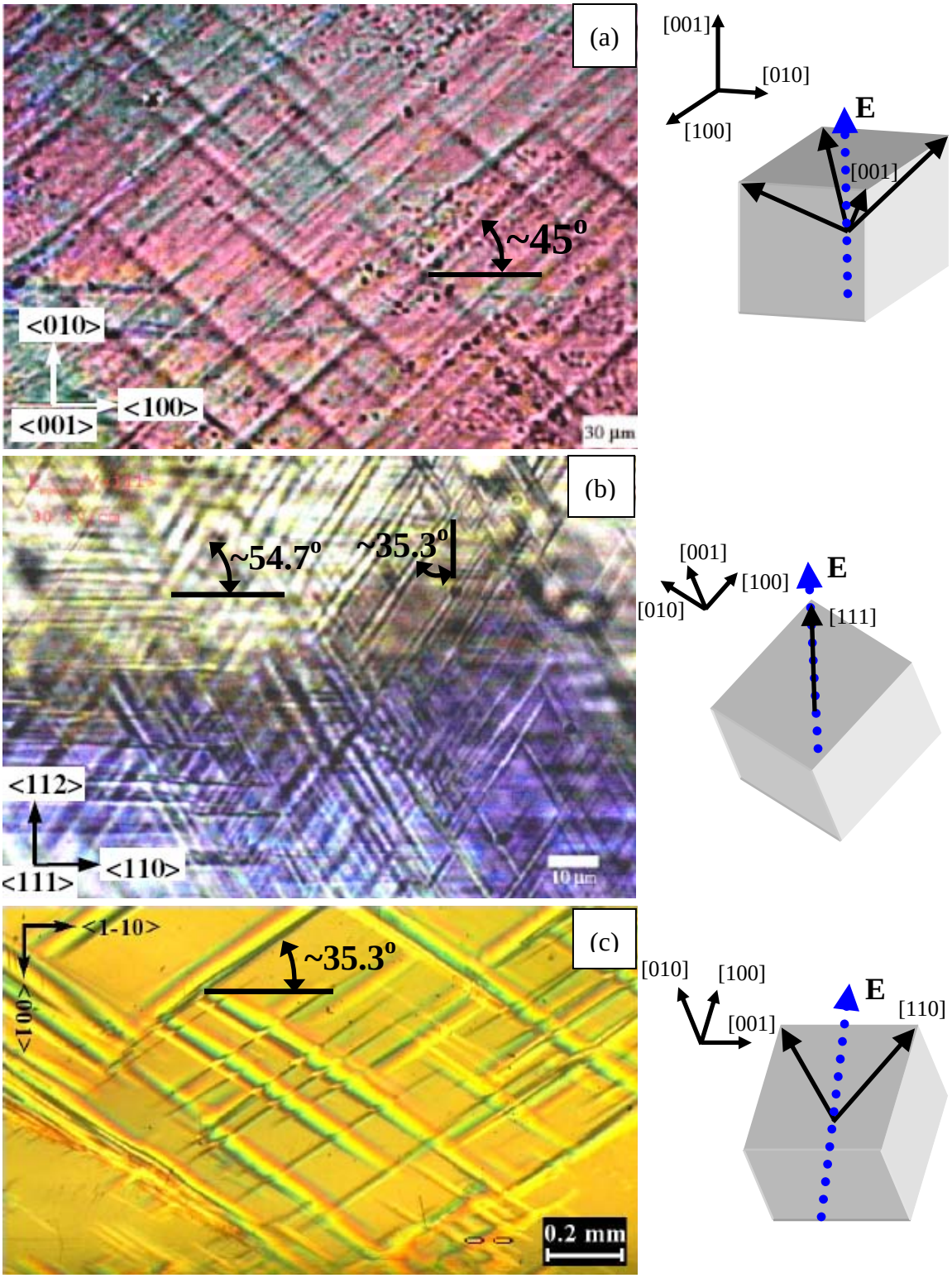

Figure 2-5. Observed domain patterns in (a) ⟨001⟩ poled [63], (b) ⟨111⟩ poled [63] and (c) ⟨110⟩ poled [64] PZN-0.045PT single crystal specimens. On the right are schematic representations showing the orientation of the perovskite rhombohedral unit cell relative to the principal crystal axes.

2.1.3 Single Crystal Grain Length Scale

Polycrystal materials are comprised of many grains, where each grain is a single crystal. After the manufacture of a polycrystal the individual grains are randomly oriented and in a multi-domain state. This results in the as-sintered polycrystalline specimen having zero remanent strain and polarization; the polycrystal must be poled by applying an appropriate electric field above the coercive field to induce piezoelectric behavior. Figure 2-6 is an electron backscatter diffraction image of a PZT composition near the MPB. This micrograph shows individual grains (larger blocks which are approximately 5 μm across), domain formation inside grains (dark and light striations), domain walls, porosity (dark areas surrounded by white), triple points (where three grains come together at the same location) and porosity at the triple points.

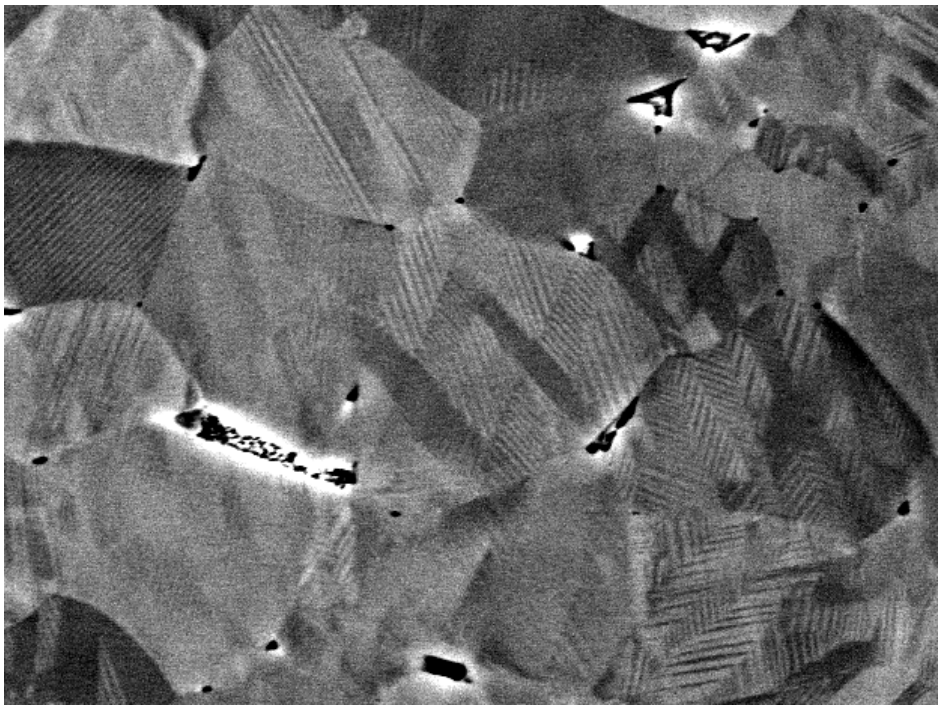

Figure 2-6. Electron backscatter diffraction image of a polished PZT specimen with a composition near the MPB (From collaboration with Dr. E. Kennik at ORNL through the SHARE program). A micrograph marker was not provided, however, the grains are approximately 5 μm wide.

A polycrystalline material is a conglomeration of single crystal grains. To accurately predict polycrystalline behavior, the orientation dependent nonlinear hysteretic response of single crystal materials must first be understood. Through the application of external fields it is possible to change the domain state of a ferroelectric single crystal. Most single crystal applications attempt to avoid large field polarization reorientation because it can cause excessive heat generation, eventual material degradation and possible component failure. However, in order to understand material behavior it is important to have experimental measurements of the large field bipolar response of single crystal switching. The electromechanical behavior of single crystal materials has been investigated by multiple authors for different compositions [29, 45, 64-69]. Ujiie and Uchino [69] observed domain reversal in relaxor ferroelectrics PZN-*x*PT using a high-resolution charge coupled device (CCD) sensor. Park and Shrout [29] measured the d_{33} coefficient of PZN-*x*PT single crystals as a function of composition showing a maximum of electromechanical response in the vicinity of the MPB on the rhombohedral side for the $\langle 001 \rangle$ crystallographic orientation. In this study the bipolar longitudinal strain and electric displacement were also measured for the $\langle 001 \rangle$ and $\langle 111 \rangle$ cut PZN-0.08PT single crystals along with the unipolar strain and electric displacement for a series of off-axis crystal cuts beginning in the $\langle 001 \rangle$ orientation and proceeding to the $\langle 111 \rangle$ crystal cut. Liu *et al.* [65] measured the dependence of selected piezoelectric properties as a function of applied electric field for $\langle 001 \rangle$ and $\langle 111 \rangle$ oriented single crystal PZN-0.045PT. Liu and Lynch [64] measured the electromechanical behavior of $\langle 001 \rangle$ and $\langle 110 \rangle$ oriented single crystal PZN-0.045PT. The experimental investigations were used to compute

piezoelectric properties for $\langle 111 \rangle$ oriented crystals. Liu and Lynch [66, 67] experimentally characterized the bipolar and unipolar behavior of off-axis cuts of single crystal PZN-0.045PT between the $\langle 001 \rangle$ and $\langle 111 \rangle$ orientations. This work extended previous works by showing the response to electric field at constant levels of stress bias and the strain and electric displacement response to a uniaxial compressive stress. McLaughlin *et al.* [45, 68] measured the strain and electric displacement response for a series of unipolar electric field and stress loadings for $\langle 001 \rangle$ and $\langle 110 \rangle$ oriented PMN-0.32PT single crystals at varying temperatures. This study showed three-dimensional plots of the electromechanical response and phase transformation behavior.

All the above reports show that the behavior of single crystals is dependent on orientation as well as applied fields and composition. After manufacturing, single crystals are typically in a multi-domain state. The domain state evolves in response to applied fields in accordance with the crystallographic orientation. Figure 2-7 shows measured polarization and strain for single crystal PZN-0.08PT in the $\langle 001 \rangle$ and $\langle 111 \rangle$ crystal cuts clearly showing orientation dependence.

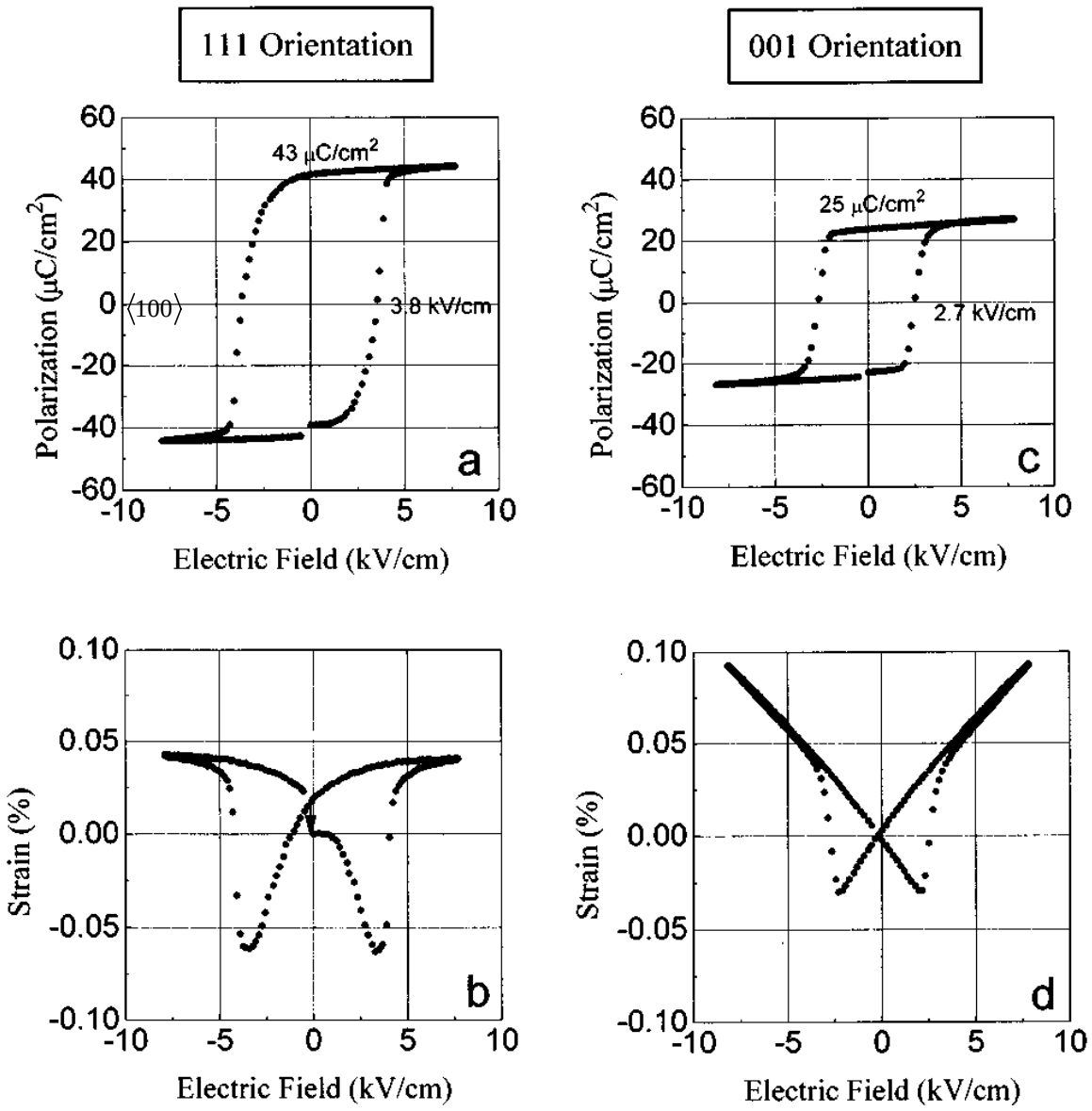

Figure 2-7. The polarization (a)(c) and longitudinal strain (b)(d) measurements of $\langle 111 \rangle$ (a)(b) and $\langle 001 \rangle$ (c)(d) oriented single crystal PZN-0.08PT versus bipolar electric field [29].

2.1.4 Polycrystalline Length Scale

At the macroscale ferroelectric polycrystals are typically modeled as a homogeneous transversely isotropic material. This methodology smears away microscale differences such as grains, domains or defects. This is a sufficient approximation for

small applied loads and low temperature where the linear characterization of the macroscopic behavior is applicable. However, ferroelectrics are in wide use in many applications that simultaneously expose the ferroelectric polycrystal material to high levels of stress, electric field and temperature. These operational conditions can cause nonlinearity by inducing polarization switching, domain wall motion and phase changes.

Many researchers have worked on the experimental characterization of major hysteresis loops in ferroelectric polycrystals. Early experimental efforts focused on the material behavior under only uniaxial electric field [70]. A number of researchers have worked to characterize the major hysteresis loops of polycrystal materials under combined stress and electric field loading [71-75]. Cao and Evans investigated the electromechanical coupling and nonlinearity in ferroelectric polycrystals [71]. Lynch [74] characterized the electromechanical behavior of soft PZT (lanthanum doped PZT, 8/65/35 PLZT) above the coercive field. In this study, initially unpoled PLZT specimens were simultaneously subjected to a uniaxial stress and electric field. Experimental efforts have focused on characterizing ferroelectric materials under other ambient conditions and loads. Chen and Lynch [72] measured the multiaxial constitutive behavior of pressurized 8/65/35 PLZT cylinders in compression. In this work they mapped a ferroelastic polarization reorientation threshold surface. Fett *et al.* [76] conducted torsion tests on thin-walled tubes of soft PZT finding good agreement with the Drucker-Prager yield criterion. Fett *et al.* [77] tested the strain response of soft PZT specimens under tensile and compressive loads which were both unpoled and poled perpendicularly to the axis of applied stress. Zhou *et al.* investigated the effects of uniaxial prestress [78] and electric field [79] on the electromechanical behavior of soft PZT. Huber and Fleck [80] and Zhou

et al. [75] have looked at the multiaxial electrical switching of ferroelectric polycrystals which have provided researchers with an understanding of switching behavior at several initial polarization orientation angles. This has provided a means with which to examine existing switching criteria in phenomenological models. Each of these studies has measured the behavior of polycrystalline specimens and speculated on the underlying mechanisms without consideration of the single crystal behavior. A polycrystalline ferroelectric material is comprised of many single crystal grains. Inhomogeneities (i.e. porosity, inclusions and cracks) can cause complex local boundary conditions for each single crystal grain. To more fully understand the magnitude of the effect of local singularities the experimental measurements of the polycrystal must be contrasted directly to experimental measurements of a comparable single crystal under similar loading conditions. Chapter 3 presents such a study.

Polycrystal materials are initially unpoled directly following manufacturing and do not display piezoelectric properties. This is because of the random distribution and domain patterns of each crystalline grain [81]. Through the application of an electric field the individual polarization directions of the grains begin to align themselves producing measurable levels of strain and electric displacement. A qualitative schematic of a polycrystal ferroelectric specimen before poling is shown in Figure 2-8a with the solid dark lines representing grain boundaries and the dashed lines representing domain walls. After an electric field is applied beyond the coercive field the polarization directions of each domain, represented by arrows, begin to align themselves with the direction of the applied electric field. When no further polar rotation is possible with increased loading the polycrystal is referred to as being in the saturated state. Domain

switching in each grain occurs at different levels of applied load. This is partly due to preferential switching orientations as well as to irregularities that affect local fields, such as grain boundaries and intergranular inhomogeneities. The particular domain patterns are dependent on defects that can either "pin" domain wall displacement by inhibiting motion, or conversely initiate it by creating areas of increased fields [6]. Both situations can cause areas of the polycrystal to begin switching at different applied loads. A schematic of a ferroelectric specimen during poling is shown in Figure 2-8b. The complete alignment of polar axes in a polycrystalline material can never be realized because of the originally random crystallographic orientation of each grain [6]. Intergranular stresses which inhibit the reorientation of domains and defects in the bulk which can cause stress concentrations act similarly by preventing the polycrystal from achieving perfect polarization (a single domain state). When the electric field is removed the dipoles will relax slightly reducing the polarization in the direction of the applied field, as shown in Figure 2-8c. Polarization rotations have been exaggerated for clarity and the corresponding points on the longitudinal strain versus electric field (ε_{33}-E_3) hysteresis loop for polycrystalline PMN-0.32PT are noted.

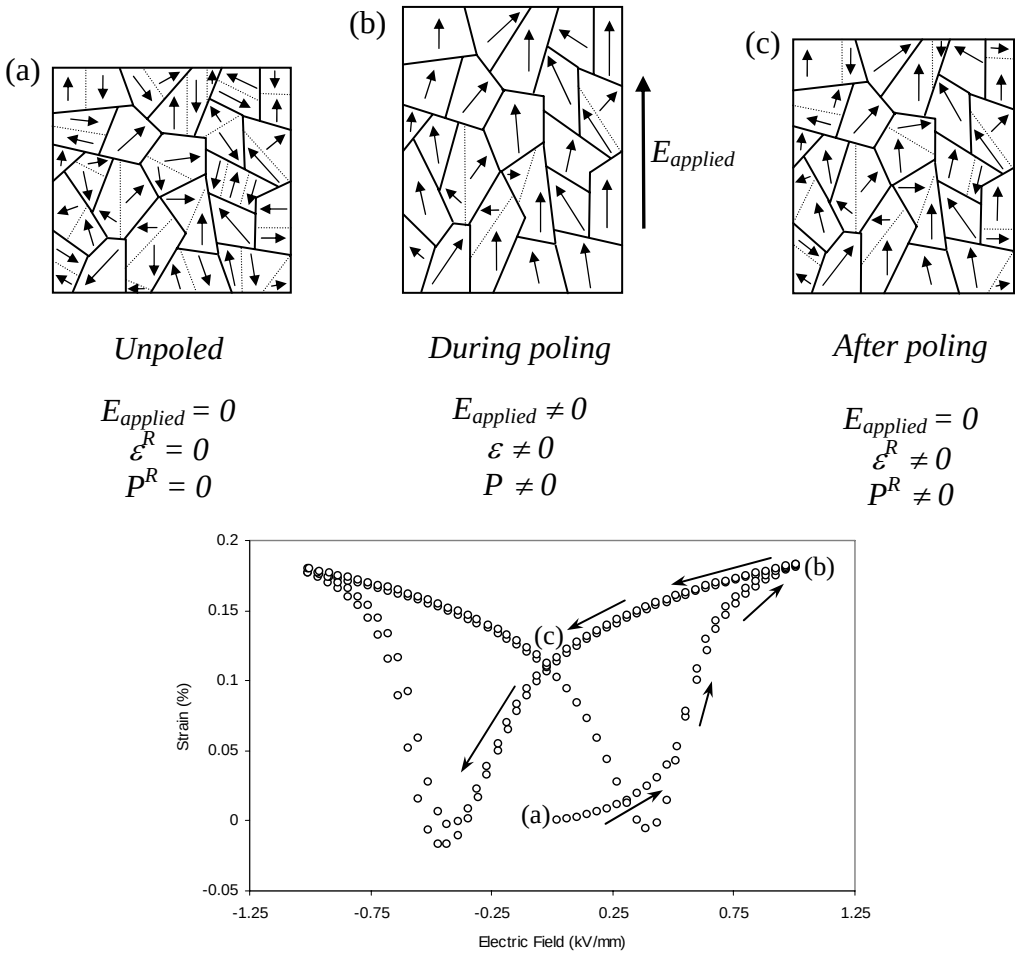

Figure 2-8. Domain orientations in a polycrystalline ferroelectric material, initially in an unpoled state with no remanent strain or polarization (a). During poling domain walls move and the polarization orientations change (b). After the release of the electric field the material relaxes slightly and some domain walls return (c). There is a remanent polarization and strain after poling operation. Experimentally measured strain versus electric field for PMN-0.32PT is labeled with corresponding domain configurations [82].

The application of a compressive stress can also produce a change in the spontaneous polarization of each grain for poled polycrystalline ferroelectrics. With the application of a compressive stress the individual polarization directions of the grains begin to reorient perpendicularly to the applied stress. This effect produces measurable levels of strain and electric displacement. Purely mechanical loading cannot force the

electric displacement to zero, which represents a polycrystal with all polarization directions oriented perpendicular to the applied field. This is not the case with strain. A qualitative schematic of a poled polycrystalline specimen is shown in Figure 2-9. The spontaneous polarization directions of the grains, shown as arrows, begin to align themselves perpendicular to the applied compressive stress. This is shown in Figure 2-9b. Upon the release of the compressive stress a number of grains regain some net out-of-plane polarization (Figure 2-9c) which could potentially be due to intergranular interactions. The qualitative schematic is compared to the experimentally measured electric displacement and strain of a poled polycrystalline 8/65/35 PLZT specimen during stress loading [74].

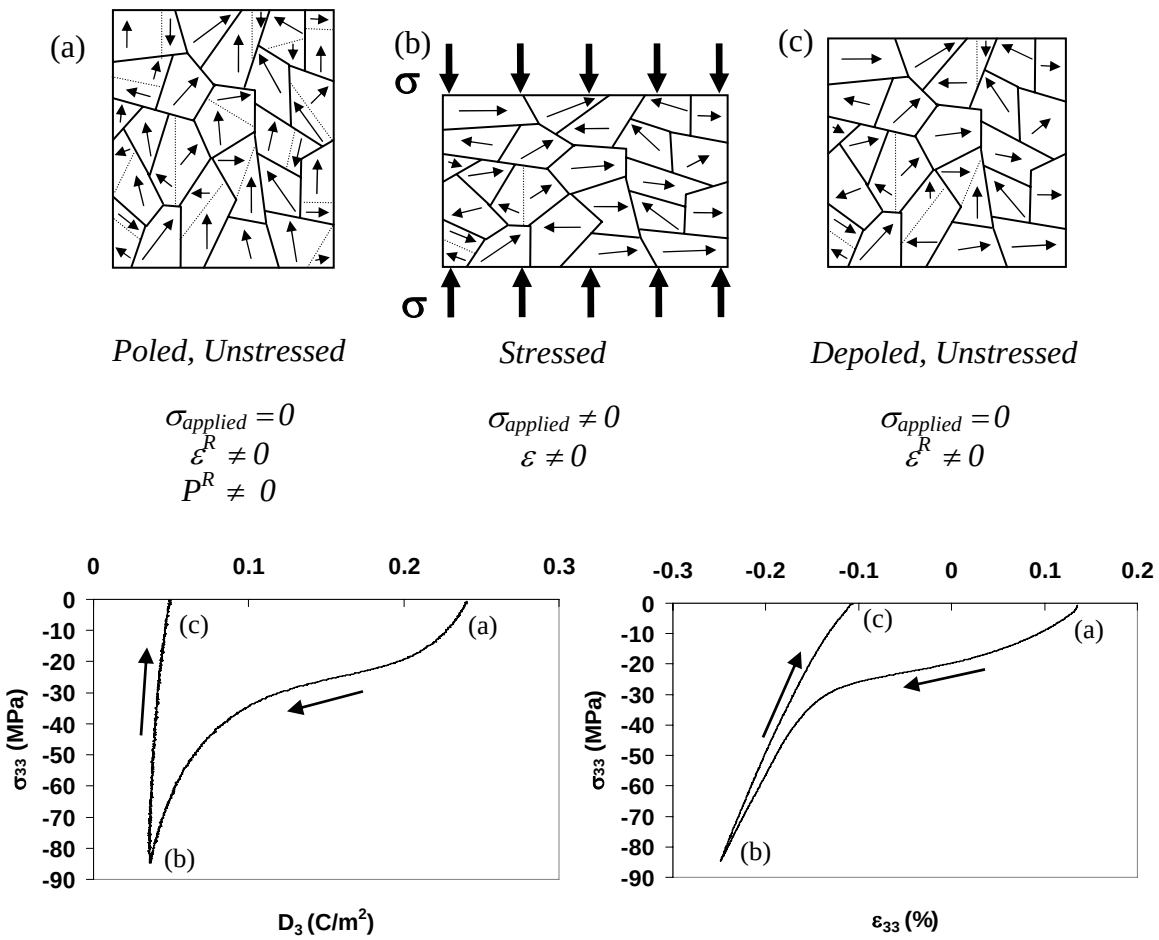

Figure 2-9. Stress induced depolarization of polycrystalline ferroelectrics. (a) The initially poled polycrystal has a remanent strain and electric displacement. (b) Upon the application of a compressive stress the spontaneous polarization of each grain begins to reorient perpendicular to the applied field, depoling the polycrystal. (c) When the compressive stress is removed some grains regain their original domain configuration. Experimental measurements of the electric displacement (D_3) and longitudinal strain (ε_{33}) of polycrystalline 8/65/35 PLZT in response to compressive mechanical stress (σ_{33}) are shown with the corresponding stage of loading labeled [74].

2.2 Modeling Techniques

Since the discovery of piezoelectricity in the 1880's (rochelle salt, quartz), single crystal ferroelectricity in 1921 (rochelle salt) and ferroelectricity in polycrystals in the 1940's (barium titanate) there has been a growing interest in ferroelectric materials. Recently developed compositions such as PMN-*x*PT and PZN-*x*PT single crystals have

been shown to be increasingly useful for numerous applications. Improved single crystal grain growth techniques and increasing number of applications for ferroelectric materials have led to research efforts focused on theoretical and numerical models of the underlying mechanisms causing their electromechanical coupling, such as domain evolution and phase transitions under applied fields [43, 83-89].

2.2.1 Linear Constitutive Relations

It can be shown that for quasi-static conditions with small perturbations the linear constitutive relationships for a piezoelectric material with applied stress, electric field and temperature as the independent variables are:

$$\varepsilon_{ij}^{L} = s_{ijkl}^{E,T}\sigma_{kl} + d_{kij}^{T}E_k + \alpha_{ij}^{E}\Delta T \tag{2-1a}$$

$$D_i^{L} = d_{ikl}^{T}\sigma_{kl} + \kappa_{ik}^{\sigma,T}E_k + q_i^{\sigma}\Delta T \tag{2-1b}$$

where ε_{ij} is the strain, s_{ijkl} is the compliance, σ_{kl} is the stress, d_{kij} is the piezoelectric constant, E_k is the electric field, α_{ij} is the coefficient of thermal expansion, ΔT is the change in temperature, D_i is the electric displacement, κ_{ik} is the dielectric permittivity and q_i is the pyroelectric coefficient; indices vary from 1 to 3. Superscript L refers to the reversible (elastic) portion of strain and electric displacement. Each of these material constants is dependent on the applied boundary conditions. Superscripts, E, σ and T refer to constant electric field, stress and temperature, respectively. These are the general equations used to describe the linear behavior of piezoelectric materials. It is important to note that these material constants are tensor components that are orientation dependent and can therefore be transformed to other orthogonal reference frames. The total strain

and electric displacement in a ferroelectric material is the summation of the linear part and remanent (nonlinear) part.

$$\varepsilon_{ij} = \varepsilon_{ij}^{L} + \varepsilon_{ij}^{R} \tag{2-2a}$$

$$D_i = D_i^{L} + D_i^{R} \tag{2-2b}$$

where the superscript *R* refers to the remanent portion of strain and electric displacement. The remanent polarization and strain are the volume average of the spontaneous polarization and strain plus and effects of stress and electric field at the local level that affect the macroscopic remanent terms. As an unpoled ferroelectric specimen is loaded, the spontaneous polarization directions begin to align themselves with the most favorable direction. When the load is removed not all domains switch back to the original configuration.

The polarization of a material is the electric dipole moment per unit volume. Electric displacement is the surface charge per unit area when there is no free charge within the dielectric. They are related through the following linear expression:

$$D_i = P_i + \varepsilon_o E_i \tag{2-3}$$

where P_i is the polarization and ε_o is the permittivity of free space which is defined as $\varepsilon_o = 8.854 \times 10^{-12} F/m$. Because of the relative size of the term $\varepsilon_o E_i$ as compared to P_i, for most ferroelectric materials it is often neglected, making electric displacement approximately equal to the polarization of a ferroelectric material. During future discussions of ferroelectric material behavior the terms polarization and electric displacement will be used interchangeably.

2.2.2 Nonlinear Constitutive Modeling

Linear piezoelectricity is a well understood phenomenon that has been extensively implemented in commercially available finite element programs such as ANSYS and ABAQUS. Current applications expose ferroelectric materials to levels of combined stress, electric field and temperature that can cause nonlinearity such as domain wall motion and phase transformation. In this region of material behavior linear relations are no longer valid.

Nonlinear ferroelectric constitutive behavior has been modeled using several different approaches that bridge multiple length scales. These include macroscale phenomenological models based on series expansions of energy functions as well as internal state variable approaches borrowed from metal plasticity used to describe yield surfaces governing polarization reorientation and hardening moduli governing polarization saturation [90, 91], micromechanics models that describe the macroscopic behavior in terms of material behavior at the level of the granular structure of the polycrystalline materials [92] and phase field models based on time dependent Ginsberg-Landau theory that describe the behavior of the grains in terms of domain structure [43, 93]. The macroscale internal state variable based phenomenological constitutive laws are the least computationally intensive; however they involve many variables that serve as fitting parameters that must be experimentally determined [94]. This requires a set of multiaxial experiments under combinations of stress and electric field that are difficult, if not impossible, to achieve experimentally. The solution to this dilemma has been to use a combination of experimental results and micromechanical simulations. The micromechanical approach is based on the multiaxial behavior of the material at the

length scale of the grains [92]. It involves representing the polycrystalline behavior as the volume average of the behavior of the single crystal grains. This approach has successfully been used in the development of multiaxial constitutive laws capable of reproducing major and minor hysteresis loops, but has had a significant shortcoming. The single crystal behavior had to be assumed and used as a fitting parameter due to a lack of available single crystal data. Chapter 6 presents a developed model which utilizes measured single domain material properties and assumptions on the nonlinear volume fraction evolution based on experimental single crystal measurements to simulate the behavior of polycrystalline specimens on a similar composition. A more thorough discussion of the micromechanical approach to modeling ferroelectric materials will be presented in Chapter 6.

2.2.3 Ferroelectric Phase Transformations

Phase transformations have been shown to occur in relaxor single crystals from the application of external stress, electric field and temperature fields [42, 45, 68]. PMN-*x*PT [95, 96] and PLZT, (Pb,La)(Zr,Ti)O_3 [97] relaxor ferroelectric materials display a gradual temperature induced phase transition with a resulting broad Curie peak rather than a distinct Curie point [98]. Continuous phase transformation behavior driven by mechanical and electrical fields has also been observed in certain compositions of relaxor ferroelectrics [45, 68]. Recent characterization of relaxor PZN-*x*PT single crystals has resulted in the observation of another distinct type of field induced phase transformation behavior. Electrically loaded $\langle 011 \rangle$ cut PZN-0.045PT shows a distinct phase

transformation field for the forward and reverse transformations resulting in a discontinuous transition [66, 67].

A commonly proposed mechanism for the observed phase transformation behavior is that the material undergoes a continual rotation through a monoclinic phase providing a gradual transition from the rhombohedral to the orthorhombic phase [29, 53, 99-102]. Phenomenological models, such as the Devonshire Theory, have been used to model phase transitions. Devonshire [103] originally explained the phase transitions of barium titanate, $BaTiO_3$, using a sixth order Ginzburg-Landau-type expansion of the free energy expression in terms of polarization. Since then, others have used the Ginzburg-Landau equations to model ferroelectric domain formation and motion [93, 102, 104, 105].

The initial explanation of the temperature induced diffuse phase transformation about the Curie point in relaxor ferroelectrics was based on the compositional fluctuations [98]. As the temperature of a relaxor ferroelectric material is increased to the Curie point nano-polar regions progressively begin to transition to the paraelectric phase, resulting in the characteristic dielectric peak. Figure 2-10 shows experimental measurements of the dielectric permittivity of polycrystalline PMN-*x*PT as a function of temperature and frequency [106].

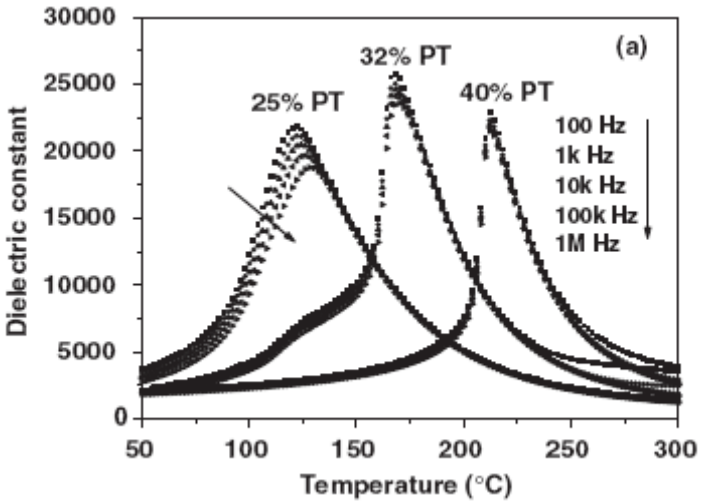

Figure 2-10. The dependence of dielectric permittivity of three compositions of polycrystalline PMN-*x*PT prepared by conventional pressure-less sintering on temperature and frequency [106].

To date, there have been no models which use this description to simulate the electric field and stress induced phase transformation shown in experimental characterizations of relaxor single crystals. Such a model would be important. Chapter 5 presents a micromechanical model of field induced phase transformations in relaxor ferroelectric single crystal specimens based on this mechanism.

2.2.4 Simulation of the Effect of Inhomogeneities in a Ferroelectric Continuum

The energy-momentum tensor (Maxwell-tensor), first described by Eshelby [107, 108], is the partial derivative of the elastic energy density with respect to the deformation gradient, where the elastic energy density is dependent on the undeformed configuration. In this classical work, Eshelby [107] studied the forces on mobile singularities in an elastic crystal lattice continuum to describe their evolution for static and dynamic cases. This idea was applied to the study of the driving forces on inhomogeneities. The term

used to describe the forces on inhomogeneities is configurational forces. Lattice defects of any dimension can be analyzed and include point charges (zero-dimensional), interstitial atoms (zero-dimensional), line defects (one-dimensional), interfaces or boundaries (two-dimensional) and inclusions or voids (three-dimensional) [109].

The development of the *J*-integral in fracture mechanics is an important use of configurational forces [110] which was later extended to fracture of piezoelectric materials [111, 112]. Recently, researchers have begun using configurational forces to study the effects of defects on the motion of domain walls [113-117], which can be considered an inhomogeneity. Mueller *et al.* [113] studied the interaction of point defects on the motion of a single 180^{o} domain wall. In this work they developed a formulation for the driving forces on a domain wall. Closely following this research, Schrade *et al.* [115] considered the kinetics of domain walls moving past various defects. Analytical results were compared to experimental measurements of domain wall velocity by Flippen [61]. Schrade *et al.* [116, 117] presented a continuum model for ferroelectric materials. In this FEM model they considered a domain wall moving over a defect.

CHAPTER 3

MEASUREMENT OF POLYCRYSTALLINE AND SINGLE CRYSTAL RELAXOR FERROELECTRIC CONSTITUTIVE BEHAVIOR

PMN-0.32PT single crystals have been characterized under combined stress and electric field loading [45, 68]. This approach is extended to PMN-0.26PT single crystals to determine compositional effects and to PMN-0.32PT polycrystalline specimens to compare with polycrystalline behavior. Electric displacement and strain were measured as a function of combinations of both unipolar and bipolar stress and electric field. The results of this study have been accepted for publication in *Acta Materialia* [60].

3.1 Introduction

Over the past fifteen years considerable effort has been devoted to the measurement of the response of ferroelectric polycrystals to combined stress and electric field loading [71, 73-75, 80]. Measurement of the constitutive behavior has been followed by the development of micromechanical constitutive laws that predict the macroscale material behavior based on a volume average of the behavior at the microscale [92, 118, 119]. At the microscale, the material behavior has been modeled by a simplified hysteresis response in the single crystal grains of the polycrystalline ferroelectric. The development of crystal growth techniques has led to the availability of larger single crystal relaxor ferroelectrics for characterization. This experimental work resulted in measured single crystal hysteresis behavior that is far more complex than the

behavior implemented in earlier micromechanics models and not only includes effects of domain wall motion (switching), but multiple field induced phase transformations.

Previous work characterizing the response of PMN-0.32PT single crystals to combined stress and electric field loading has led to the question of whether this measured single crystal behavior can be used to predict the behavior of polycrystalline ceramics of the same composition through micromechanical modeling. Such models would take into account effects of orientation, intergranular interactions, ferroelectric and ferroelastic polarization reorientation and field induced phase transformations; and use volume averaging techniques to predict the material behavior at the macroscale. These models would be extremely useful in providing a fundamental understanding of the behavior of polycrystalline ceramics, including textured ceramics and thin films under large in-plane biaxial stress. To date, there has not been sufficient experimental data on single crystal and polycrystalline specimens of the same composition to construct micromechanical models without the introduction of a number of simplifying assumptions for the single crystal behavior. The work presented in this chapter has provided data on the constitutive behavior that is used in Chapter 6 for the development of an improved micromechanical model. The following sections begin with a review of the measured behavior of single crystal and polycrystalline ferroelectric materials. This is followed by the presentation of the results of characterizing the response of single crystal PMN-0.26PT and polycrystalline PMN-0.32PT.

The response of relaxor single crystals to combined stress and electric field loading has been experimentally determined by various authors. McLaughlin *et al.* characterized the response of $\langle 001 \rangle$ and $\langle 011 \rangle$ oriented PMN-0.32PT single crystals at

various temperatures [45, 68]. In this work the electric displacement and strain were measured as a function of stress, electric field and temperature. The results were presented as three-dimensional surface plots which identify the effects of field induced phase transformations. Phase transformation maps were created which show the dependence of the transformation on applied fields. Park and Shrout [29]measured the d_{33} piezoelectric coefficient as a function of composition for the $\langle 001 \rangle$ and $\langle 111 \rangle$ oriented PZN-0.045PT single crystals. In addition, the electric displacement and strain were measured in response to bipolar and unipolar electric field loading, respectively, for crystal cuts between the $\langle 001 \rangle$ and $\langle 111 \rangle$ orientations. Liu and Lynch [66, 67] have measured the unipolar and bipolar response of PZN-0.045PT for a series of crystal cuts. Cyclic electric field was applied at multiple angles between the $\langle 001 \rangle$ and $\langle 111 \rangle$ orientation directions. The results showed that the effects of domain wall motion on the hysteresis behavior are strongly orientation dependent. Liu and Lynch characterized the electromechanical response of PZN-0.045PT single crystals for the $\langle 001 \rangle$, $\langle 011 \rangle$ and $\langle 111 \rangle$ orientations [64]. This work utilized a combination of measured piezoelectric coefficients together with orthogonal transformations to determine a full set of piezoelectric coefficients in the single domain $\langle 111 \rangle$ orientation. This study also presented measured double loop behavior, evidence of an electric field induced phase change. The hysteretic phase change was shown to be accompanied by a jump in strain and electric displacement in contrast to the more gradual electric field induced phase transformation seen in PMN-*x*PT specimens [46].

Studies have shown that PMN-*x*PT and PZN-*x*PT specimens near the morphotropic phase boundary (MPB) have an intricate multiphase state consisting of tetragonal, rhombohedral, orthorhombic and monoclinic phases [39, 47, 49]. The phase state of a relaxor single crystal is dependent on applied fields such as stress, electric field and temperature in addition to the composition and the history of the sample. Many researchers have shown experimental evidence of rhombohedral to orthorhombic ($R \rightarrow O$) [25, 27, 50, 102, 103] and rhombohedral to tetragonal ($R \rightarrow T$) [12, 47, 104, 105] phase transformations in relaxor single crystals from the application of external fields. It was shown from these studies that the relative orientation between the applied loads and the principle crystallographic axes affected both the initiation point and the type of phase transformation. Experimental studies have shown that PMN-*x*PT and PZN-*x*PT single crystals of varying compositions with an electric field in the $\langle 110 \rangle$ orientation or a stress in the $\langle 001 \rangle$ direction display an $R \rightarrow O$ phase transformation [45, 68, 120]. Alternately, applying and electric field in the $\langle 001 \rangle$ orientation has been shown to initiate an $R \rightarrow T$ phase transition in PMN-*x*PT and PZN-*x*PT single crystals [121-123]. Some of these experimental studies have shown that increasing temperature also affects phase transformation behavior by decreasing the applied fields required to cause a phase transition.

Many researchers have worked on the characterization of major hysteresis loops in ferroelectric polycrystals under combined stress and electric field loading [53, 56, 57, 106]. Cao and Evans [71] investigated the electromechanical coupling and irreversibility in ferroelectric polycrystals. In their study, hard and soft PZT specimens, a relaxor ferroelectric material (PMN-0.1PT), and an antiferroelectric ($PLSn_{0.27}ZT$) were poled and

subjected to a uniaxial compressive stress. Several significant observations were made. First, when a compressive stress is applied normal to the polarization direction, 180^{o} switching decreases. Second, nonlinear deformation is related to the deviatoric components of stress and strain. Third, when uniaxial stress is applied to a specimen parallel to the polarization there is a subsequent change in the Poisson ratio that is associated with a transition from ferroelastic switching to purely elastic strain. They also proposed a material specific constitutive law. Lynch [74] characterized the large field electromechanical behavior of lanthanum doped 8/65/35 PLZT. In this study, initially unpoled PLZT specimens were subjected to a uniaxial stress and electric field. This work provided measurements of the strain/electric field, polarization/electric field, stress/polarization, and stress/strain hysteresis loops. It also provided several observations along with a discussion of the possibility of modeling the intergranular stress effects using a variation of an Eshelby inclusion model for intergranular constraints [124]. More recent experimental efforts have focused on characterizing ferroelectric materials under other loading. Huber and Fleck [125] and Zhou *et al.* [75] have looked at the multi-axial electrical switching of ferroelectric polycrystals, and Chen and Lynch [72] characterized polycrystalline 8/65/35 PLZT tubes under multiaxial mechanical loading.

This study presents a comparison of the measured large field constitutive behavior of polycrystalline PMN-0.32PT and single crystal PMN-0.26PT. It also presents a comparison of measured single crystal behavior with previously published results for single crystal PMN-0.32PT. This gives a direct indication of the effect of composition (proximity to the MPB) on the single crystal behavior. The results are discussed in terms of the effects of domain wall and phase boundary motion.

3.2 Experimental methodology

This section describes the specimen preparation, the experimental arrangement and the results of the single crystal and polycrystalline characterization.

3.2.1 Single Crystal Specimen Manufacturing and Preparation

PMN-0.26PT and PMN-0.32PT are each in the rhombohedral phase at room temperature, with the PMN-0.32PT being very close to the morphotropic phase boundary. The spontaneous polarization of the rhombohedral phase lies in one of the eight possible $\langle 111 \rangle$ directions. When an electric field in excess of the coercive field is applied along the $\langle 001 \rangle$ direction as shown in Figure 3-1, the spontaneous polarization will re-orient such that four of the eight possible $\langle 111 \rangle$ crystal variants are present.

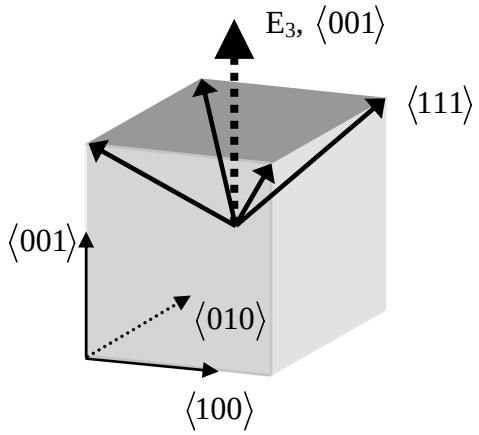

Figure 3-1. Possible variants in the $\langle 001 \rangle$ poled rhombohedral phase.

The single crystal specimens were provided by TRS Technology, Inc. Specimens were cut from a single crystal boule. Each specimen measured 5mm x 5mm x 5mm and

was oriented with the $\langle 001 \rangle$ (cubic referenced) crystallographic axis parallel with the mechanical and electrical loading direction. No further polishing or cutting was performed on the specimens; testing was done in the as received condition. Prior to testing, each crystal was cleaned in an ultrasonic cleaner with acetone followed by ethanol alcohol. Two opposing faces were sputtered with a thin layer of gold to serve as electrodes. Three cubes were stacked and bonded together and the center cube was instrumented with strain gages. This novel testing method was developed to increase the aspect ratio and to produce a uniform uniaxial stress in the center specimen (where strain was measured) by decreasing clamping effects at the edges during loading. Buehler Crystalbond mounting wax was used to bond the electroded sides of each specimen together with alignment of each crystal relative to one another. A copper foil mesh with a thickness of 0.025mm was placed between each crystal in the bonded region to ensure electrical contact and to serve as an electrical connection point. A schematic of this experimental setup is shown in Figure 3-2.

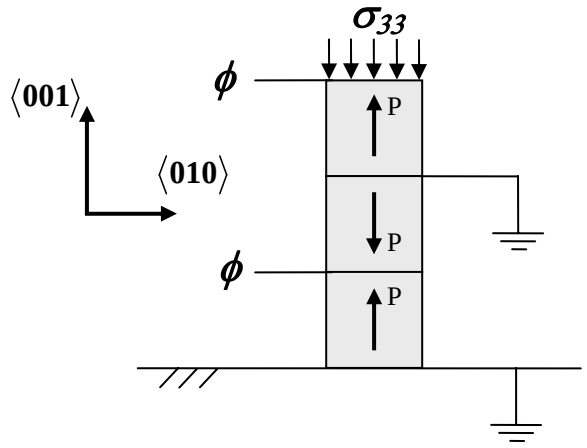

Figure 3-2. Three single crystal specimens were bonded and subjected to electrical and mechanical loading as shown.

3.2.2 Polycrystalline Specimen Manufacturing and Preparation

PMN-0.32PT polycrystalline specimens were manufactured at the Darmstadt University of Technology in Darmstadt, Germany. The chemicals used to produce these specimens were PbO (>99.0%, Alfa Aesar, Germany), $MgCO_3Mg(OH)_2{\cdot}6H_2O$ (99.5%, Alfa Aesar, Germany), Nb_2O_5 (99.9%, ChemPur, Germany) and TiO_2 (99.9%, Alfa Aesar, Germany). The columbite precursor method was employed to prepare $0.68Pb(Mg_{1/2}Nb_{2/3})O_3$-$0.32PbTiO_3$ powder. The columbite, $MgNb_2O_6$ (MN), was synthesized by attrition-milling $MgCO_3Mg(OH)_2{\cdot}6H_2O$ and Nb_2O_5 for 12 hours, followed by calcination at 1200 ^oC for 4 hours. The dried MN powder, PbO and TiO_2 were weighed according to the stoichiometric formula and ball-milled in ethanol for 24 hours with a planetary mill and yttrium-stabilized zirconia balls of 5mm in diameter. The mixed powder was then calcined in an alumina crucible at 850 ^oC for 2 hours. After calcination, the powder was further ground for 24 hours using the above-mentioned ball mill. Rectangular bars were uniaxially pressed in a stainless steel die, followed by a cold isostatic pressing at 300 MPa. Sintering was conducted in air at 1200^oC for 3 hours at a heating rate of 300^oC/hr with the specimens buried by the powder of the same composition to minimize the lead volatilization, and covered by double alumina crucibles as well. After that, the sintered samples were ground and polished on all sides until the defined dimensions of 8mm x 8mm x 12mm were reached.

Prior to testing, each specimen was cleaned in an ultrasonic cleaner with acetone followed by ethanol. Gold electrodes were sputtered onto opposing 8mm x 8mm faces. Polycrystalline specimens were not tested in a stacked configuration because of their prohibitive size.

3.2.3 Experimental Arrangement

Mechanical and electrical loads were applied simultaneously using the fixture shown in Figure 3-3. Uniaxial compressive load was applied by a screw-type load frame. The bottom of the specimen rested on a steel plate which was attached in series with a capacitor to ground potential. During testing each sample was submerged in a bath of Fluorinert™ FC-70 electrical liquid. Electrical isolation from the load frame was accomplished by placing alumina blocks above and below each specimen. This experimental setup has been used previously by other researchers to characterize ferroelectric materials.

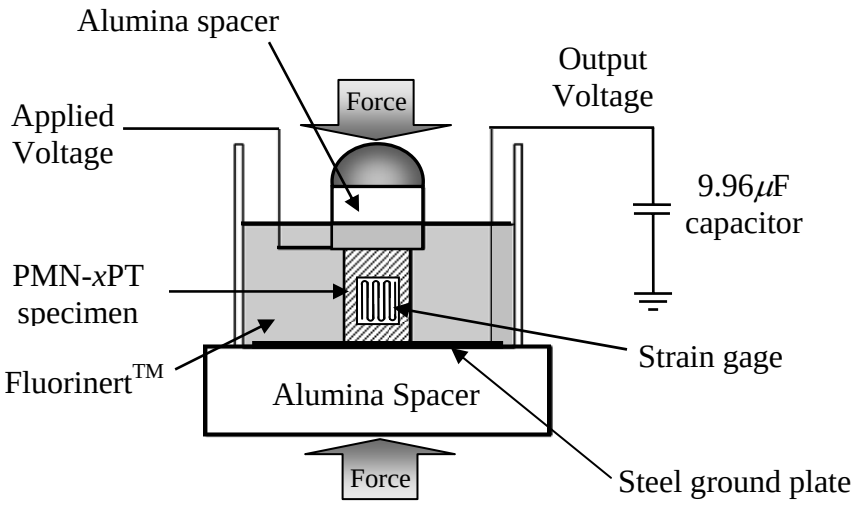

Figure 3-3. Schematic of testing arrangement.

3.2.4 Data Measurement Methodology

The analog output signal of each instrument was recorded using an analog to digital data acquisition system.

Strain: Strain gages were attached to all specimens. Strain for polycrystalline specimens was measured both longitudinal (X_3) and transverse (X_1, X_2) to the direction of the polarization. Two longitudinal/transverse 90 degree strain gage rosettes were attached to opposing faces of the specimen, while on the other two faces strain gages measuring only the longitudinal strain were attached. Figure 3-4a illustrates the strain gage orientation used on each polycrystalline specimen. Due to their smaller size, single crystal specimens were only instrumented with two longitudinal strain gages on opposing faces. Figure 3-4b shows the strain gage placement on the single crystal specimens. The Micro-Measurements 2110A strain gage signal conditioner output was recorded. The strain measurements were averaged to obtain an average material response.

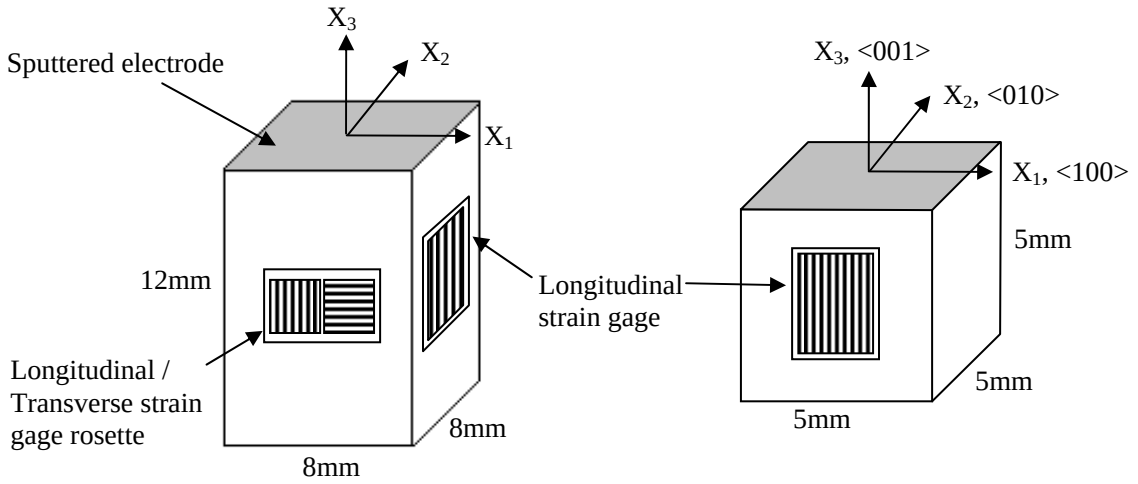

Figure 3-4. Specimen showing the strain gage configuration for (a) the polycrystalline specimens and (b) the single crystal specimens.

Electric field: A triangular wave at 0.02 Hz was applied to the top electrode with the bottom electrode connected to ground. This frequency can be considered quasi-static. A Wavetek 10 MHz DDS Model 29 function generator was used to create the reference

signal that was amplified 2000 times by a TREK Model 20/20A amplifier. The monitor voltage from the amplifier was recorded.

Load: Load was applied using a DDL screw-type load frame with a 4.45 kN load cell. Rubber blocks were placed under the testing fixture in the load path to create sufficient compliance for a constant load condition. The rubber did not affect the specimen response, or the measured load.

Electric displacement: The electric displacement of the specimen was measured by monitoring the voltage across a 9.96μF capacitor in a Sawyer-Tower arrangement. The capacitor was connected from the bottom electrode of the specimen to ground. The voltage was measured using a high input impedance Keithley 6512 electrometer. The analog output signal of the electrometer was recorded.

3.3 Experimental Results

3.3.1 Bipolar PMN-0.26PT Single Crystal

Figure 3-5 shows the two-dimensional plots of the longitudinal strain (Figure 3-5a) and electric displacement (Figure 3-5b) response under room temperature (20^{o}C) bipolar electric field loading at various stress levels (-0.4, -16, -32, -48, -64 MPa). Figure 3-5a displays the longitudinal strain in response to electric field. The dotted line illustrates the reduction in coercive field associated with applied stress.

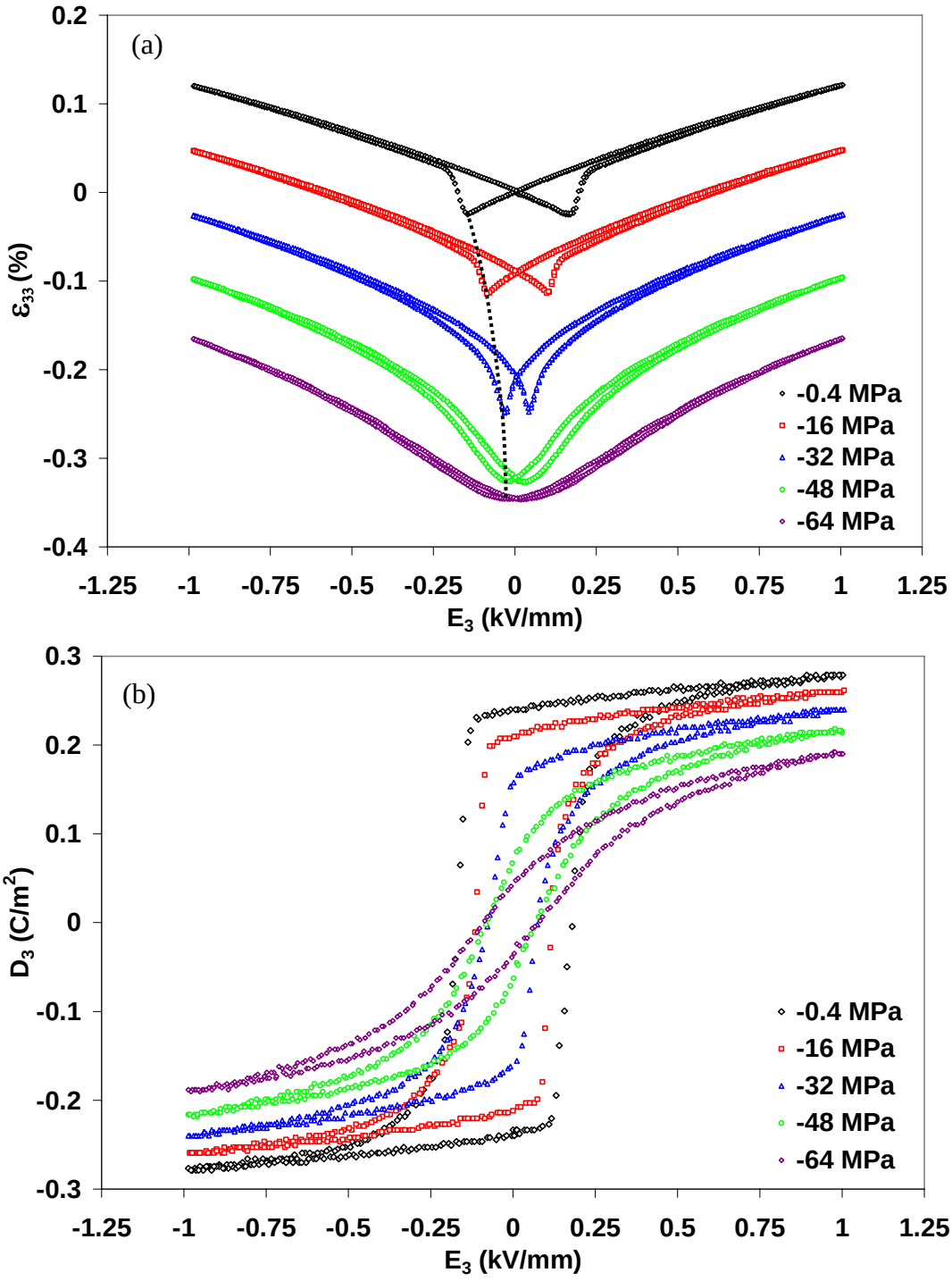

Figure 3-5. (a) Longitudinal strain (ε_{33}) and (b) electric displacement (D_3) measured during combined mechanical and electrical loading of single crystal $\langle 001 \rangle$ PMN-0.26PT. A dotted line is shown (a) which connects the coercive field value for each stress bias level. Experimental characterizations were done at 0.02Hz.

3.3.2 Unipolar PMN-0.26PT Single Crystal Experimental Results

Figure 3-6 shows the two-dimensional plots of unipolar electrical and mechanical loading. Figure 3-6a shows the electric displacement plotted against the applied unipolar electric field. Figure 3-6b shows the longitudinal strain response to applied electric field at constant compressive stress levels. Figure 3-6c displays the electric displacement change during compressive stress loading at constant electric field bias levels. Figure 3-6d illustrates the longitudinal strain during application of unipolar stress at constant electric field levels.

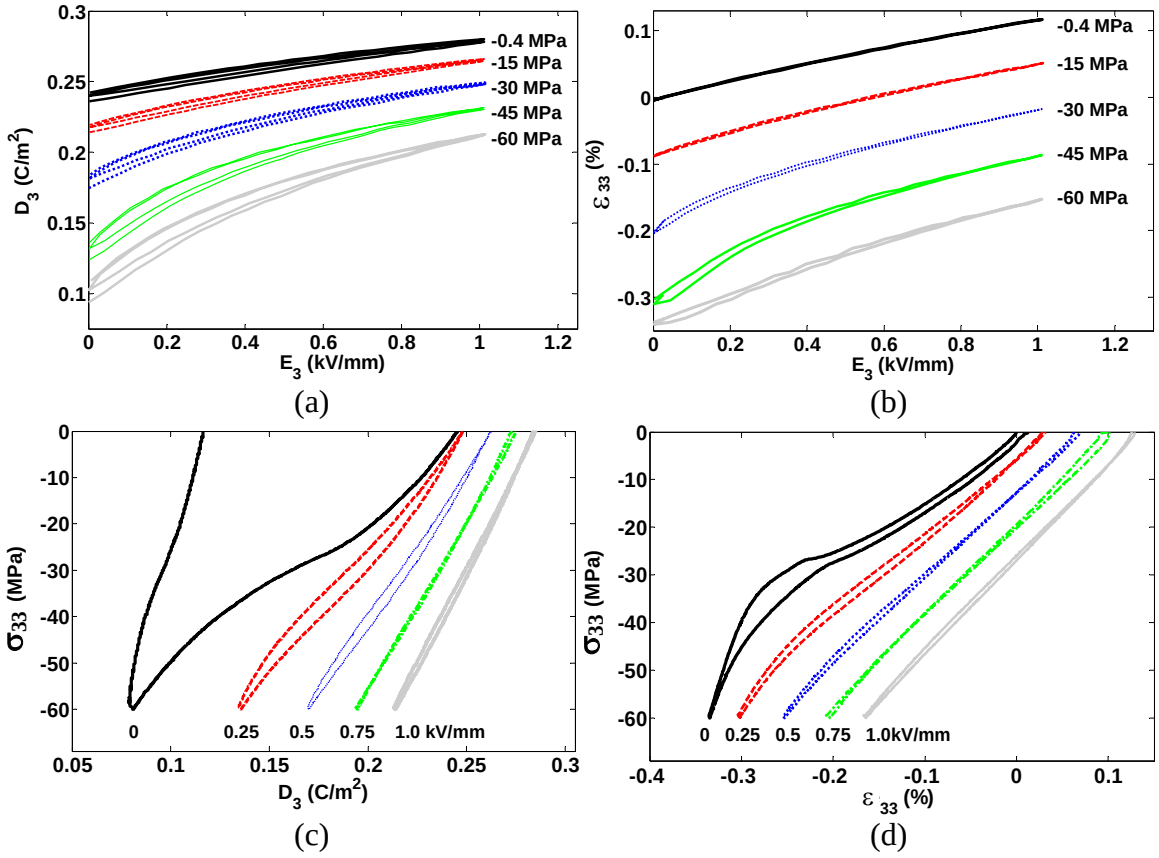

Figure 3-6. Two-dimensional plots of mechanical and electrical unipolar loading at 20°C of single crystal $\langle 001 \rangle$ PMN-0.26PT. (a) Electric displacement versus applied electric field at constant stress levels, D_3-E_3; (b) longitudinal strain versus electric field at constant stress levels, ε_{33}-E_3; (c) electric displacement versus stress at constant electric field bias levels, D_3-σ_{33}; and (d) longitudinal strain versus stress at constant electric field bias levels, ε_{33}-σ_{33}. Electric field loading was done with a frequency of 0.02Hz and stress cycling was carried out with a frequency of 0.01Hz, both considered quasi-static. Two cycles were used during unipolar electric field stress cycling utilized one cycle.

The non-linearity can be visualized well using a three-dimensional plot. Figure 3-7 shows the three-dimensional plots produced from the unipolar loading data. Figure 3-8 shows the comparison of the unipolar loading data to the bipolar loading data.

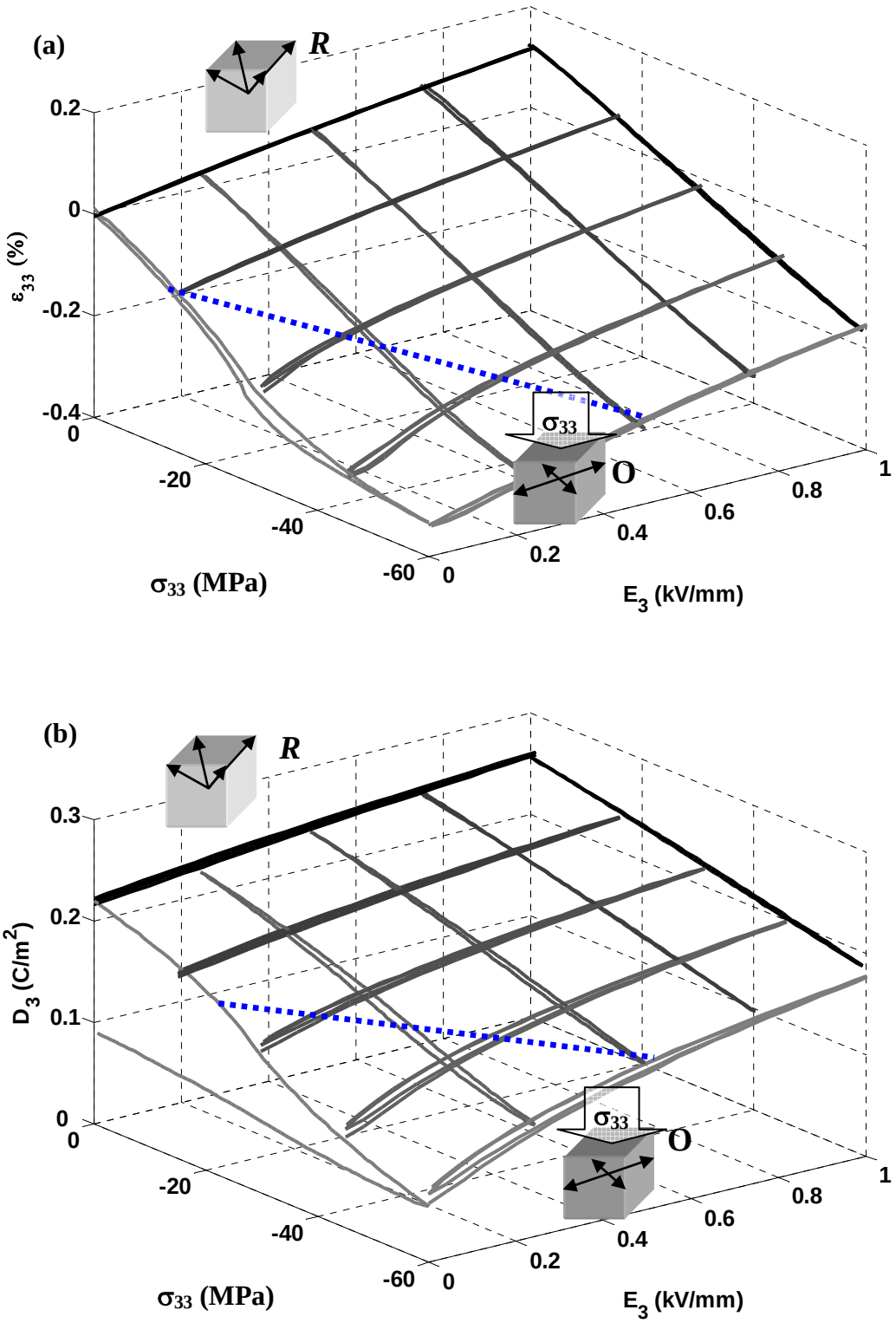

Figure 3-7. Three-dimensional phase transformation map of (a) strain as a function of stress and electric field, ε_{33}-E_3-σ_{33}; and (b) electric displacement as a function of stress and electric field, D_3-E_3-σ_{33}, for [001] poled PMN-0.26PT single crystal. Dotted lines represent the initiation of the phase transition which was determined by where the slope deviated from the linear modulus by 5% of the slope.

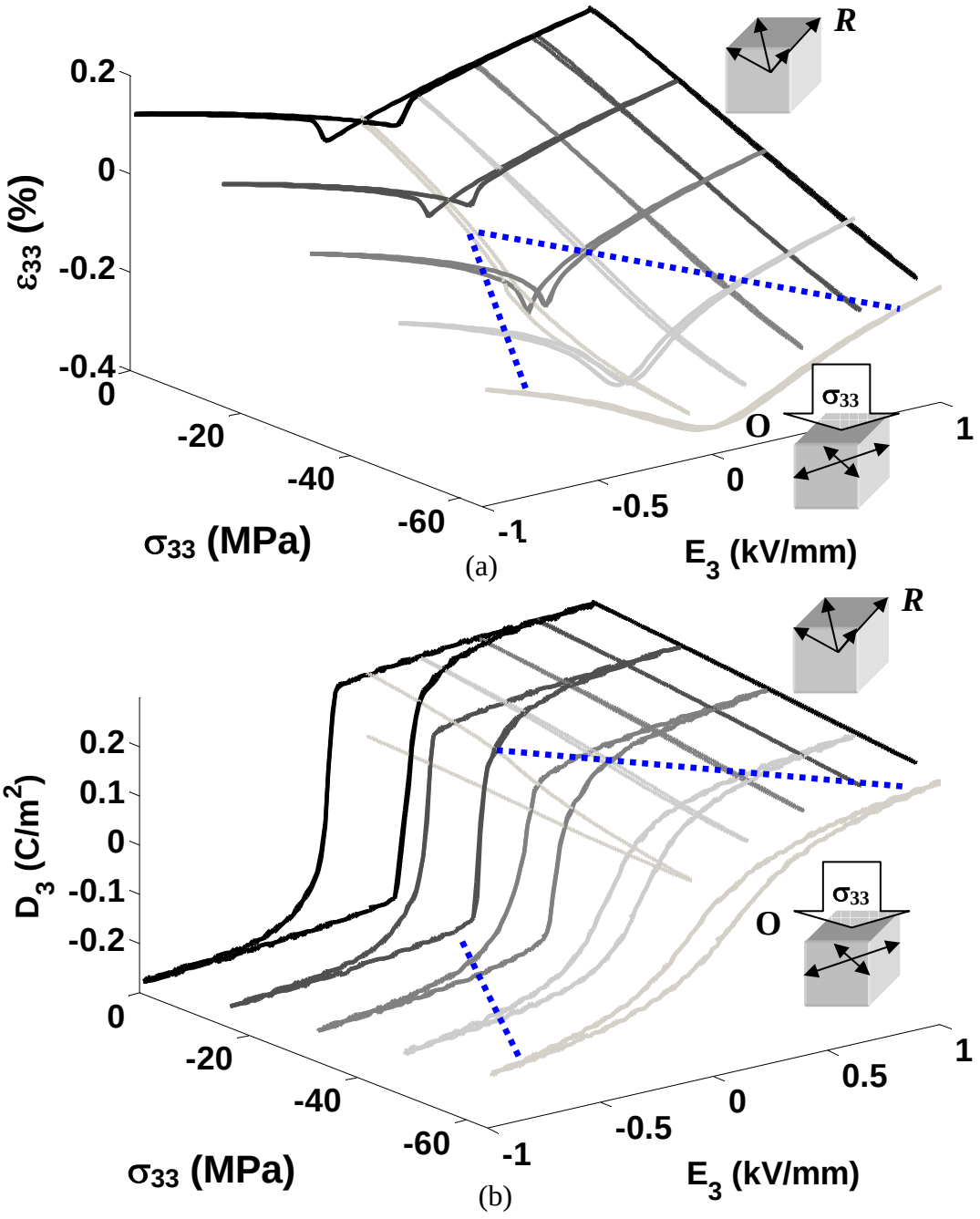

Figure 3-8. Comparison of the longitudinal strain (a) and electric displacement (b) measured during bipolar and unipolar application of external loads for [001] poled PMN-0.26PT single crystal. The dotted lines approximately represent the phase transformation initiation. Inset figure represents the rhombohedral phase with variants present.

3.3.3 Stress-Induced Polarization Reversal

Figure 3-9 shows the measured electric displacement during mechanical loading with a small bias field of 0.008 kV/mm applied to the specimen. The solid line represents the electric displacement when the electric field and polarization direction are initially in the same direction. The dotted line shows the electric displacement curve when the electric field is applied opposite to the initial polarization direction.

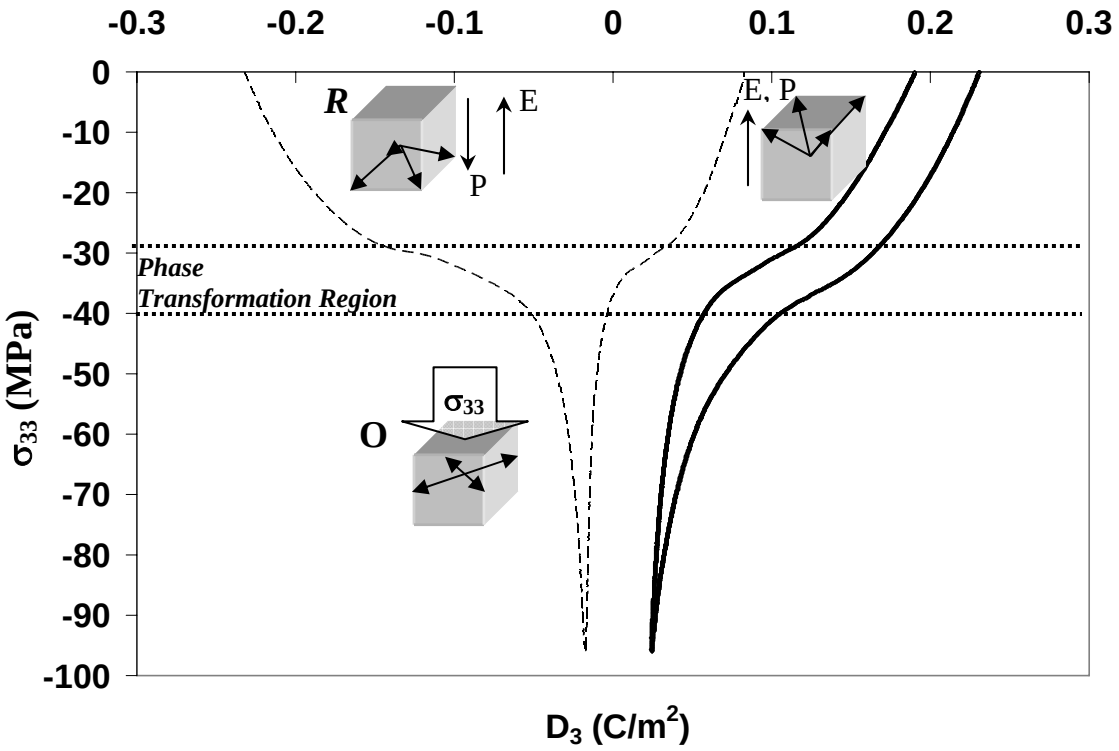

Figure 3-9. The stress induced depolarization in the presence of a small bias electric field of 0.008 kV/mm shows the effect of the quasi-static stress reducing the coercive field to near zero for [001] poled PMN-0.26PT single crystal.

3.3.4 Polycrystalline PMN-0.32PT

In the polycrystalline specimen setup, the strain response varied between the four gages during the stress induced polarization reorientation. This was not an alignment

issue. Specimens were removed, rotated and replaced and the loading repeated multiple times. Each time the same side always gave the same behavior. These specimens, when subjected to compressive stress depolarization, did not ferroelastically depole uniformly. The ferroelastic behavior consistently started at one side and moved across the specimen. The results presented are the average of the four strain gages.

The following figures are the experimental results of mechanical and electrical loading of polycrystalline specimens of PMN-0.32PT composition. Multiple specimens were tested and the results shown here are representative of all the specimens tested. For clarity the electric displacement and strain data are shown separately for each prestress level.

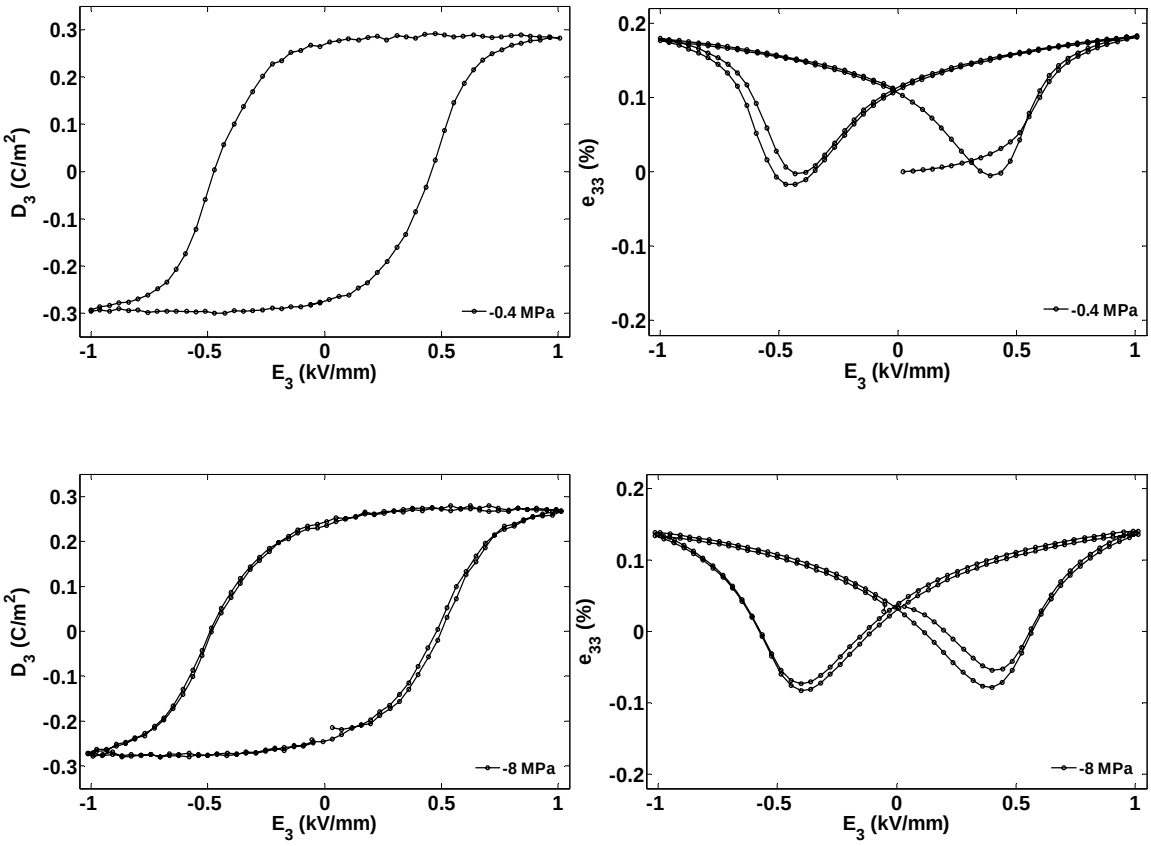

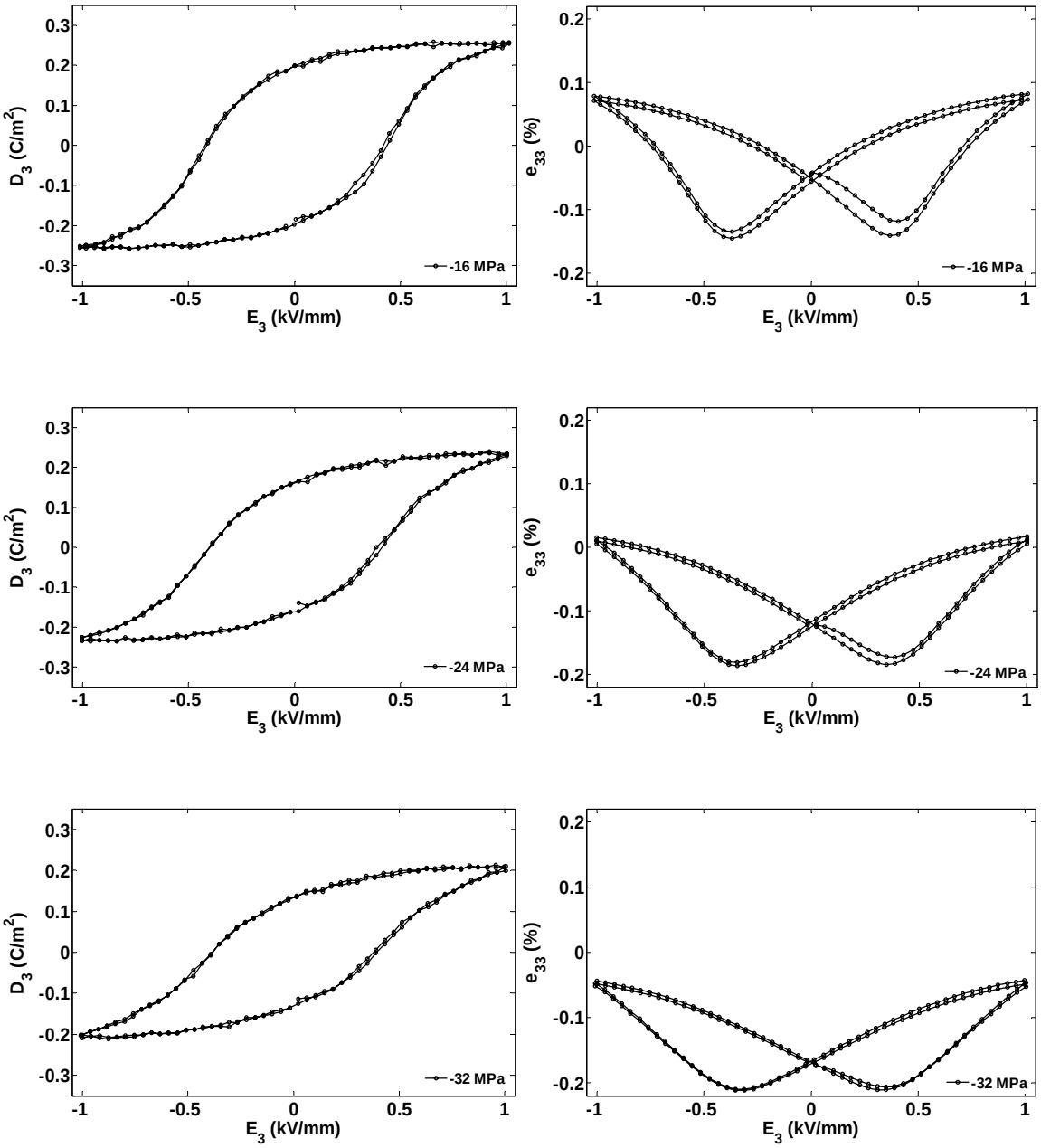

Figure 3-10. Longitudinal strain and electric displacement versus electric field at various preload stress levels for polycrystalline PMN-0.32PT at a frequency of 0.02Hz.

3.4 Discussion

The non-linearity observed in Figures 3-5, 3-6 and 3-7 for the PMN-0.26PT single crystal, is indicative of a phase transformation driven by the applied compressive stress in

the $\langle 001 \rangle$ direction and domain wall motion caused by electric field loading. Before load was applied to the single crystal it was in the rhombohedral phase near the morphotropic phase boundary. There are four possible variants when a single crystal material in the rhombohedral phase is poled in the $\langle 001 \rangle$ orientation. In the unstressed four variant state the polarized crystal displayed a linear response to the applied electric field. As mechanical stress was increased a phase transitioned from rhombohedral with $\langle 111 \rangle$ spontaneous polarization to what is most likely orthorhombic with spontaneous polarization in the $\langle 110 \rangle$ orientation took place. Due to the limited hysteresis and the continuous nonlinear change in elastic, dielectric and piezoelectric crystal properties observed during the phase transformation, it appears that there was either a continuous rotation of the polarization through an intermediate monoclinic phase or a continuous evolution of the volume fraction of the orthorhombic phase as applied stress was increased. Upon unloading of the mechanical stress the crystal structure transforms back into the rhombohedral phase. A schematic of this is shown in Figure 3-11.

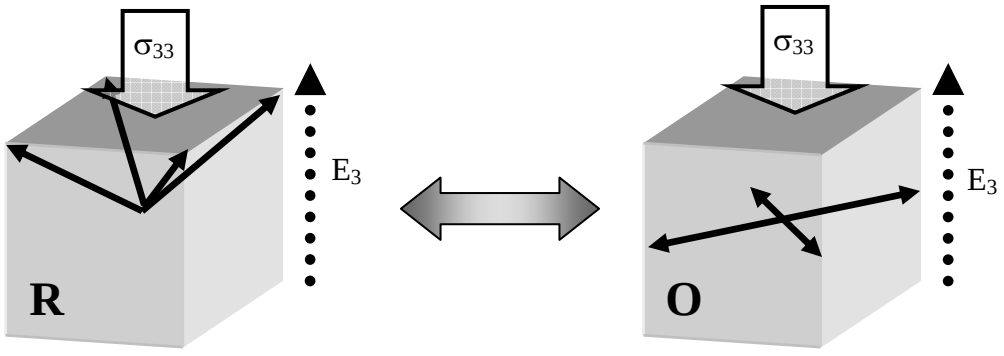

Figure 3-11. Phase transformations between the rhombohedral and orthorhombic phases induced by stress [45].

Mechanical load in the $\langle 001 \rangle$ crystallographic orientation is depolarizing the single crystal. A single crystal with $\langle 001 \rangle$ orientation in the orthorhombic phase which has four possible variants perpendicular to the applied mechanical load is fully depolarized and has an effective d_{333} piezoelectric coefficient of zero. This behavior is seen the Figures 3-5a and 3-6b. At the largest stress levels there is no strain response to small electric fields. As the electric field increased the spontaneous polarization began to rotate through the monoclinic phases towards the rhombohedral phase resulting in the observed quadratic electrostrictive behavior seen in the bottom curve of Figure 3-5b.

The coercive field is the magnitude of the reverse electric field required to reorient the remnant polarization of a ferroelectric material and has been identified in Figure 3-5a and Figure 3-10a as the location where the butterfly loops are at the lowest value. When the electric field that opposes the polarization has been increased to the point where local resistance to polarization switching is overcome, the longitudinal strain begins to increase. Application of a mechanical load decreases the coercive field by reducing the energy barrier to polarization reversal. The reduction of coercive field values due to mechanical loading is shown by the dotted line in Figure 3-5a and 3-10a. Both the polycrystalline and single crystal specimens show a decreasing coercive field, although the effect in the single crystal is more pronounced. The polycrystalline specimens initially had a larger coercive field than that of the single crystal specimens. This may be due to a number of factors including grain size effects, orientation effects, intergranular interactions and the effects of inhomogeneities such as porosity and inclusions. The crystallite size in a polycrystalline ferroelectric material can greatly influence the dielectric properties by “locking in” their polarization direction, thus

increasing the coercive field value over an unconstrained single crystal [6]. Figure 3-12 shows the measured coercive field values for the single crystal and polycrystalline specimens during bipolar electric field loading at constant stress bias levels.

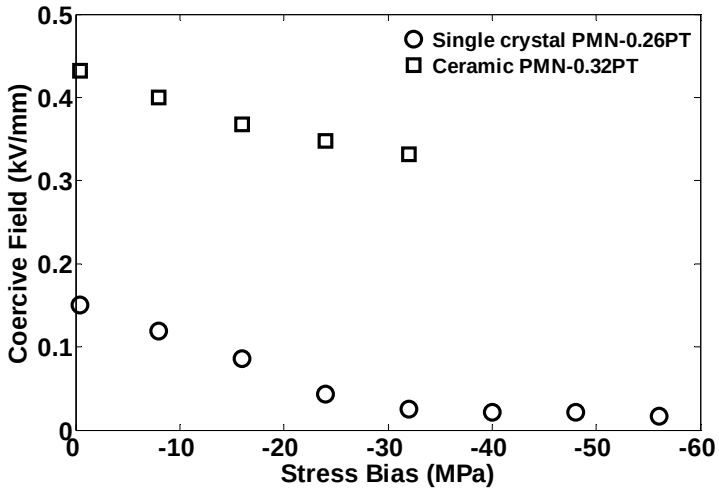

Figure 3-12. Measured coercive field values for $\langle 001 \rangle$ single crystal PMN-0.26PT and un-textured polycrystalline PMN-0.32PT during bipolar electric field loading at different levels of constant stress bias.

Comparison of Figures 3-5 and 3-10 show that during bipolar loading there was more hysteresis in the polycrystalline material than the single crystal. Experience with PZN-0.045PT single crystals [48, 49] has shown that when the electric field direction is rotated from $\langle 001 \rangle$ toward $\langle 011 \rangle$ the strain-electric field hysteresis loops change shape. If the behavior in the PMN-0.26PT is analogous, the orientation effect may play a significant role in causing the differences between the single crystal and polycrystalline specimens. There may also be differences due to intergranular interactions and inhomogeneities in the polycrystal that are not present in single crystals. A single crystal

does not have grains, or grain boundaries, that can act as a barrier to switching. This may allow the single crystal to more readily reorient to the electric field direction.

At very low stress it can be seen in Figures 3-5a and 3-5b that the single crystal specimen had a linear strain and electric displacement response to the applied electric field. It can be seen in Figure 3-9a and 3-9b that during preload the initial response to an applied electric field was nonlinear.

Evidence of a phase transformation can be seen in the three-dimensional plots, Figure 3-7. The $\langle 001 \rangle$ oriented single crystal can be driven to a different phase through the application of a compressive stress along the $\langle 001 \rangle$ direction, and can be subsequently pulled back from that phase to the rhombohedral phase through an electric field in the $\langle 001 \rangle$ direction. This illustrates that the applied stress and electric field act as competing driving forces. This behavior is seen in Figure 3-7 by the dotted line which approximately represents the dividing line between the rhombohedral phase and the phase transition region. This same general behavior was seen in earlier experimental characterization of PMN-0.32PT single crystals [68]. In that study $\langle 001 \rangle$ oriented single crystal specimens were subjected to combined unipolar electromechanical loading at various temperatures with the resulting strain and electric displacement measured. PMN-0.32PT is closer to the MPB than PMN-0.26PT [47]. The PMN-0.32PT and PMN-0.26PT show similar material behavior, however, there are important differences that show the compositional dependence of constitutive behavior. The piezoelectric coefficient of PMN-0.32PT was reported as 2100 *pC/N* which is approximately 42% larger than that measured in the PMN-0.26PT material. In addition, it is also apparent that lowering the amount of PT increases the stress at which a phase transformation

initiates while simultaneously increasing the material stiffness. PMN-0.26PT shows the beginning of a phase transition region when no electric field was applied at approximately -34 MPa, while PMN-0.32PT began at approximately -20 MPa. The trend is that as the composition is moved away from the MPB, on the rhombohedral side, the stiffness increases, the piezoelectric coefficient decreases, the dielectric constant decreases and the energy barrier to the phase transformation increases. It is also interesting to note that in Figure 3-7 the effects of stress on crystal depolarization can be seen. During unipolar electric field loading it can be seen that the specimen repoles some of the stress depoled regions. This has the effect of increasing the remnant strain and electric displacement value at that stress preload.

Figure 3-8 shows the comparison of the measured data during bipolar and unipolar loadings. It can be seen in this three-dimensional plot that the data corresponds well. Similarly to Figure 3-7 it can be seen that the remnant strain and electric displacement values at the various stress bias levels are higher than that measured in the unipolar stress loading at no electric field. This is likewise due to stress induced depolarization. The dotted line represents the approximate line separating the rhombohedral phase from the phase transformation region.

Figure 3-9 shows the stress induced depolarization of the single crystal material in the presence of an electric field well below the coercive field. During a unipolar stress cycle in the absence of an applied electric field it was shown that single crystal PMN-0.26PT was driven to the depolarized orthorhombic phase. Without a suitable externally applied driving force, such as a small bias electric field, the spontaneous polarization direction can reorient either in the $\langle 111 \rangle$ or $\langle 11\bar{1} \rangle$. This results in the strain returning to

the original preload value, while the electric displacement moves closer to zero. However, when the mechanical loading/unloading cycle is done in the presence of a small electric field, each unit cell has an externally applied driving force large enough to provide a preferred polarization direction.

From Figure 3-10 it is apparent that the polycrystalline specimen has undergone significant changes due to loading. It can be seen that the amount of hysteresis present during bipolar electric field loading decreased as the uniaxial stress was increased. This may be due to the local barriers to switching being overcome by the applied mechanical energy. The polycrystalline specimens initially had a nonlinear response to electric field. When the electric field reached a critical level the response became approximately linear. This is in contrast to the behavior of the single crystal.

To contrast the differences in the linear material properties of single crystal and polycrystalline specimens the measured elastic, piezoelectric and dielectric coefficients are presented in Table 3-1. The linear material coefficients were obtained by measuring the initial slope of the corresponding small field strain and electric displacement data associated with an increasing field. The single crystal piezoelectric and dielectric properties have been listed only for the rhombohedral phase.

Table 3-1. Elastic, piezoelectric, and dielectric material properties for single crystal PMN-0.26PT and polycrystalline PMN-0.32PT. All experimental data was collected at 0.02Hz.

Material Property	$\langle 001 \rangle$ Single Crystal PMN-0.26PT		Polycrystalline PMN-0.32PT
	R	O	
Compliance $S_{3333}^{E} \quad (10^{-12} m^2 / N)$	59.5	12.4	13.5
Piezoelectric $d_{333} \quad (pm/V)$	1475	--	1350
$d_{311} = d_{322} \quad (pm/V)$	--	--	550
Relative Permittivity $\kappa_{33}^{\sigma} / \varepsilon_0$ $\left(\varepsilon_0 = 8.854 \times 10^{-12} F / m\right)$	5500	--	8385

The single crystal behavior depends on various factors and nonlinear processes such as crystal orientation angle, crystal cut, temperature, phase transformation behavior and domain wall motion. The polycrystalline behavior is the result of a complex arrangement of these effects in addition to effects of intergranular interactions and dispersed inhomogeneities. This creates a complex network of nonlinear local effects which can influence overall material constitutive behavior.

3.5 Concluding Remarks

The strain and polarization of $\langle 001 \rangle$ single crystal PMN-0.26PT and polycrystalline PMN-0.32PT specimens have been characterized in response to combined large electric field and stress. Testing was done at room temperature. Single crystal specimens showed clear evidence of a stress induced phase transformation from the

rhombohedral phase to the depolarized orthorhombic phase. It was also shown that an electric field applied in an opposing direction to the stress was able to overcome the applied stress and return the specimen to the rhombohedral phase. Three-dimensional plots were created from the measured single crystal unipolar longitudinal strain and electric displacement response to applied loads. Polycrystalline specimens were characterized under bipolar electric fields at various stress levels.

These results are important for future modeling efforts. They illustrate the important differences between the observed single crystal and polycrystalline behavior.

CHAPTER 4

COMPOSITIONAL DEPENDENCE OF PHASE TRANSFORMATION AND CONSTITUTIVE BEHAVIOR IN ⟨001⟩ SINGLE CRYSTAL PMN-*x*PT

The constitutive behavior of two compositions of relaxor ⟨001⟩ oriented single crystal PMN-*x*PT (x = 0.27 and 0.29) was characterized at various temperatures in response to stress and electric field loading. The experimental results are presented as three-dimensional surface plots that show the effect of applied fields and are compared to those of other studies on different compositions of ⟨001⟩ PMN-*x*PT single crystals near the morphotropic phase boundary. The effects of composition on the phase transformation behavior and linear material properties are compared and discussed. This work is presently being prepared for submission to *Acta Materialia* and was the product of collaboration with Harold C. Robinson at NUWC Division Newport. Robinson supervised a technician and performed initial data reduction for the experimental measurements of the PMN-0.27PT and PMN-0.29PT single crystals. Webber handled the plotting, analysis and discussion of results.

4.1 Introduction

Single crystals of relaxor ferroelectric PMN-*x*PT in the rhombohedral phase display extraordinary piezoelectric properties. Ongoing work has focused on developing an understanding of the compositional dependence of these properties. The nonlinear piezoelectric and dielectric material properties are hysteretic, anisotropic and dependent

on the phase state as well as the crystallographic orientation relative to the loading direction. The reported phases that can occur in these crystals are: cubic (C), tetragonal (T), rhombohedral (R), orthorhombic (O) or an intermediary monoclinic (M_A, M_B, M_C) phase. Each phase possesses a different crystal symmetry and spontaneous polarization direction. The phase is determined by the material composition and applied fields such as temperature, electric field and stress. At temperatures above the Curie point the crystal is in the cubic phase. At room temperatures the phase is either rhombohedral for a composition of $x < 0.3$ or tetragonal $x > 0.35$ to 0.37 [47, 48]. These phase regions are separated by a morphotropic phase boundary. X-ray and neutron structural studies have shown a complex phase structure in the vicinity of the MPB. A number of researchers have shown experimental evidence of monoclinic phases (M_A, M_B and M_C) for various compositions of PMN-*x*PT and PZN-*x*PT specimens near the MPB [47, 50-53, 123, 126]. It has been proposed that the monoclinic phase is due to residual stresses caused by the coexistence of incompatible phases forcing one another to take on a monoclinic phase [127].

The application of stress, electric field and temperature can produce phase transformations that significantly change the material behavior. There have been numerous investigations into the effects of electric field [29, 45, 60, 68, 122, 128], uniaxial stress [45, 60, 68, 129, 130] and temperature [106, 131, 132] on polarization reorientation and phase transformations in PMN-*x*PT and PZN-*x*PT single crystals. Recent research has presented results of the experimental characterization of PMN-*x*PT single crystal constitutive behavior comparing material response at different orientation angles [29, 45, 66-68, 133, 134]. Park *et al.* measured the electromechanical behavior of

PMN-*x*PT and PZN-*x*PT relaxor ferroelectrics as a function of composition and orientation angle [29]. This seminal work helped to identify preferred crystal compositions and crystal cuts to maximize behavior, or reduce hysteresis. Webber *et al.* measured the bipolar electromechanical response of $\langle 001 \rangle$ PMN-0.32PT single crystal specimens [60]. Wan *et al.* measured the polarization and strain response of $\langle 001 \rangle$, $\langle 011 \rangle$ and $\langle 111 \rangle$ oriented PMN-0.32PT single crystals to bipolar electric field at constant stress preloads [134]. Feng *et al.* measured the unipolar electric field induced strain response of $\langle 001 \rangle$, $\langle 011 \rangle$ and $\langle 111 \rangle$ oriented PMN-*x*PT single crystals of varying compositions [133]. This study provided experimental evidence of an optimal compositional range for high strain response and low hysteresis in $\langle 001 \rangle$ oriented PMN-*x*PT single crystals, however, the effects of compressive stress and electric field on the initiation of phase transitions and linear material properties were not considered. A recent study has shown that there exist a linear relationship between the relative dielectric constant and the d_{33} piezoelectric coefficient for five different compositions (x = 0.045, 0.06, 0.07, 0.08 and 0.09) of single crystal PZN-*x*PT [135]. In this work it was theorized that polarization rotation occurs more easily in materials with higher piezoelectric and dielectric material properties. It is reasonable to speculate that a similar statement can be said for phase transformation behavior.

The present study addresses the macroscopic behavior of $\langle 001 \rangle$ oriented PMN-0.27PT and PMN-0.29PT single crystal specimens measured in response to simultaneously applied mechanical and electrical loads at various temperatures. A comparison to previous experimental measurements for $\langle 001 \rangle$ PMN-*x*PT single crystal

specimens with different compositions is presented and the compositional dependence of phase transformations and material properties are discussed.

4.2 Experimental methodology

4.2.1 Specimen preparation

Single crystal specimens were manufactured and prepared by TRS Technologies, Inc. Each specimen was cut from a single crystal boule of PMN-*x*PT material in such a way that the $\langle 001 \rangle$ crystallographic directions were oriented perpendicular to each face. The final dimensions of the specimens were 4 x 4 x 12mm, providing a 3:1 aspect ratio. Cr/Au electrodes were sputtered onto the 4 x 4mm faces and each specimen was poled along the 12mm axis. Prior to testing, each specimen was cleansed in an ultrasonic cleaner with ethanol for 15 minutes.

4.2.2 Experimental arrangement

Experimental measurements were performed at NUWC Division Newport using the stress dependent electromechanical characterization system (SDECS). This system is capable of simultaneously applying controlled thermal, electrical and mechanical loads while measuring the material response of strain and electric displacement [45]. Electric field cycling was done at 10Hz and stress cycling was done at 0.07Hz. For clarity error bars were omitted from the following figures. All experimental data is subject to 5% error.

Specimens were aligned in the $\langle 001 \rangle$ orientation and antagonistically loaded in the 33-mode. Antagonistically loaded is a term used to describe the case where the electric field is driving an elongation in the $\langle 001 \rangle$ direction and the uniaxial stress is driving a contraction in the same direction. Figure 4-1 illustrates a representative unit cell which qualitatively shows the possible spontaneous polarization directions, or variants, during stress and electric field loading. In the unloaded $\langle 001 \rangle$ poled state the rhombohedral phase has four possible variants. The application of external fields of sufficient magnitude can cause a phase transition. A compressive stress in the $\langle 001 \rangle$ crystallographic direction causes an $R \rightarrow O$ phase change through the monoclinic phase, M_B [44]. An electric field causes an $R \rightarrow T$ phase transformation through the M_A monoclinic phase [44].

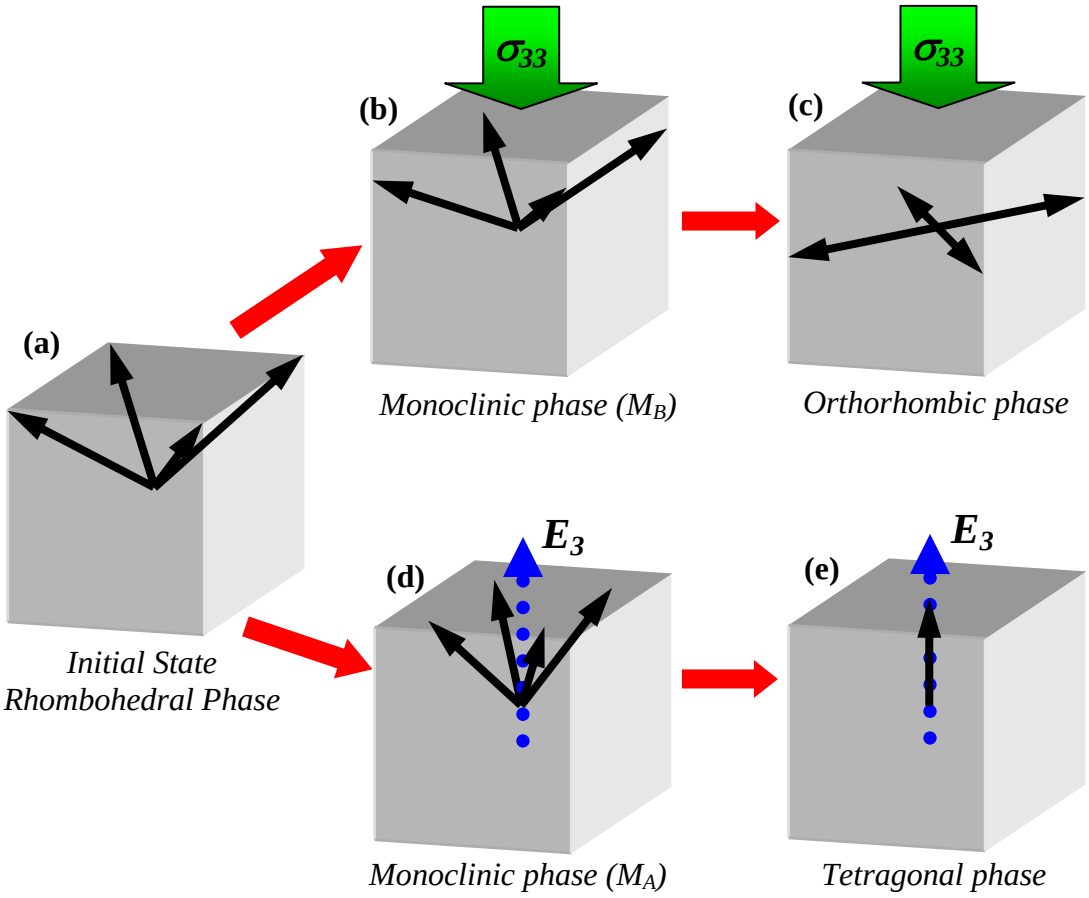

Figure 4-1. Possible spontaneous polarization directions under various loading conditions. (a) The unloaded PMN-*x*PT unit cell is in a rhombohedral phase state with spontaneous polarization directions in the ⟨111⟩ orientation. Increased stress can potentially transform the specimen from an initially rhombohedral phase through a monoclinic phase (b) to an orthorhombic phase (c) with spontaneous polarization oriented in the ⟨011⟩ crystallographic direction. Electric field applied to the rhombohedral unit cell can cause a phase transformation through a monoclinic phase (d) to a tetragonal phase that has spontaneous polarization directions in the ⟨001⟩ directions.

Electric field was applied through the sputtered electrodes on the 4 x 4mm faces. Mechanical load was applied parallel to the electric field along the ⟨001⟩ direction. During testing a minimum compressive load of -2 MPa was used to maintain constant electrical contact. Unidirectional longitudinal strain gages were attached at the center of

two of the opposing non-electroded 4 x 12mm faces. The clamping effects at the ends of the specimen were minimized by the location of the strain gages and the 3:1 aspect ratio. Strain measurements were obtained with a Wheatstone bridge and recorded. The electric displacement was measured using modified Sawyer–Tower circuitry. A low pass filter was utilized on the electric field, electric displacement, strain and mechanical load signals that were recorded by the SDECS's dynamic signal analyzer.

The loading consisted of: (1) a 10Hz cyclic unipolar electric field at constant stress preloads; and (2) 0.07Hz unipolar cyclic stress at constant electric field preloads. Loading was repeated in a range of temperatures. Electric field was applied using a high voltage power amplifier. The voltage was recorded with a high voltage probe. Mechanical load was applied through a pneumatic cylinder with load monitored with a load cell and recorded. During testing the specimen was submerged in a bath of Fluorinert to electrically isolate the applied high voltage. An environmental chamber was used to control the temperature.

4.3 Results

4.3.1 Initial Data Analysis

During experimentation the remnant polarization and remnant strain values were reset to zero between each loading cycle by the SDECS system. This is an unchangeable feature of this measurement system. Experimental data was analyzed in a post-processing program which restored the remnant values by applying the corresponding measured value in both electric field and stress cycling. Previous experimental investigations have determined the remanent polarization values for PMN-0.26PT [60]

and PMN-0.32PT [68] single crystals to be 0.24 and 0.20, respectively. It was assumed that the remanent polarization values varied linearly. The remanent polarization for PMN-0.27PT and PMN-0.29PT at no load were found to be 0.23 C/m^2 and 0.22 C/m^2, respectively. These values were used as the base values from which all other remnant polarization values were referenced. The post-processing program reset remnant values for each unipolar electric field cycle at a constant stress preload by measuring the corresponding polarization and strain from the unipolar stress loading with no applied electric field bias. The opposite process was used to reset the remnant polarization and strain of the unipolar stress experiments. All experimental measurements are subject to a 5% error; for clarity error bars are omitted in each figure.

4.3.2 PMN-0.27PT Experimental Measurements

Figure 4-2 shows two-dimensional plots of the data collected at 40°C. Longitudinal strain (ε_{33}) and electric displacement (D_3) were measured in the x_3 direction in response to stress and electric field; both applied along the x_3 axis. Figures 4-2a and 4-2b show the measured electric displacement and strain during 10Hz unipolar electric field loading at constant stress preloads. The stress preloads used for this study were 0, -13.8 and -27.6 MPa (Labeled as F, G and H, respectively, in Figure 4-2a and 4-2b). Figure 4-2c and 2d show the electric displacement and strain for 0.07Hz unipolar compressive stress loading at constant electric field levels of 0, 0.5, 1, 1.5 and 1.67 kV/mm (Labeled as A, B, C, D and E, respectively, in Figure 4-2c and 4-2d). Figure 4-2c also shows the effects of nonlinear electrical leakage.

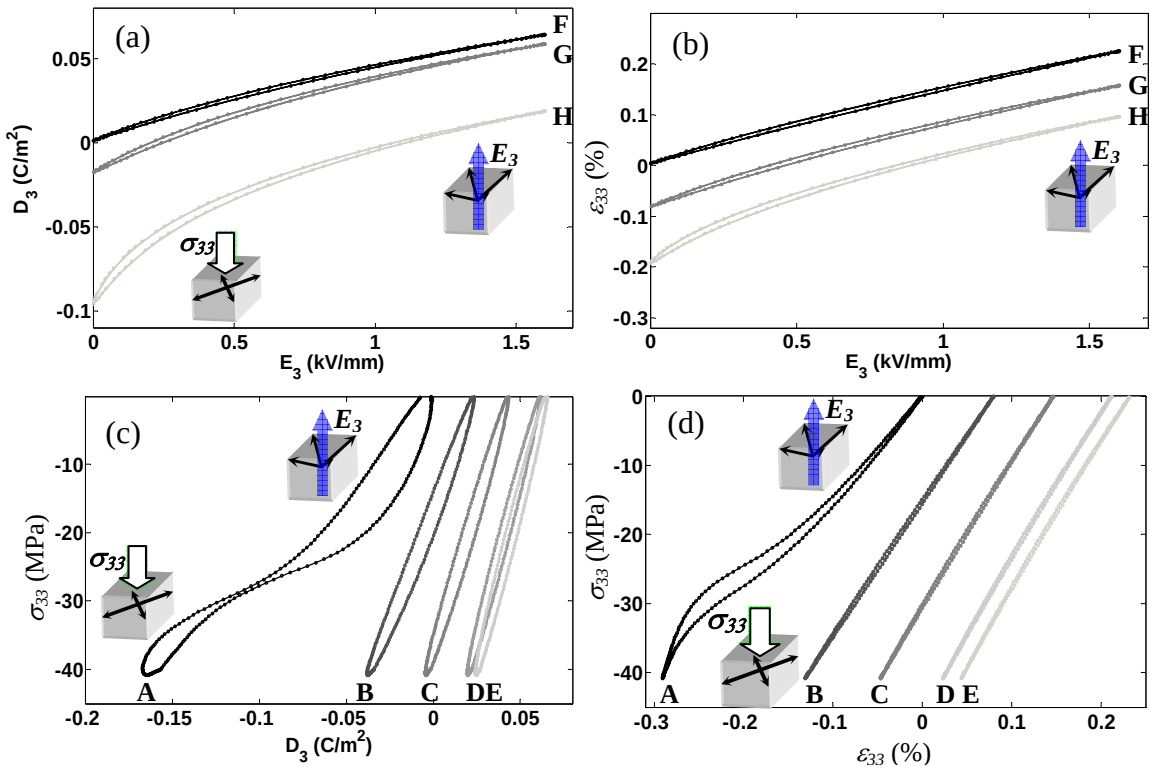

Figure 4-2. Two-dimensional plots of the measured strain and electric displacement versus the applied electric field and stress for single crystal ⟨001⟩ PMN-0.27PT specimens tested at 40°C; (a) $D_3 - E_3$ at various stress preloads; (b) $\varepsilon_{33} - E_3$ at various stress preloads; (c) $D_3 - \sigma_{33}$ at different electric field preloads; and (d) $\varepsilon_{33} - \sigma_{33}$ at different electric field preloads. The stress preloads of 0, -13.8 and -27.6 MPa are labeled as F, G and H, respectively. The constant electric field bias levels of 0, 0.5, 1, 1.5 and 1.67 kV/mm are labeled as A, B, C, D and E, respectively.

The electromechanical responses from Figure 4-2 can be combined into a single three-dimensional surface plot that succinctly illustrates the phase transformation behavior under applied fields. Figure 4-3 shows the longitudinal strain (ε_{33}) and the polarization (D_3) constitutive behavior surface plots under applied stress and electric field for three different ambient temperatures (T = 5, 20, 40°C).

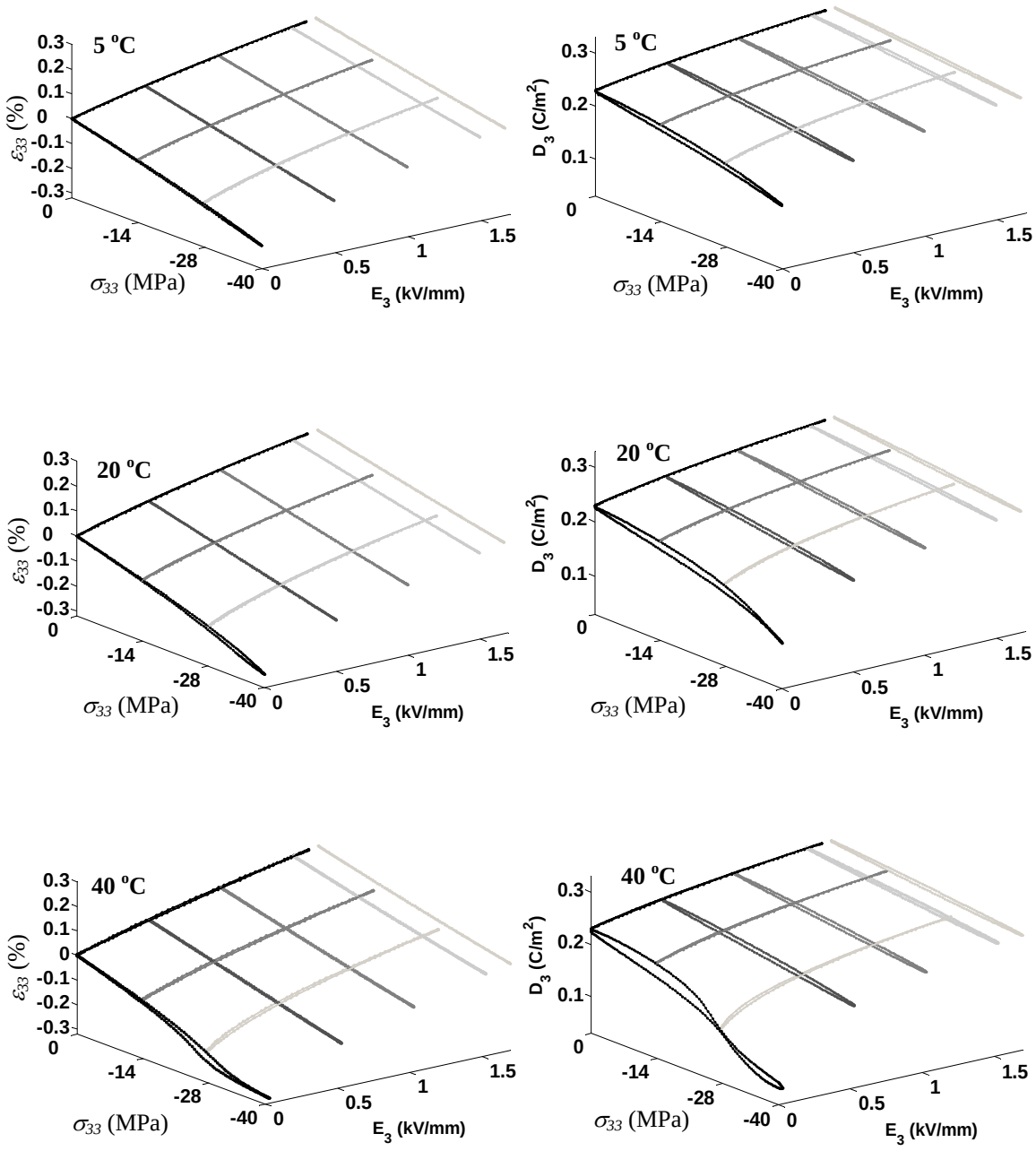

Figure 4-3. Measured longitudinal strain (ε_{33}) and electric displacement (D_3) under combined quasi-static mechanical, electrical and thermal loading of single crystal $\langle 001 \rangle$ PMN-0.27PT.

4.3.3 PMN-0.29PT Experimental Measurements

Measured electromechanical behavior was combined into three-dimensional surface plots for PMN-0.29PT. Figure 4-4 shows the longitudinal strain (ε_{33}) and the polarization (D_3) constitutive behavior surface plots under applied stress and electric field at four different ambient temperatures (T = 5, 20, 40, 60^{o}C). The stress preloads used during 10Hz unipolar electric field cycling from 0 to 1.5kV/mm were 0, -13.8, and -27.6 MPa. The electric field preloads utilized during 0.07Hz unipolar compressive stress loading from -2 to 25 MPa were 0, 0.25, 0.5, 0.75, 1, 1.25, 1.5 kV/mm.

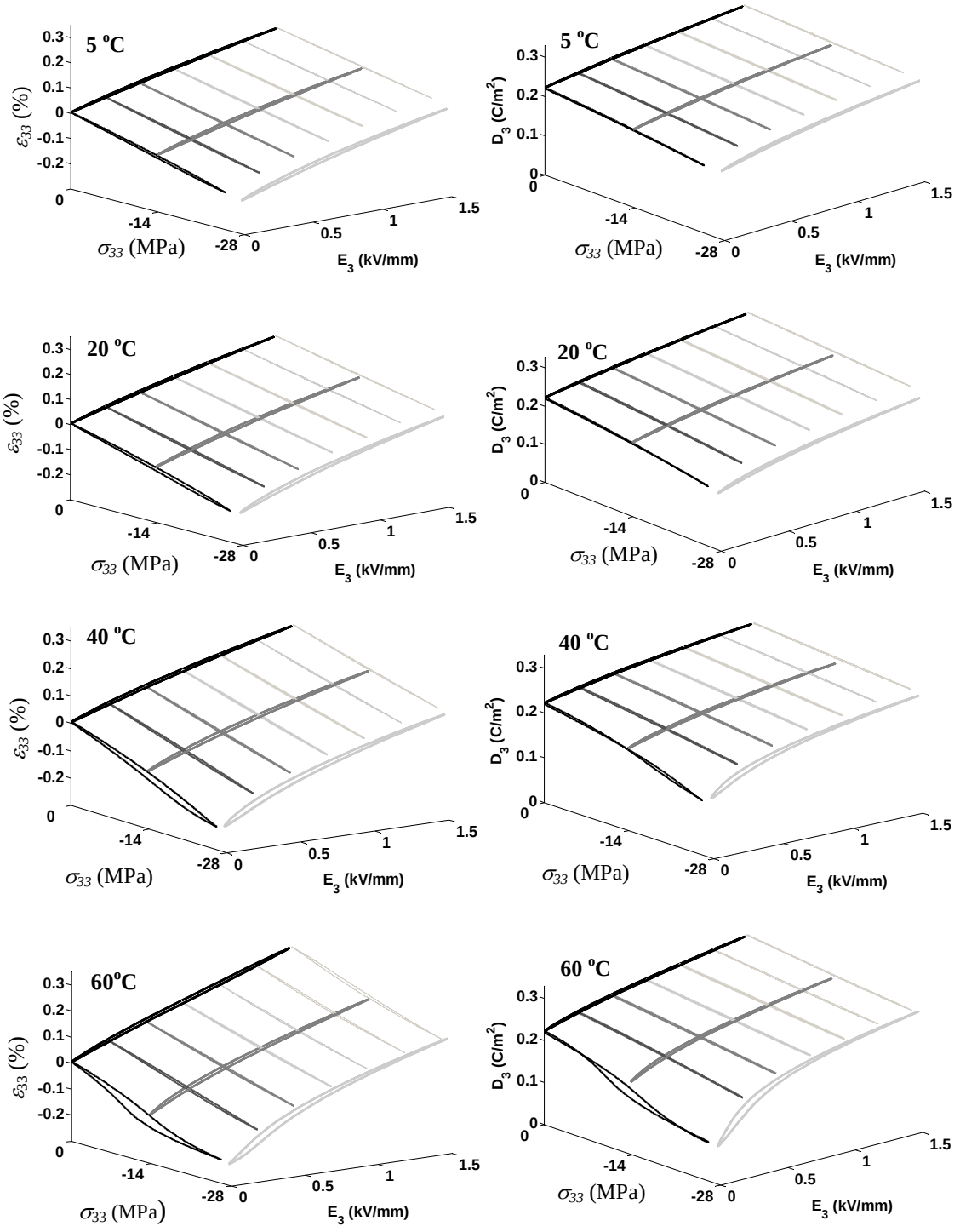

Figure 4-4. Surface plots of the longitudinal strain (ε_{33}) and electric displacement (D_3) for $\langle 001 \rangle$ PMN-0.29PT single crystal under combined quasi-static mechanical, electrical and thermal loading. Note that the scale on the stress axis is different than that used for the $\langle 001 \rangle$ PMN-0.27PT experimental measurements.

4.4 Discussion

The following discussion of phase transformations is based on the crystal symmetry of the corresponding phase with respect to the applied loading direction. Figure 4-2 shows that increasing the $\langle 001 \rangle$ compressive stress increases the $\langle 001 \rangle$ electric field required to cause a phase transformation in an antagonistic loading scheme. This was found to be the same for both compositions. Prior to testing, the poled specimens were in a four domain state in the rhombohedral phase. An applied electric field in the $\langle 001 \rangle$ crystallographic direction drives a transformation to the tetragonal phase, while a compressive stress in the $\langle 001 \rangle$ orientation causes a transition to the orthorhombic phase. These two competing fields counteract the effects of one another. This is the reason that a nearly complete $R \rightarrow O$ phase transformation did not occur in PMN-0.27PT until the temperature was increased to 40^{o}C. PMN-0.29PT specimen showed a nearly complete $R \rightarrow O$ phase transformation at 60^{o}C. Because the PMN-0.27PT specimen was tested to a higher stress a phase transformation occurred at a lower ambient temperature than in the PMN-0.29PT specimen. An increase of temperature reduces the energy barrier for phase transformation required to be overcome by applied electrical or mechanical loads. Even at the highest temperature tested for each specimen it appears from the curve that there was an incomplete phase change to the orthorhombic phase during unipolar stress cycling at zero electric field. With the addition of an electric field, the applied stress is no longer large enough to cause a phase change. In these experiments there was insufficient electric field applied to provide the work necessary to overcome the energy barrier and drive an $R \rightarrow T$ phase transformation.

The surface plots in Figures 4-3 and 4-4 demonstrate the effects of temperature on the initiation of a phase transformation. As the temperature of the specimen is increased the material response begins to progressively become more nonlinear. This indicates that increasing specimen temperature causes phase transformations to occur at lower levels of applied electric field and stress. It can also be seen that the R phase state is stable and occurs at lower field levels while the O phase appears only at increased $\langle 001 \rangle$ compressive stress levels. It has been shown experimentally that a $R \rightarrow O$ phase transition can also be driven by electric field applied in the $\langle 011 \rangle$ direction [45].

Components of the compliance, piezoelectric and dielectric property tensors at low fields were measured from the experimental data and are listed in Table 4-1. This table only contains compliance, piezoelectric and dielectric coefficients for the R phase; a complete phase transformation to the O phase did not occur during testing.

Table 4-1. Measured material properties of rhombohedral $\langle 001 \rangle$ oriented PMN-0.27PT and PMN-0.29PT single crystals. Linear compliance coefficient was measured at 0.07Hz. The linear piezoelectric and dielectric coefficients were measured at 10Hz.

Material Property	Temperature	PMN-0.27PT	PMN-0.29PT
Compliance S_{3333}^{E} $(10^{-12} m^2 / N)$	5°C	50.2	50.8
	20°C	53.1	52.1
	40°C	59.9	59.8
	60 °C	--	68.5
Piezoelectric d_{333} (pm/V)	5°C	1467	1614
	20°C	1635	1774
	40°C	1710	2212
	60 °C	--	2970
Relative Permittivity $\kappa_{33}^{\sigma} / \varepsilon_0$ $\left(\varepsilon_0 = 8.854 \times 10^{-12} F / m\right)$	5°C	5260	6100
	20°C	6124	6765
	40°C	6617	8690
	60 °C	--	12260

4.4.1 Compositional Dependence

The phase transformation behavior and material properties of relaxor PMN-*x*PT single crystal are dependent on composition and applied fields. Effects of phase transformations can be seen in the three-dimensional surface plots as the regions of rapidly changing slope. The $R \rightarrow O$ phase transformation is not a sudden jump-type switch in the PMN-*x*PT single crystals, but rather a gradual transition. For this reason the applied electric field, stress and temperature at the initiation of the $R \rightarrow O$ phase transformation were measured for each composition and are compared in Figure 4-5. Initiation was determined by the approximate point at which the strain response began deviating from linear during loading. The relationships between the $R \rightarrow O$ phase

transition temperature and applied loads for $\langle 001 \rangle$ oriented PMN-0.32PT single crystals was previously determined by McLaughlin *et al.* as $T = 73.5 + 165E_3 + 4.10\sigma_{33}$ [68]. The R→O phase transformation temperature function for PMN-0.27PT and PMN-0.29PT were experimentally determined in this study as $T = 95 + 5.0\sigma_{33}$ and $T=82.1 + 4.6\sigma_{33}$, respectively. There was insignificant data to reliably determine relationships which included applied electric field.

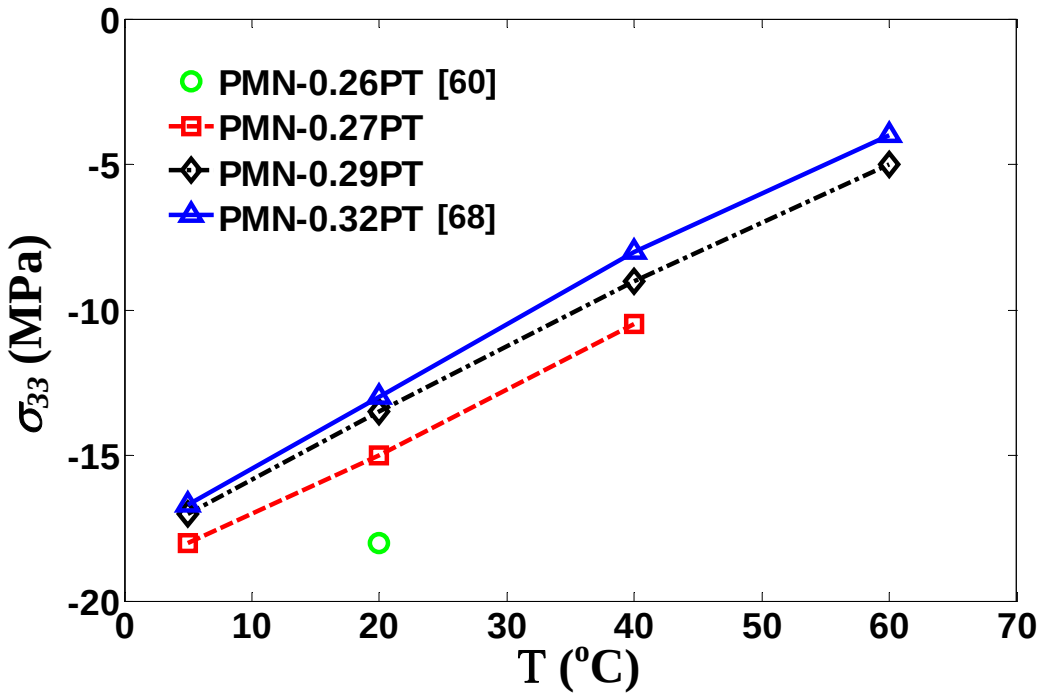

Figure 4-5. Comparison of the quasi-static $\langle 001 \rangle$ compressive stress induced initiation of the R→O phase transformation for various compositions and temperatures. For clarity error bars were omitted; the experimental data is subject to 5% error. The lines connecting points are to guide the eye and do not represent experimental data or a model.

Figure 4-5 shows the strong dependence of composition on phase transformations in relaxor ferroelectric PMN-*x*PT. As the level of PT decreases, moving the composition away from the MPB, there is an increase in stress required to initiate a phase change.

Figure 4-5 also shows that the required stress to initiate a phase change is strongly affected by temperature. Accompanying the change in phase transition behavior, the linear material properties also show composition dependence. Figure 4-6a shows the experimentally measured compliance component term S_{3333}^{E} plotted against the material composition measured from the unipolar compressive stress loading at zero electric field bias. Figure 4-6b shows the piezoelectric coefficient d_{333} versus material composition measured during unipolar electric field loading at -2 MPa stress preload. Figure 4-6c shows the relative dielectric permittivity coefficient versus the material composition measured as the slope of the electric displacement versus electric field data at -2 MPa preloaded stress. Tangent moduli were fit to the loading and unloading portions of the measured minor hysteresis loop and averaged to determine the linear compliance, piezoelectric and dielectric material properties. Only the data in the initial 5% of the maximum load was used in this process. The response in this region was linear and represents the zero field material behavior.

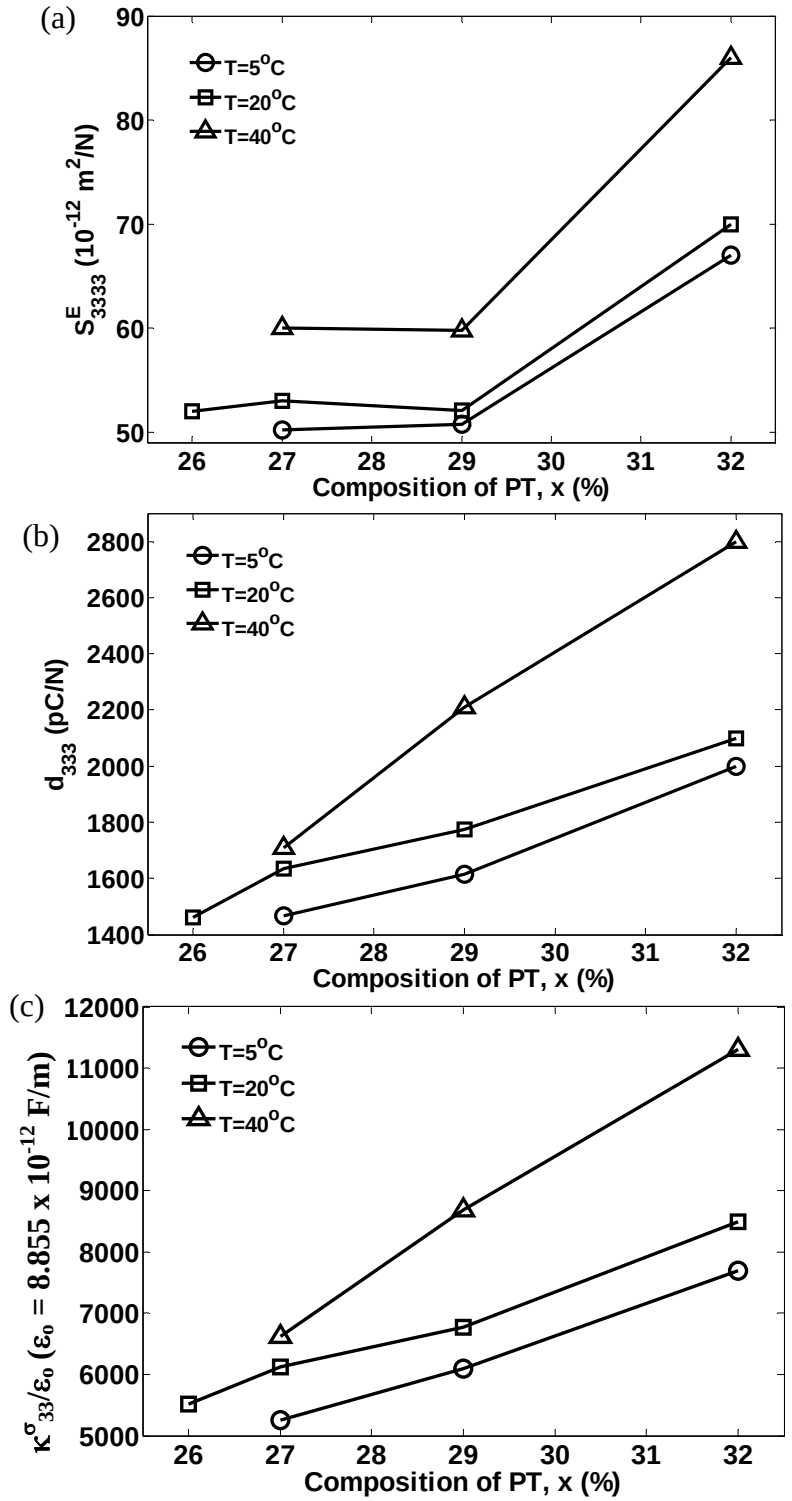

Figure 4-6. Measured linear compliance (a) as a function of composition and temperature during unipolar stress loading at zero electric field for single crystal PMN-*x*PT. Piezoelectric constants (b) and dielectric permittivity (c) were measured during unipolar electric field loading at -0.4MPa preload stress for the same single crystal specimen. The lines connecting points are to guide the eye and do not represent experimental data or a model. Error bars were omitted for clarity; experimental data is subject to 5% error.

Figure 4-6 shows that as the composition of *x*PT decreases some of the electromechanical coupling coefficients are diminished. The shown trend is an augmentation in material properties as the composition is increased. This effect has diminishing returns. Experimental investigations have suggested an optimum compositional region for maximized strain response and minimized hysteresis for $\langle 001 \rangle$ oriented PMN-*x*PT single crystal as $0.29 \leq x \leq 0.31$ [133]. Figure 4-6 shows that an increase in temperature is followed by an increase in the measured material properties. Similar to the subsequent decrease in material properties due to a stress induced phase transformation, a temperature above the material specific Curie point will result in a loss of all electromechanical response as the material transformation to the cubic phase. Noheda *et al.* [47] have presented a phase diagram of PMN-*x*PT which shows that the Curie points for PMN-0.32PT, PMN-0.29PT, PMN-0.27PT and PMN-0.26PT are approximately 417K, 399K, 388K and 382K, respectively.

4.4.2 Bias Field Effects

The linear material properties of $\langle 001 \rangle$ oriented single crystal PMN-*x*PT are load dependent. An increased compressive stress causes an $R \rightarrow O$ phase transition which initiates a marked nonlinear transition. In the loading orientation used in this work, an applied electric field counteracts the compressive stress and opposes the $R \rightarrow O$ phase transformation. Both applied fields change the measured compliance, piezoelectric and dielectric material properties of PMN-0.27PT single crystal specimens. Figure 4-7 shows the measured linear material properties as a function of stress or electric field bias levels, dependent on which loading scheme the coefficient was measured. To determine the

linear material properties at small field the moduli of the initial 5% of the maximum applied load was measured to obtain the linear compliance, piezoelectric and dielectric material properties. The material response in this region was found to be linear.

(a)

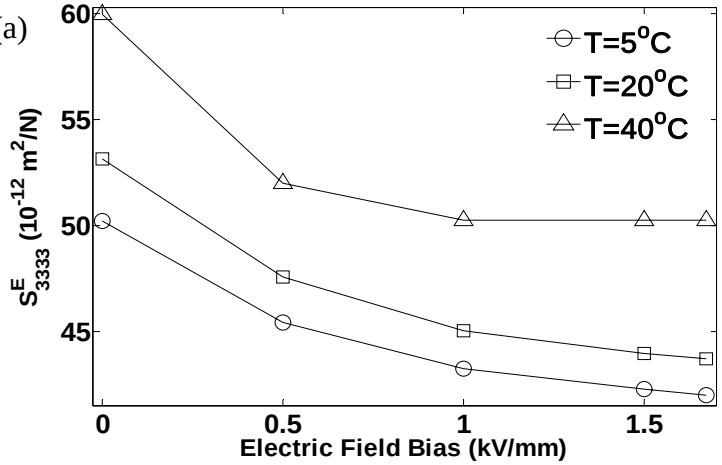

(b)

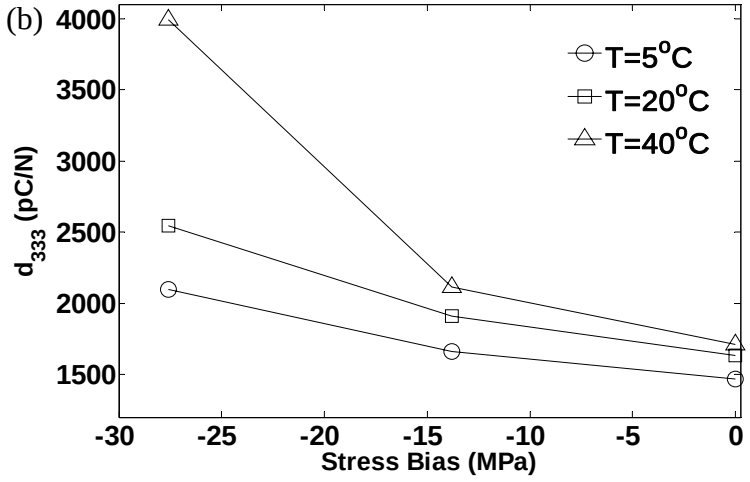

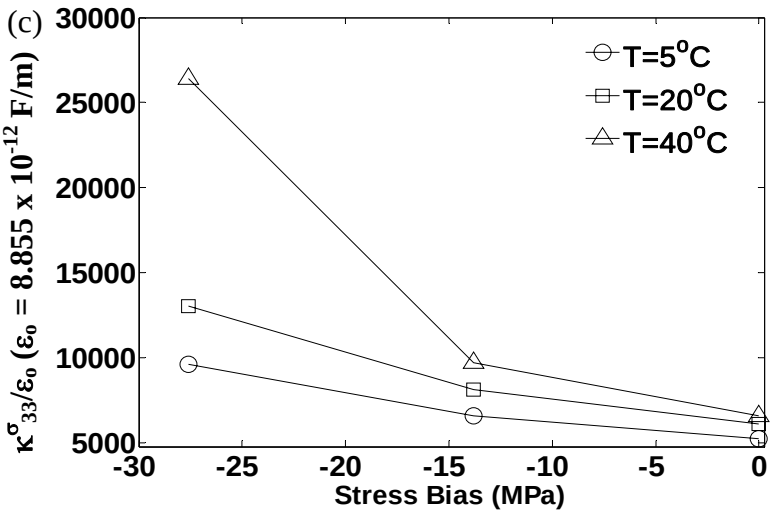

Figure 4-7. Measured compliance (a), piezoelectric (b) and dielectric permittivity (c) as a function of applied bias field and temperature for single crystal PMN-0.27PT. The lines connecting points are to guide the eye and do not represent experimental data or a model. Error bars were omitted for clarity; experimental data is subject to 5% error.

Figure 4-7 shows how the material properties change in response to the applied bias fields. Figure 4-7a shows that the measured compliance decreases as the applied electric field bias increases. This is because the electric field is moving the PMN-0.27PT material further from the $R \rightarrow O$ phase transformation initiation point and closer to the $R \rightarrow T$ phase transition. This behavior was also observed in PMN-0.26PT, PMN-0.29PT and PMN-0.32PT single crystal specimens in the $\langle 001 \rangle$ orientation. It can be seen from Figure 4-3 that a compressive stress applied along the $\langle 001 \rangle$ crystallographic direction causes a phase transformation to the O phase and a nonlinear change in material properties. As the applied stress bias was increased and the phase transformation was initiated there was an increase in the piezoelectric and dielectric material constants. This is because the stress bias causes a partial change to the O phase and then an electric field pulls it back to the R phase, thus increasing the piezoelectric and dielectric material

constants. Although not shown in the measured data, this behavior would be followed by a decrease to zero of the material constants for the fully depolarized orthorhombic phase. Recent research by Davis *et al*. [123] have characterized $\langle 001 \rangle$ PZN-*x*PT (*x* = 5, 6.5, 8.5) and $\langle 001 \rangle$ PMN-*x*PT (*x* = 25, 30.5, 31) single crystal under unipolar electric field cycling at various temperatures. This work showed that as the specimen temperature was increased there was a corresponding increase in the d_{333} piezoelectric coefficient and a simultaneous decrease in the electric field required to initiate a phase transformation.

The measured piezoelectric and dielectric coefficients shown in Figures 4-7b and 4-7c, respectively, are taken at points where the material has not been mechanically driven into the fully depolarized state. Continued increasing of the bias stress causes these coefficients to reach a maximum and then decrease. This behavior can be seen in experimental measurements of $\langle 001 \rangle$ PMN-0.26PT specimens that were applied with a bias stress large enough to drive the full transformation. Figure 4-8 shows the zero field piezoelectric coefficient, d_{333}, plotted against the applied compressive bias stress for $\langle 001 \rangle$ PMN-0.26PT.

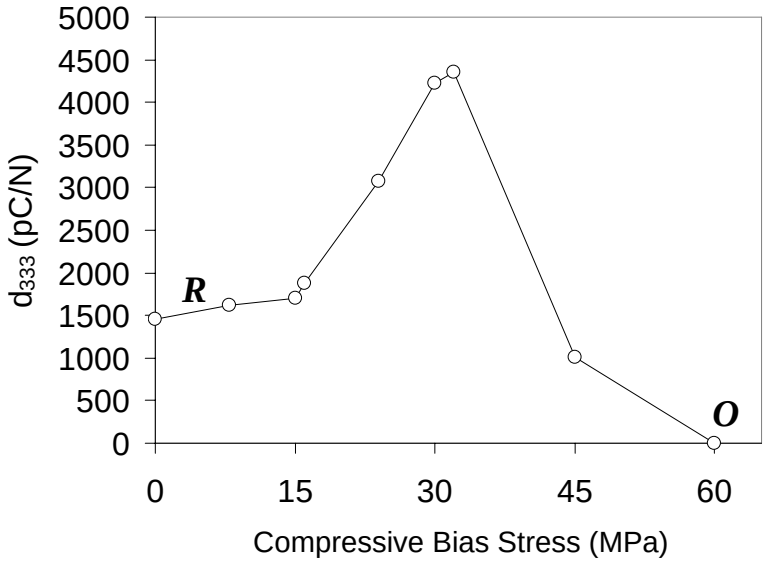

Figure 4-8. Piezoelectric coefficient, d_{333}, measured during bipolar electric field cycling at zero field for $\langle 001 \rangle$ PMN-0.26PT. The rhombohedral and orthorhombic phases are labeled. The lines connecting points are to guide the eye and do not represent experimental data or a model.

4.5 Concluding Remarks

The electromechanical response and phase transformation behavior of relaxor based $\langle 001 \rangle$ oriented single crystal PMN-0.27PT and PMN-0.29PT specimens were measured under combined mechanical, electrical and thermal fields. Three-dimensional surface plots were utilized to clearly illustrate phase transformations. Experimental results were compared to previous studies to show the dependence of constitutive behavior and $R \rightarrow O$ phase transformations on material composition and temperature. As the temperature and percent composition of *x*PT decrease there was a reduction in the measured linear electromechanical response and the stress required for initiation of the $R \rightarrow O$ phase transformation.

CHAPTER 5

A MODEL OF THE CONTINUOUS FIELD DRIVEN PHASE TRANSFORMATIONS OBSERVED IN PMN-*x*PT RELAXOR FERROELECTRIC SINGLE CRYSTALS

The field driven phase transformation behavior of relaxor ferroelectric single crystal PZN-*x*PT is discontinuous and displays well-defined forward and reverse coercive fields [136], whereas the same transformation in PMN-*x*PT is nearly continuous and occurs over a range of field levels [45]. In analogy to the broad Curie range in relaxor ferroelectrics arising from property fluctuations at the nanometer length scale, the continuous field driven phase transformations in PMN-*x*PT are modeled as a step-like series of discontinuous transformations associated with similar spatial property fluctuations. An increase in applied field gradually increases the volume fraction of the new phase at the expense of the old phase resulting in a continuous transition between phases. The model simulation produces excellent agreement with the measured material response of $\langle 011 \rangle$ cut PMN-0.32PT single crystals under conditions of cooperative stress and electric field loading. This work has been accepted for publication in *Acta Materialia* [137] and was the result of collaborative work between Elizabeth McLaughlin at the Naval Undersea Warfare Center Division Newport and Prof. George Rossetti at The University of Connecticut, Storrs, Connecticut. Elizabeth McLaughlin provided the experimental measurements of the PMN-0.32PT single crystal specimens for previously published studies [45, 68]. Prof. George Rossetti provided discussion concerning the relaxor ferroelectric behavior.

5.1 Introduction

Relaxor ferroelectric materials display a diffuse phase transformation between the high temperature paraelectric and lower temperature ferroelectric phases that is characterized by a broad Curie range instead of the single Curie point that is observed with a normal ferroelectric phase change [98]. This broadened phase transformation behavior is observed in a number of complex perovskite-structured compounds and solid solutions that include PMN, PMN-*x*PT and PLZT, (Pb,La)(Zr,Ti)O_3 [138]. Figure 5-1 shows the dielectric permittivity as a function of temperature and frequency for PLZT 6/80/20 [139] .

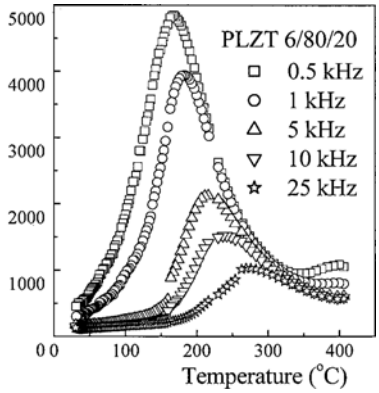

Figure 5-1. Dependence of the dielectric permittivity for PLZT 6/80/20 on temperature and frequency [139].

Recent characterization of relaxor ferroelectric single crystals has resulted in the observation of two distinct types of phase transformation behavior under the application of externally applied loads. As shown in Figure 5-2a, when the transverse strain is measured perpendicular to the direction of the applied electric field, electrically loaded $\langle 011 \rangle$ cut PZN-0.045PT shows well-defined coercive fields for the forward and reverse transformations. The transformation is accompanied by a discontinuous change in strain

and strong hysteresis that is characteristic of a first-order phase change [66, 67, 123]. These observations are to be contrasted with those shown in Figure 5-2b, which shows the results of similar measurements for electrically loaded $\langle 011 \rangle$ cut PMN-0.32PT. For PMN-0.32PT there is a nearly continuous phase transformation that is spread over a range of field values that shows markedly less hysteresis than is observed for $\langle 011 \rangle$ cut PZN-0.045PT [45]. In both cases the transformation is understood to be from the initial rhombohedral phase to a field-induced orthorhombic phase.

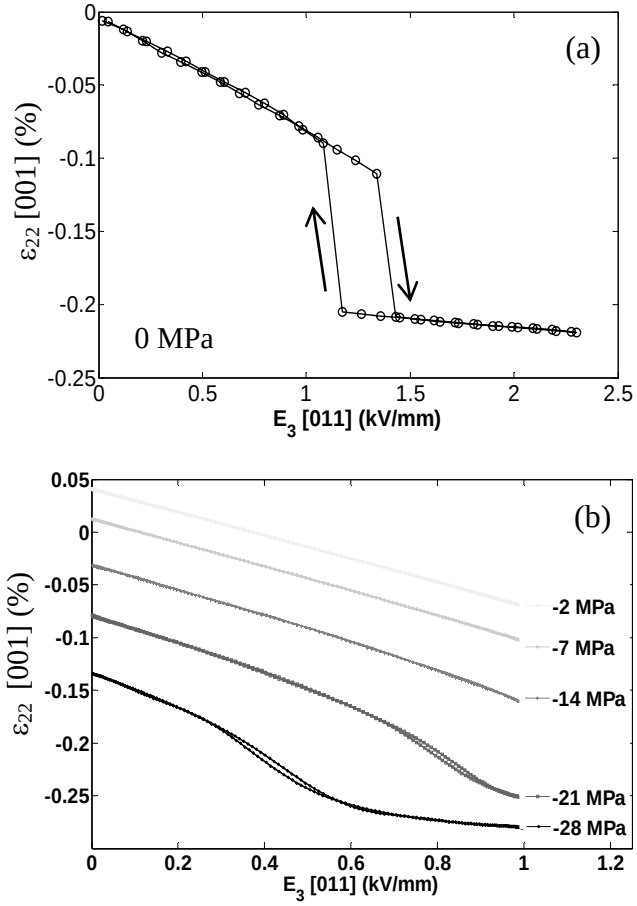

Figure 5-2. (a) PZN-0.045PT [64] and (b) PMN-0.32PT [45] strain versus electric field behavior during field induced phase transformations. The constant uniaxial compressive stress in the PMN-0.32PT was in the $\langle 001 \rangle$ direction.

Field induced phase transformation behavior has been measured in several compositions of PMN-*x*PT. The transformation fields were found to increase as the PT concentration (*x*) was decreased and the average composition was moved away from the morphotropic phase boundary and toward the PMN end member. Frequency-dependent dielectric permittivity measurements made on polycrystalline PMN-*x*PT compositions reveal relaxor ferroelectric behavior when $x < 0.35$ and normal ferroelectric behavior for $x > 0.35$ [140]. Based on neutron diffraction data [140], it is reported that three phases of monoclinic symmetry interleave the rhombohedral and tetragonal phases of the conventional morphotropic phase diagram. However, close to the morphotropic boundary region, complex microstructures are observed in single crystal PMN-*x*PT that are characterized by hierarchical domain structures with domain sizes ranging from nanometers to millimeters and with spatial configurations that are dependent on the thermal and electrical history of the specimen [141]. Chemical heterogeneity persisting at the nanometer length scale is understood to be the origin of the broad Curie temperature region and frequency dispersive properties of relaxor ferroelectrics [98, 138]. Here it is proposed that spatial, chemical and structural heterogeneities may play a similar role in the observed broadening of the field-induced transformations that take place between two ferroelectric phases in relaxor single crystals. Following this interpretation the macroscopically observed material behavior can be the result of the volume average of the behavior of many small regions, each region displaying the discontinuous type transformation observed in PZT-0.045PT, but with spatial fluctuations in material properties about their mean values resulting in a distribution of forward and reverse phase transformation fields.

A model is presented based on the volume average of a sub-scale property distribution mechanism and is shown to provide excellent ability to fit the observed material behavior over a range of stress, electric field, temperature and composition.

5.2 Model Methodology

The sub-scale material behavior is assumed to follow an idealized discontinuous phase transformation from a phase with linear material response to another phase with linear response, as shown in Figure 5-3. In this figure, the driving field can be either stress or electric field and the response can be either strain or electric displacement. For each phase, the moduli of the phases are m^{α} and m^{β}. R_r^{α} and R_r^{β} represent the remanent values for either strain or electric displacement of the α and β phases. F_1^c and F_2^c represent the value of the applied field, either electric field or stress, which drives the transformation from α to β and from β to α, respectively.

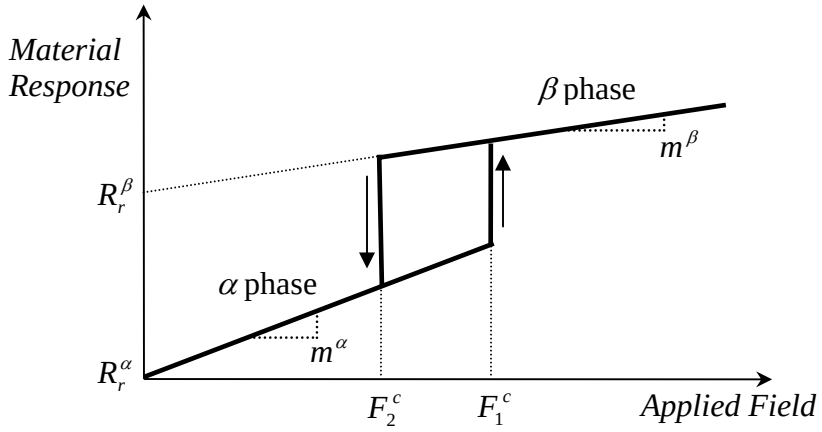

Figure 5-3. Step-like field driven transformation behavior from phase α to phase β is shown schematically. The labels indicate the moduli, the remanent values, and both the forward and reverse transformation fields.

Some relaxor single crystal compositions undergo a phase change that is nearly continuous [45, 68]. This phase transformation behavior is modeled by simulating the material as a heterogeneous medium comprised of numerous regions that each have ideal discontinuous switching behavior but with each region differing in the local values of coercive field for the forward and reverse transformations, F_1^c and F_2^c. This produces a series of step-like discontinuous transformations, the volume average of which results in a gradual change in strain and electric displacement as the applied field increases and progressively more regions transform. The differences between the forward and reverse coercive field values for the various regions are approximated to be constant. The moduli of the initial phase are assumed to be the same in all untransformed regions and the moduli of the final phase are assumed to be the same in all fully transformed regions. This is an approximation as it is known that the moduli are both composition and temperature dependent. These approximations enable modeling each region as having a unique and finite hysteresis. Taking the difference between the forward and reverse transformation fields to be a constant and the moduli of the two phases of each region to be the same leads to the hysteresis loops having different areas due to the different moduli of the two phases. Figure 5-4 shows a schematic illustrating a qualitative representation of three different local material regions and their respective hysteresis loop size as implemented in this model.

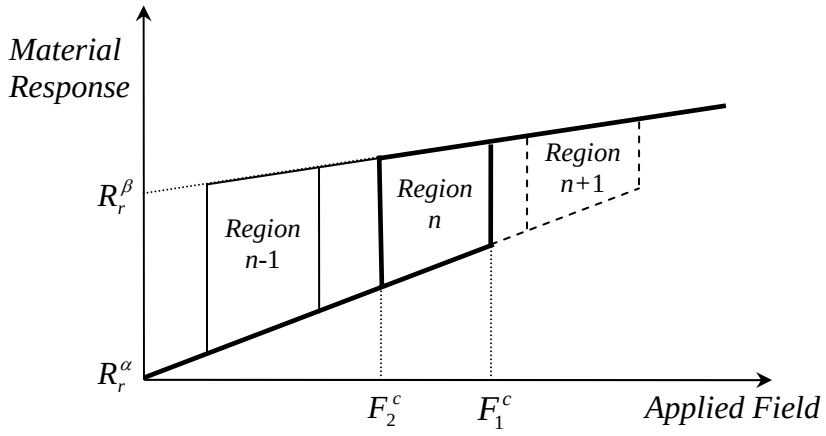

Figure 5-4. Step-like switching behavior from α to β due to an applied field for various regions of material. Switching between phases for each region is initiated at a different applied field levels.

Modeling the distributed phase transformation behavior required identification of the driving force interval over which the transformation is distributed and a distribution function which describes the way in which the regions are distributed. The start and finish points of the interval for the forward transformation were determined by measuring the location where the experimental data displayed a 5% variation of slope from the linear material response. This identified a range of threshold values from the lowest field needed for transformation initiation to the highest field required for transformation completion, *i.e*. a range of F_1^c values. Next, the width of the hysteresis area at the widest location was measured. This measurement was taken to represent the difference between the forward and reverse transformation fields and thus to provide the range for reverse phase transformation, *i.e*. a range of F_2^c values. A normal distribution was used within the threshold interval to describe the variation of local materials properties about their mean value. The distribution functions used were identical for both the forward and

reverse threshold intervals, only shifted relative to one another. For the simulations +/- 2.58σ was chosen to set the end points of the distribution function to match the end points of the transformation interval. This fitting parameter adjusts the shape of the normal distribution within the interval. The normal distribution function is shown in Equation (5-1).

$$f(X) = \frac{1}{\sigma\sqrt{2\pi}} e^{-\frac{1}{2}\left[\frac{X-\mu}{\sigma}\right]^2}, \qquad -2.58\sigma < X < 2.58\sigma \tag{5-1}$$

where σ is the standard deviation, μ is the mean coercive field, and *f(X)* represents the volume fraction of regions with coercive field *X*. Figure 5-5 shows an example of the determination of the linear material coefficients and remanent values for the R and O phases as well as the endpoints for the range of forward transformation fields for $\langle 110 \rangle$ PMN-0.32PT.

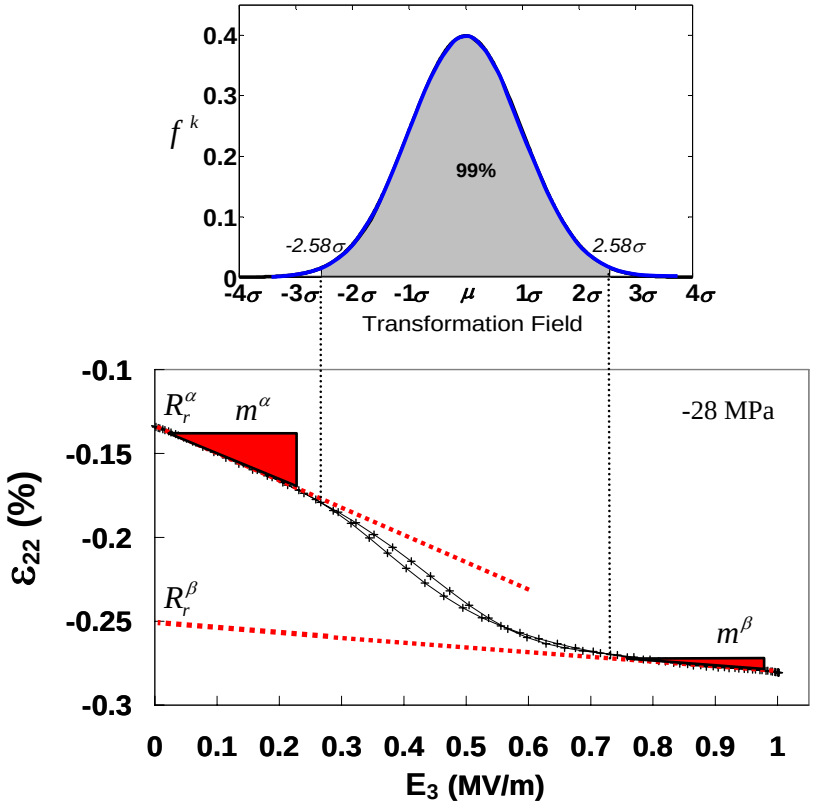

Figure 5-5. Determination of linear material properties, remanent values and range of transformation fields for $\langle 110 \rangle$ PMN-0.32PT.

In setting up the numerical simulations, the interval was subdivided into *n* distinct sub-intervals *k* with the volume fraction f^k of material within each sub-interval determined using the normal distribution. The volume average strain and electric displacement were computed using Equations (5-2) and (5-3).

$$\hat{\varepsilon}_{ij} = \sum_{k=1}^{n} f^k \left(\varepsilon_{ij}\right)^k \tag{5-2}$$

$$\hat{D}_m = \sum_{k=1}^{n} f^k \left(D_m\right)^k \tag{5-3}$$

where $\hat{\varepsilon}_{ij}$ and $\hat{D}_m$ are the macroscopic strain and electric displacement, respectively, $(\varepsilon_{ij})^k$ and $(D_m)^k$ are the local strain and electric displacement response of region *k* to the applied fields.

Equations (5-4) and (5-5) are the constitutive laws used to describe each crystal phase.

$$\varepsilon_{ij} = \varepsilon_{ij}^L + \varepsilon_{ij}^s = s_{ijkl}^E \sigma_{kl} + d_{kij}^\sigma E_k + \varepsilon_{ij}^s \tag{5-4}$$

$$D_i = D_i^L + P_i^s = d_{ikl}^E \sigma_{kl} + \kappa_{ik}^\sigma E_k + P_i^s \tag{5-5}$$

where ε_{ij}^L is the reversible strain, ε_{ij}^s is the spontaneous strain, s_{ijkl} is the compliance, σ_{kl} is the stress, d_{kij} is the piezoelectric constant, E_k is the electric field, D_i^L is the reversible electric displacement, P_i^s is the spontaneous polarization, and κ_{ik} is the dielectric permittivity; indices vary from 1 to 3. The superscripts *E* and σ refer to constant electric field and stress, respectively.

Electrical and mechanical loads applied simultaneously can either work together to drive the transformation (cooperative loading) or against one another where one load drives the transformation and the other load hinders it (antagonistic loading). McLaughlin *et al.* [45, 68] have observed this behavior experimentally in PMN-0.32PT single crystal specimens. The present model has been setup to simulate cooperative loading in which the electric field is applied in the $\langle 011 \rangle$ direction and the stress in the $\langle 100 \rangle$ direction.

The combination of simultaneously applied electrical and mechanical fields is handled by recognizing that there is an energy difference between the phases that represent a barrier to the transformation and that the applied loads must perform sufficient work to drive the material past this energy barrier. The mechanical work is found from the scalar contraction of the applied stress with the strain change that takes place during the transformation and the electrical work is found from the scalar contraction of the electric field with the electric displacement change that takes place during the transformation. The initial interval for electric field loading is identified at a particular constant stress level. If this stress level is changed, the interval shifts by the change in mechanical work that takes place during the transformation. The interval shift can be found from the increment in reversible work density done on an isothermal body using Equation (5-6).

$$\Delta w^{\alpha\to\beta} = \Delta w_{mech}^{\alpha\to\beta} + \Delta w_{elec}^{\alpha\to\beta} = \sigma_{ij}\Delta\varepsilon_{ij}^{\alpha\to\beta} + E_m\Delta D_m^{\alpha\to\beta} \tag{5-6}$$

where $\Delta w^{\alpha\to\beta}$ is the total increment in work to transform from phase α to β, σ_{ij} is the applied stress, $\Delta\varepsilon_{ij}^{\alpha\to\beta}$ is the change in strain, E_m is the applied electric field, and $\Delta D_m^{\alpha\to\beta}$ is the change in electric displacement. It follows from Equation (5-6) that the simultaneous application of a constant compressive stress and unipolar electric field will change the threshold for the phase transformation. In fact, one of the checks on the validity of this modeling approach is to use the parameters determined from the electrical loading data to simulate mechanical loading and then compare with measured mechanical loading data.

The jump in strain and electric displacement caused by a phase change from a single applied load can be measured for each material region. During a unipolar electric field load, the application of a compressive stress does mechanical work during the phase change. During a unipolar compressive stress cycle the application of an electric field bias does electrical work during the phase transformation. The addition of mechanical or electrical work changes the phase transformation behavior and results in a shift of the interval of coercive field values according to Equation (5-6). Figure 5-6 shows a schematic of step-like behavior during phase transformation with illustration of the change in strain and electric displacement which were utilized in Equation (5-5) and (5-6).

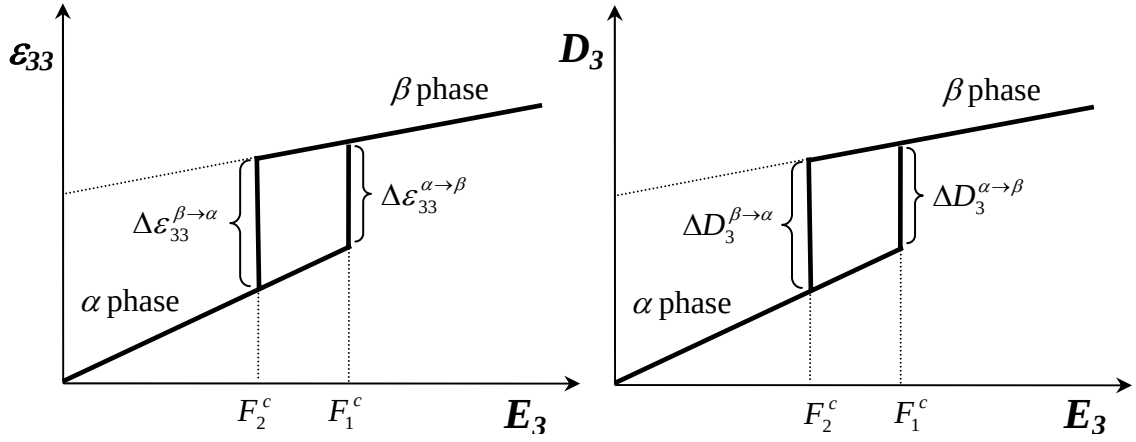

Figure 5-6. Phase transformation from phase α to β, illustrating the change in strain and electric displacement during the transformation.

In addition to shifting the transformation interval, the application of an additional load shifts the starting point of the strain and electric displacement values due to the compliance, piezoelectricity, and permittivity.

5.3 Results

Experimental measurements were performed using the stress-dependent electromechanical characterization system (SDECS) located at Naval Undersea Warfare Center (NUWC) Division Newport. The SDECS system measures the response of piezoelectric materials to electrical, mechanical and thermal fields. The specimens were oriented with the polarization direction aligned along the $\langle 011 \rangle$ crystallographic axis creating a two variant state. An electric field was applied along the $\langle 011 \rangle$ axis while a compressive stress was applied perpendicular along the $\langle 100 \rangle$ axis. This load orientation is described as cooperative because both the stress and electric field provide a positive driving force for the rhombohedral to orthorhombic phase transformation. Strain and electric displacement were measured while the crystal was loaded with both unipolar electric field at several constant stress levels and unipolar stress at several constant electric field levels. All measurements were carried out at 298 K.

The material properties and the difference between the forward and reverse coercive field values were determined from the experimental data. Table 5-1 shows the measured material properties.

Table 5-1. Measured material properties of $\langle 011 \rangle$ PMN-0.32PT single crystal during unipolar electric field and compressive stress loading

	Unipolar Electric Field	Unipolar Stress
$\left(\varepsilon_{22}^{R}\right)^{\alpha}$ (%)	0.0390	0.0390
$\left(\varepsilon_{22}^{R}\right)^{\beta}$ (%)	0.0175	0.0240
$\left(D_{3}^{R}\right)^{\alpha}$ (C/m^2)	0.301	0.301
$\left(D_{3}^{R}\right)^{\beta}$ (C/m^2)	0.340	0.332
$\left(d_{322}^{E}\right)^{\alpha}$ (pm/V)	-1120	-1120
$\left(d_{322}^{E}\right)^{\beta}$ (pm/V)	-320	-320
$\left(\kappa_{33}^{\sigma}\right)^{\alpha}$ (nF/m)	27	--
$\left(\kappa_{33}^{\sigma}\right)^{\beta}$ (nF/m)	10	--
$\left(s_{2222}^{E}\right)^{\alpha}$ ($10^{-12}\ m^2/N$)	--	-63.2
$\left(s_{2222}^{E}\right)^{\beta}$ ($10^{-12}\ m^2/N$)	--	-21.0
$min\left(F_1^c\right)$, $max\left(F_1^c\right)$	1.4, 2.05 kV/cm	23, 38 MPa
$min\left(F_2^c\right)$, $max\left(F_2^c\right)$	1.37, 2.02 kV/mm	22.25, 37.25 MPa

The difference in total strain values between the phases are needed to compute the mechanical work done during the stress driven transformation and the difference in total electric displacement values between the phases can be used to compute the work done during an electric field driven transformation. These values were determined from the remanent strain or electric displacement values, the moduli of the associated phase, and the load level at which the transformation is taking place using Equations (5-4, 5-5). Figure 5-6 shows the experimental data and simulations using the phase transformation model. For the experimental curves, the error bars are roughly the thickness of the lines used to plot the results and thus are not shown. The insets in Figure 5-6a show the

symmetry equivalent orientations of the polarization vector along the pseudo-cubic $\langle 111 \rangle$ directions of the rhombohedral (R) phase and the $\langle 110 \rangle$ directions of the orthorhombic (O) phase in relation to the directions of the applied electric field and mechanical stress.

Figure 5-7 shows two-dimensional plots of the measured strain and electric displacement compared to model simulations. Figures 5-8 and 5-9 combine the two-dimensional plots into three-dimensional surface plots that straightforwardly show the phase transformation behavior. The insets in Figure 5-8a represent the crystal variants present in the corresponding rhombohedral (R) or orthorhombic (O) phase.

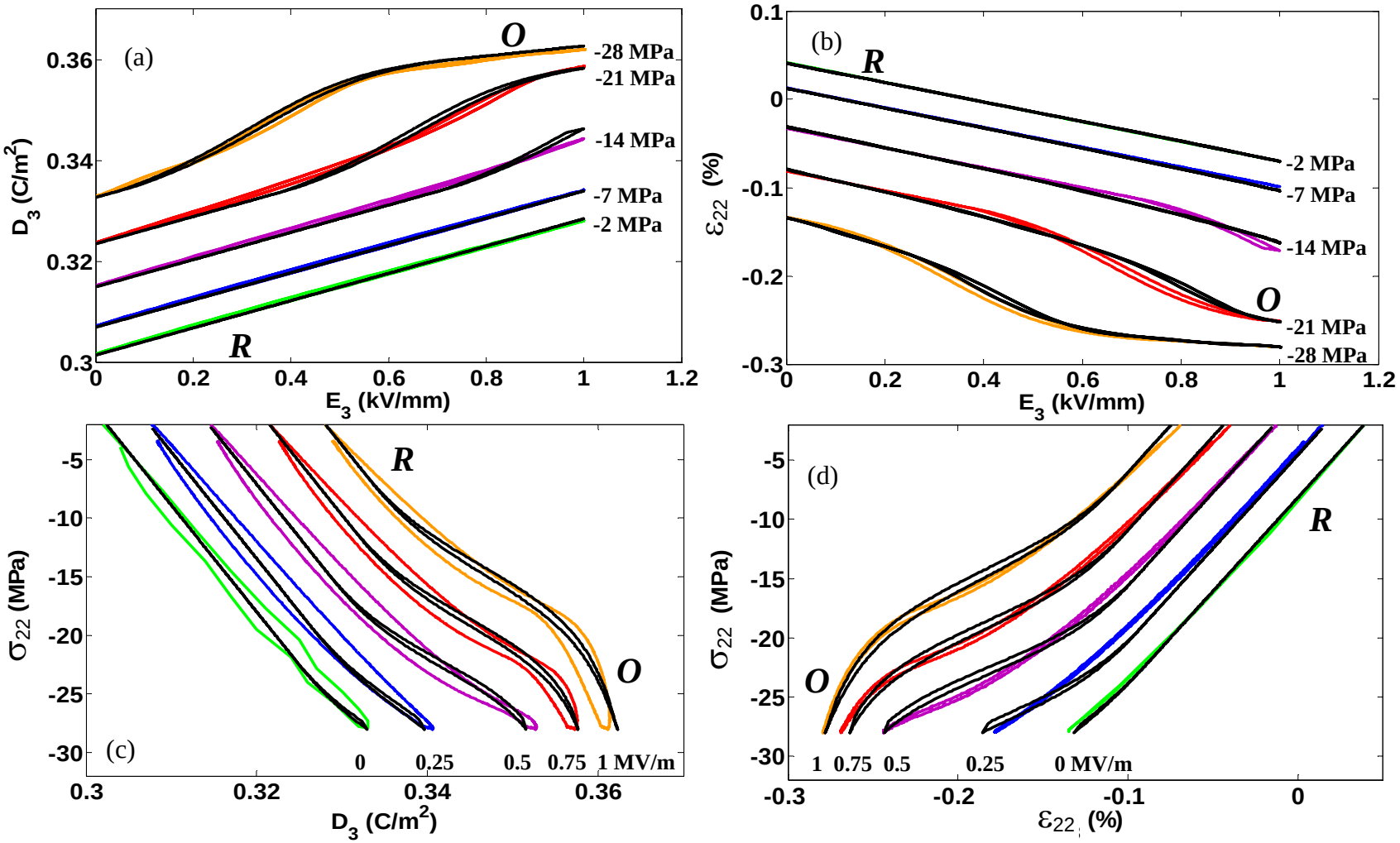

Figure 5-7. Comparison of the experimentally measured ⟨110⟩ PMN-0.32PT single crystal (colored lines) and simulated (black lines) strain and electric displacement during electric field and stress induced R→O phase transformation. The applied bias values are noted next to the corresponding hysteresis loop. The phase is labeled for the rhombohedral and orthorhombic phases.

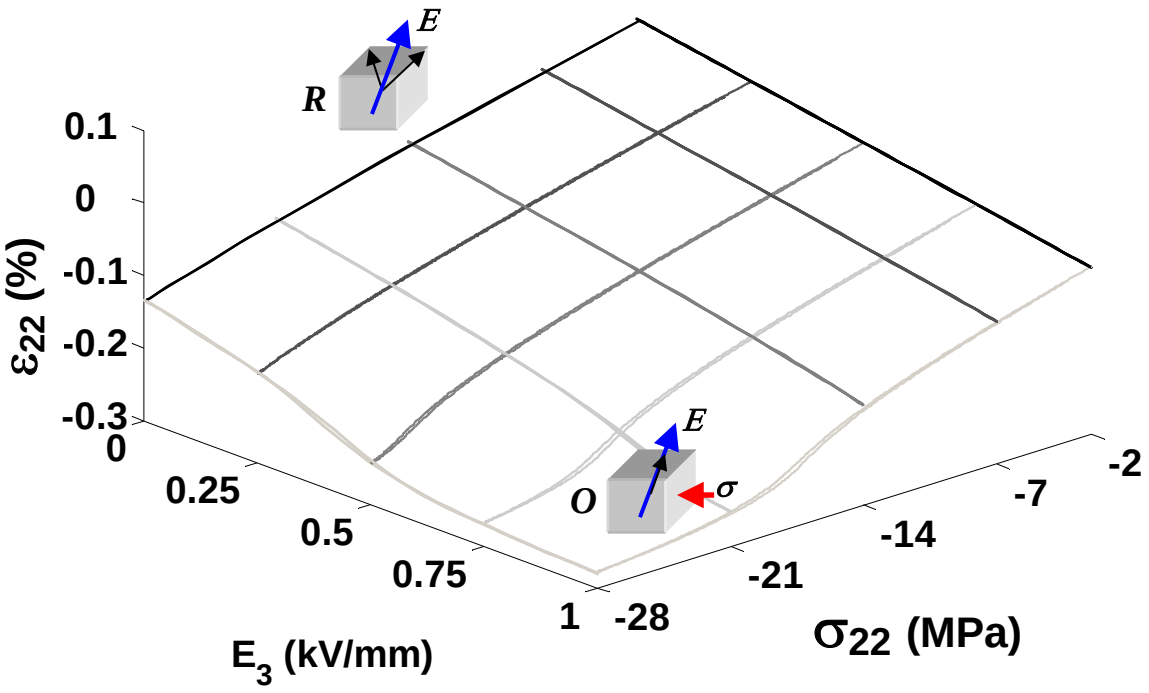

(a)

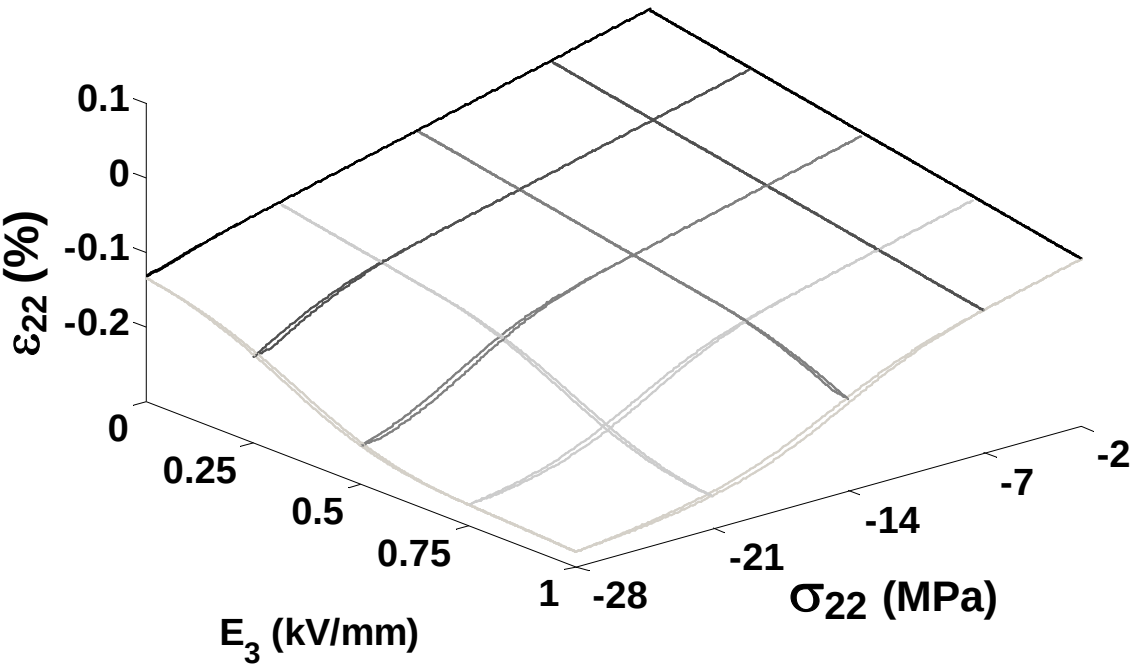

(b)

Figure 5-8. Comparison of the experimentally measured (a) and simulated (b) longitudinal strain of $\langle 001 \rangle$ single crystal PMN-0.32PT under 32-mode loading.

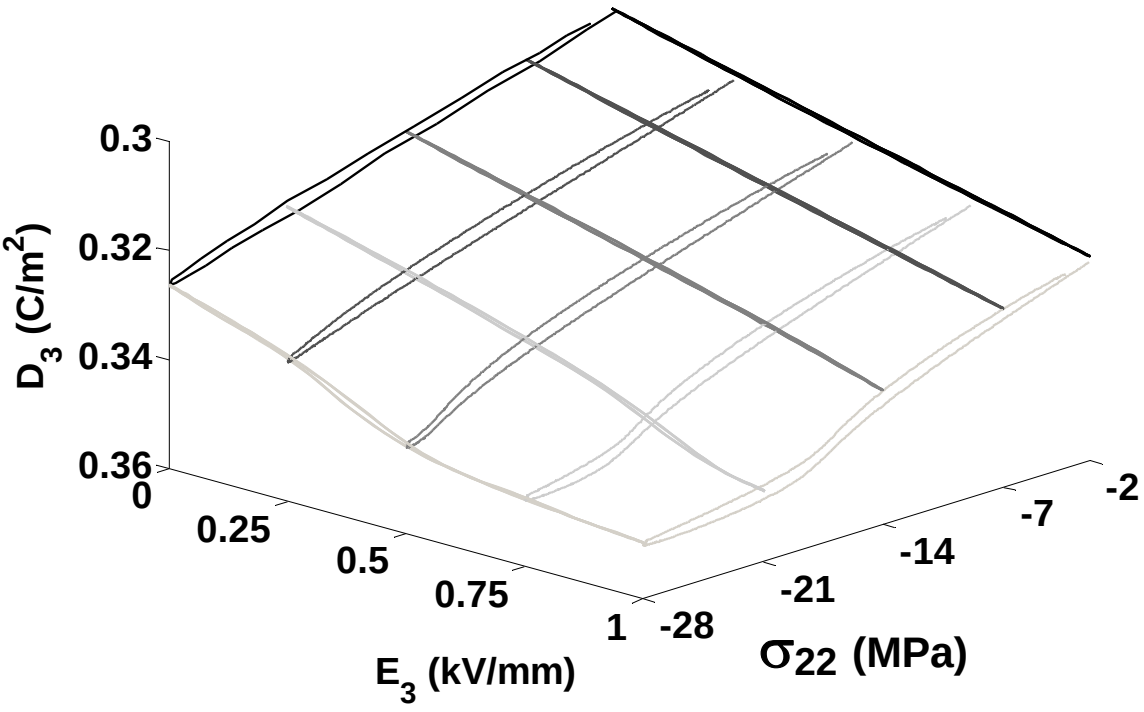

(a)

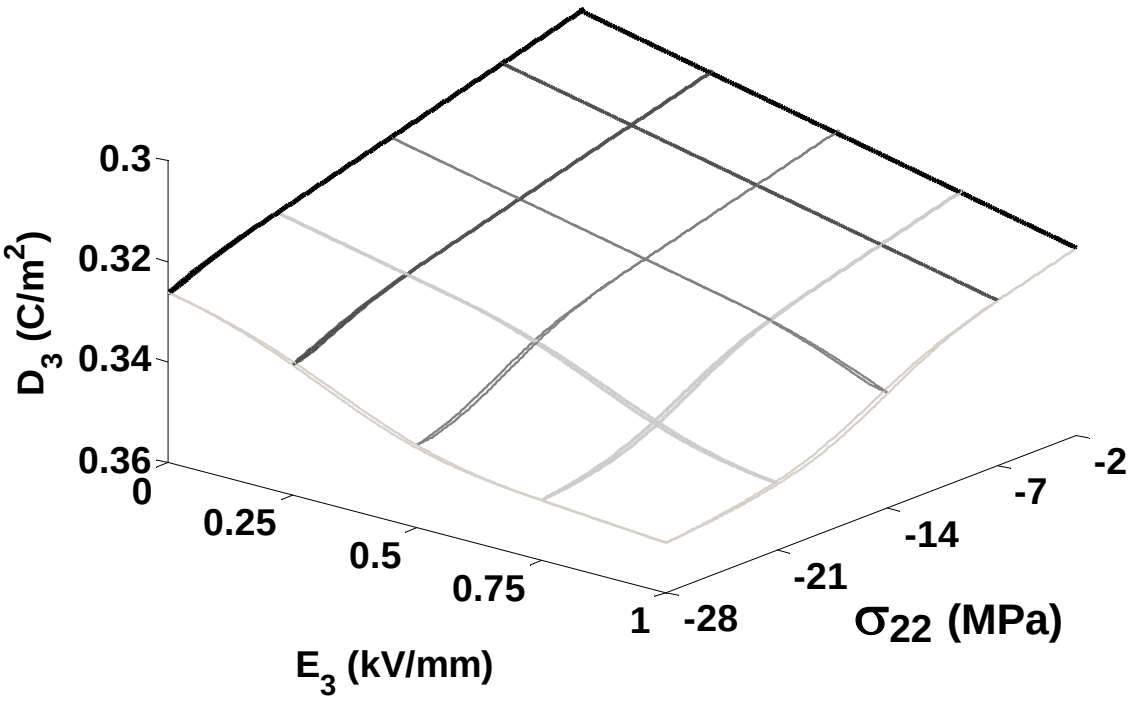

(b)

Figure 5-9. Comparison of the experimentally measured (a) and simulated (b) electric displacement of $\langle 001 \rangle$ single crystal PMN-0.32PT under 32-mode loading.

5.4 Discussion

The predictive capability of this distributed property mechanism based model is excellent. Simulations of the three-dimensional surface plots of Figure 5-6 only required a limited number of parameters, the measured linear material response of each phase, the measured remanent strain and remanent electric displacement of each phase, the width of the hysteresis loop during the electric field driven transformation, and the measured field levels for the start and end of the phase transformation. The only fitting parameter was the number of standard deviations that were contained within the interval of transformation. This controlled the shape of the normal distribution function used to simulate the distribution of regions. For the simulations presented, a standard deviation of +/- 2.58 was found to best fit the data. With a small number of measured parameters this model accurately simulates the phase transformation behavior during multiaxial loading. Temperature effects are not included in the model, but can be included by accounting for the shift in relative energy levels of the phases associated with a change in temperature and a shift of the moduli with temperature.

The amount of hysteresis in the model is controlled by the difference between the forward and reverse coercive fields. The level of hysteresis observed in the experimental results, Figure 5-7c, does not match that of the simulations. The reason for this appears to be because the unipolar stress loading was done at a low frequency where the SDECS instrumentation appears to have had some drift in the electric displacement measurement system. This drift was a known problem with the data and it is likely that the simulation of the stress-electric displacement curves based on the parameters taken from the electric

field loading are more accurate than the measured data. An attempt to represent this with error bars in Figure 5-7c would simply present bars that span the open loop.

The mechanism that this model is based on, namely that there are sub-scale regions with different properties, is presently the subject of intense discussion. This concerns the relation of the structural state near the morphotropic phase boundary in relaxor ferroelectric single crystals such as PMN-*x*PT to the nature of the phase transformations that may occur between ferroelectric phases subject to a change in temperature, composition and/or externally applied loads [142]. Two distinct explanations have emerged to reconcile how it is possible for a continuous transformation to occur in relaxor single crystals between two ferroelectric phases that do not share symmetry group-subgroup relations. In one explanation the phase transformation behavior observed in morphotropic PMN-*x*PT materials is associated with the presence of one or more monoclinic phases positioned in a region of the composition-temperature phase diagram adjacent to the morphotropic boundary [143]. It is proposed that these monoclinic phases serve as structural bridges in which there is a polarization rotation that provides a pathway for transitions between ferroelectric phases of different symmetry [144]. Following this interpretation the observed macroscopic material response arises as a consequence of the intrinsic properties of the monoclinic bridging phases.

An alternative explanation [145] has been proposed based on the adaptive state theory of martensites, wherein the diffraction data attributed to homogeneous phases of monoclinic symmetry are instead the result of heterogeneous stress-accommodating domain structures with ultra-low domain wall energies and spatial dimensions reduced to the nanometer scale [146]. Following this interpretation the observed macroscopic

material response is extrinsic in nature and arises as a consequence of the gradual reconfiguration of the nano-domain states under the application of external forces [147]. The hierarchical microstructures associated with these nano-domain states have been directly confirmed in PMN-0.33PT single crystals by a combination of transmission electron microscopy, convergent beam electron diffraction and polarized light microscopy [148] and their reconfiguration has been connected with the high sensitivity of the phase stability near the morphotropic boundary of PMN-*x*PT to crystal orientation under applied electric field [149].

The model presented in this chapter follows the second description wherein chemical and structural heterogeneities at the nanometer length scale lead to spatial property fluctuations. The origins of these spatial property fluctuations have been attributed to the chemical heterogeneities that are inherent to relaxor ferroelectrics [98, 138] and to the microstructural heterogeneities that are inherent to morphotropic ferroelectric solid solutions [150]. The present model is therefore conceptually similar to the earliest distributed Curie temperature model used to explain the broadened dielectric permittivity peak seen in same materials and which also display the diffuse phase change [26].

5.5 Concluding Remarks

A phase transformation model has been presented which simulates the effects of variations in material properties among local regions in relaxor ferroelectric materials. Each of these local regions was assumed to respond with discontinuous phase transformation behavior with an instantaneous change in the elastic, piezoelectric, and

dielectric material properties. Results of simulations are in excellent agreement with experimental data.

CHAPTER 6

RATE INDEPENDENT MICROMECHANICAL MODEL OF NONLINEAR VOLUME FRACTION EVOLUTION IN RELAXOR FERROELECTRICS

The non-linear and hysteretic constitutive behavior of polycrystalline ferroelectric materials is governed by mechanisms at several smaller length scales and over multiple time scales. These include the length scales of grains, domains, defect structures and unit cells. This work presents a micromechanical model of the constitutive behavior of single crystal PMN-0.26PT based on the evolution of the volume fraction of crystal variants, which is then used as the foundation for a micromechanical model of polycrystalline PMN-0.32PT. In the presented micromechanical approach, the behavior of each grain is modeled as the volume average of the behavior of the rhombohedral crystal variants. The variant volume fractions evolve in response to local stress and electric fields. The behavior of the grains is then volume averaged to obtain the behavior of the polycrystalline ceramic. The multiaxial model results are compared with measured single crystal and with polycrystalline behavior. This work is presently being prepared for submission to *Acta Materialia*

6.1 Introduction

Developing micromechanical constitutive models of ferroelectric material is a multifaceted problem where nonlinear hysteretic behavior at multiple length scales contributes to the observed behavior. Simulations based on the underlying mechanisms are inherently multiaxial and give insight into the various contributions of the

fundamental phenomena. They also provide the capability to perform accurate multiaxial simulations suitable for the tuning of macroscale multiaxial phenomenological models [151]. Such models can be used in finite element codes for device design and optimization. Many applications expose ferroelectric materials to high stress, high electric field and changing temperatures. Domain wall motion is a primary contributor to nonlinearity and hysteresis in ferroelectrics below the Curie point [6]. The mobility of domain walls is dependent on time, field strength, frequency and inhomogeneities at various length scales.

The micromechanical approach models polycrystalline ferroelectric constitutive behavior as the volume average of the behavior of an orientation distribution of single crystal grains (typically random or uniform, but textured polycrystals can readily be simulated using this approach). Early micromechanical models assumed there were no interactions between grains and that loading was quasi-static, isothermal and well away from phase transition temperatures [92, 152-160]. Each grain was assumed to have Priesach step-like switching behavior [92]; therefore domains and domain walls were not explicitly modeled. This effectively combined the behavior at multiple smaller length scales using a single simplifying assumption. In these early models, each unit cell was typically modeled as tetragonal with spontaneous polarization in one of six possible directions. Multiple grains were modeled; each with a random orientation of the crystal structure relative to a macroscale coordinate system and each given an initial random polarization direction. This resulted in an initial value of zero remanent (volume average) polarization and strain of the polycrystalline ferroelectric. Application of stress and electric field resulted in evolution of the remanent polarization and strain. This

occurred due to the polarization of the single crystal grains switching to align with the applied stress or electric field in a manner that maximized the work done by the external driving forces, as described by Equation (6-1). This states that when the work per unit volume that would be done in a virtual switch of the polarization from one of the tetragonal directions to another exceeds an energy barrier, then the switch will take place [92].

$$w = \sigma_{ij}\Delta\varepsilon_{ij}^{s} + E_i\Delta D_i^{s} \geq 2E_c P^{s} \tag{6-1}$$

where σ_{ij} is the applied stress, E_i is the applied electric field, $\Delta\varepsilon_{ij}^{s}$ and ΔD_i^{s} are the change in the spontaneous strain and electric displacement that would take place were the polarization to reorient to one of its other equilibrium orientations, E_c is the coercive electric field and P^s is the magnitude of the spontaneous polarization. It is apparent from Equation (6-1) that under purely mechanical loading there is no driving force for 180^o polarization reorientation since this provides no change in strain. Only 90^o polarization reorientations occur under this condition. However, when an electric field is applied in the absence of mechanical load, 180^o and 90^o reorientation are both possible depending on the orientation of the electric field with respect to the initial polarization direction.

Subsequent micromechanical models addressed the material behavior associated with domain switching, volume fraction evolution of variants, phase transitions and domain engineering in single crystals [90, 118, 136, 161-168]. McMeeking and Hwang [159] and Chen and Lynch [118, 161] proposed models that used interaction functions to approximate the interactions between grains using a simplified inclusion approach. Chen and Lynch used different energy levels for 90^o and 180^o switching and included the

effects of intergranular interactions through semi-empirical fitting parameters to model piezoelectric polycrystalline ceramics. Huber *et al.* [90, 162] implemented a crystal plasticity based model governing the evolution of a switching surface (this is similar to a yield surface in phenomenological plasticity) and volume fractions of crystal variants. This model assumed that once a critical yield value was reached, volume fraction evolution proceeded in a steady-state dissipative process while the critical yield value remained constant. Landis and McMeeking [169] presented a self-consistent constitutive model for barium titanate. This model considered simplified domain wall motion which was primarily due to 180^{o} switching and modeled the ferroelectric grains as spherical crystallites. Mauck and Lynch [165, 166] proposed models which included thermal and rate effects. Rodel and Kreher [167] described the effects of intergranular interactions using a statistical method and a simplified domain configuration. Chen *et al.* [153] and Lu *et al.* [170-172] both proposed a domain switching model that considered each domain to be an ellipsoidal inclusion in an infinite piezoelectric solid. The energy due to the existence of individual domains and the domain interaction energy were formulated in a thermodynamics framework to determine the volume fractions of each variant. Fan [119] utilized domain wall nucleation and evolution rate equations to describe the nonlinear hysteresis behavior of PMN-based polycrystals near the phase transition temperature where the permittivity is at a maximum. In this work, he developed a domain switching model which utilized the applied mechanical and electrical loads to determine the driving force for volume fraction evolution. Fan *et al.* [173] then developed a model to describe the transition from an initially soft material to the subsequent hardening due to polarization saturation. This model relied heavily on curve

fitting experimental polycrystalline data and did not take into account the volume fraction evolution of crystal variants that occurs during loading. Other authors have also utilized micromechanical modeling to describe observed nonlinear ferroelectric behavior [101, 174, 175].

Although micromechanical modeling has provided considerable insight into non-linear and hysteretic material behavior, these models used the sub-scale (single crystal) behavior as a fitting parameter for the observed macroscale polycrystalline behavior. In the following work, a micromechanical model is developed from measured single crystal behavior and the results compared to measured behavior of polycrystalline specimens of a similar composition.

6.2 Model Methodology

In this work, a model of macroscale ferroelectric behavior is developed based on several underlying sub-scale phenomena. This involves the development of models governing the sub-scale behavior followed by implementation of a volume averaging scheme to determine the macroscale material response. Volume averaging was performed in which the domain types (crystal variants) are volume averaged to obtain the grain level remanent polarization and strain. This was accomplished by weighting the spontaneous strain and polarization of each of the crystal variants present by the volume fraction of that variant. It was assumed that compatible domain walls were formed, and thus interaction energies between domain walls were not considered. Because the maximum measured field induced strain was smaller than 0.5% the following formulation is restricted to small strain.

6.2.1 Constitutive Behavior

The materials under consideration are single crystal and polycrystalline PMN-*x*PT compositions near the morphotropic phase boundary (MPB) which are in the rhombohedral phase at room temperature (293K). The rhombohedral phase is a member of the trigonal crystal class that possesses 3*m* symmetry [176]. Miller indices were used to define the orientation of the crystal variants where $[mnp]$ denotes a specific crystallographic direction and $\langle mnp \rangle$ indicates all vectors that are equivalent to $[mnp]$ by symmetry. The rhombohedral phase has eight possible spontaneous polarization directions that are oriented towards the corners of the unit cell along the $\langle 111 \rangle$ directions. A variant coordinate system was defined for each of the possible spontaneous polarization directions in the unit cell. The choice of variant coordinate system affects the coefficients. The variant coordinate system for the rhombohedral structure poled in the $\langle 111 \rangle$ direction was defined as such: the variant axes $\hat{x}_1$-$\hat{x}_2$-$\hat{x}_3$ lie along the $\langle \bar{1}10 \rangle$-$\langle \bar{1}\bar{1}2 \rangle$-$\langle 111 \rangle$ cubic referenced directions, respectively, where $\hat{x}_3$ is the variant spontaneous polarization direction. This coordinate system was chosen because the principal axes of each variant could be conveniently defined with the cubic referenced axes, simplifying implementation. Figure 6-1 shows a schematic of the rhombohedral unit cell illustrating possible polarization directions as well as the crystal (cubic referenced) and variant referenced coordinate systems. A similar variant coordinate system was defined for each of the other 7 rhombohedral variants.

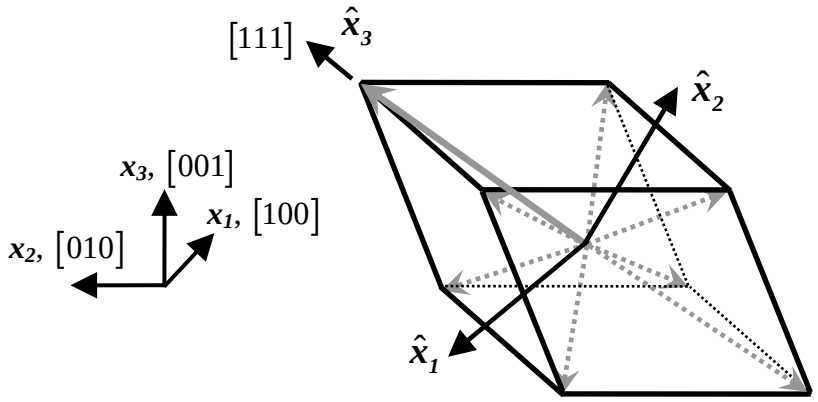

Figure 6-1. Structure of the rhombohedral unit cell illustrating the crystal (x_k) and variant ($\hat{x}_k$) coordinate systems.

The governing equations are presented using indicial notation; summation is implied on repeated indices. The single variant behavior is modeled using a linear piezoelectric constitutive law.

$$\varepsilon_{ij} = \varepsilon_{ij}^{L} + \varepsilon_{ij}^{s} = s_{ijkl}^{E}\sigma_{kl} + d_{kij}E_k + \varepsilon_{ij}^{s} \tag{6-2}$$

$$D_i = D_i^{L} + D_i^{s} = d_{ikl}\sigma_{kl} + \kappa_{ik}^{\sigma}E_k + P_i^{s} \tag{6-3}$$

where ε_{ij} is the total strain, ε_{ij}^{s} is the spontaneous strain tensor, s_{ijkl} is the compliance, σ_{kl} is the stress, d_{kij} is the piezoelectric constant, E_k is the electric field, D_i is the total electric displacement, P_i^{s} is the spontaneous polarization and κ_{ik} is the dielectric permittivity; indices vary from 1 to 3. Superscripts L and s refers to the reversible (elastic) and spontaneous (nonlinear) portions of strain and electric displacement, respectively. Superscripts, E and σ refer to constant electric field and stress, respectively. The spontaneous strain and polarization for the $\langle 111 \rangle$ variant are shown in Equations (6-4) and (6-5).

$$\varepsilon_{ij}^{s} = \begin{bmatrix} -0.5\varepsilon^{s} & 0 & 0 \\ 0 & -0.5\varepsilon^{s} & 0 \\ 0 & 0 & \varepsilon^{s} \end{bmatrix} \tag{6-4}$$

$$P_{i}^{s} = \begin{bmatrix} 0 \\ 0 \\ P^{s} \end{bmatrix} \tag{6-5}$$

where ε^{s} is the spontaneous strain and P^{s} is the spontaneous polarization along the $\hat{x}_3$ axis.

6.2.1.1 Rhombohedral Single-Domain Properties

In this study the compliance, piezoelectric and dielectric properties of each rhombohedral variant were taken to possess to 3*m* symmetry [24]. The associated non-zero components of each material matrix for each rhombohedral variant are shown in Equations (6-6 – 6-8). The compliance matrix shown in Equation (6-6) is symmetrical about the leading diagonal.

$$s_{ij} = \begin{bmatrix} s_{11} = s_{22} & s_{12} & s_{13} = s_{23} & s_{14} = -s_{24} = \frac{1}{2}s_{56} & 0 & 0 \\ & s_{22} = s_{11} & s_{23} = s_{13} & s_{24} = -s_{14} = -\frac{1}{2}s_{56} & 0 & 0 \\ & & s_{33} & 0 & 0 & 0 \\ & & & s_{44} = s_{55} & 0 & 0 \\ & & & & s_{55} = s_{44} & s_{56} = -2s_{24} = 2s_{14} \\ & & & & & s_{66} = 2(s_{11} - s_{12}) \end{bmatrix} \tag{6-6}$$

$$d_{ij} = \begin{bmatrix} 0 & 0 & 0 & 0 & d_{15} = d_{24} & d_{16} = -2d_{22} = 2d_{21} \\ d_{21} = -d_{22} = \frac{1}{2}d_{16} & d_{22} = -d_{21} = -\frac{1}{2}d_{16} & 0 & d_{24} = d_{15} & 0 & 0 \\ d_{31} = d_{32} & d_{32} = d_{31} & d_{33} & 0 & 0 & 0 \end{bmatrix} \quad (6\text{-}7)$$

$$\kappa_{ij} = \begin{bmatrix} \kappa_{11} = \kappa_{22} & 0 & 0 \\ 0 & \kappa_{22} = \kappa_{11} & 0 \\ 0 & 0 & \kappa_{33} \end{bmatrix} \quad (6\text{-}8)$$

The complete set of nonzero piezoelectric coefficients for the $\langle 111 \rangle$ variant was established using the ratio of material properties determined from previous experimental investigations of single crystal PMN-0.3PT specimens [136] in conjunction with our measurements. A full set of piezoelectric coefficients for $\langle 111 \rangle$ oriented PMN-0.3PT single crystals have been determined by Liu and Lynch [136] through a combination of experimentation and computation. The relative ratio of the piezoelectric constants from their study was maintained, but scaled by the smaller magnitude of measured piezoelectric coefficients in the composition under consideration during this study. Equation (6-9) shows the orthogonal transformation of the piezoelectric coefficients from one right-handed orthogonal coordinate system to another.

$$d'_{ijk} = a_{im} a_{jn} a_{kp} d_{mnp} \quad (6\text{-}9)$$

where a_{ij} are components of the transformation matrix and summation is implied. Expanding Equation (6-9) and substituting in the components of the direction cosine matrix determined from coordinate systems for the $\langle 001 \rangle$ and $\langle 111 \rangle$ yields Equation (6-10) which can be used to determine the relationship between the measured piezoelectric

coefficient, $d_{33}^{\langle 001 \rangle}$, and the nonzero components of the piezoelectric tensor in the $\langle 111 \rangle$ oriented PMN-*x*PT single crystal [64]. It is assumed that the $\langle 001 \rangle$ poled single crystal contains equal volume fractions of the $\langle 111 \rangle$, $\langle \bar{1}11 \rangle$, $\langle 1\bar{1}1 \rangle$ and $\langle \bar{1}\bar{1}1 \rangle$ rhombohedral variants.

$$d_{33}^{\langle 001 \rangle} = 0.3849 d_{31}^{\langle 111 \rangle} + 0.1925 d_{33}^{\langle 111 \rangle} + 0.3849 d_{15}^{\langle 111 \rangle} - 0.2722 d_{16}^{\langle 111 \rangle} \tag{6-10}$$

where the superscripts $\langle 001 \rangle$ and $\langle 111 \rangle$ refer to the crystallographic orientation of the material coefficient. With the determined coefficient ratios, the single-domain properties can be estimated for PMN-0.26PT from Equation (6-10).

The nonzero components of the compliance and dielectric tensors were determined in a similar scaling method to the piezoelectric coefficients. Zhang *et al.* [177-179] have experimentally determined a complete set of compliance and dielectric tensors for $\langle 111 \rangle$ and $\langle 001 \rangle$ PMN-0.33PT single crystal along with the material properties for other compositions of $\langle 001 \rangle$ PZN-*x*PT and PMN-*x*PT single crystal specimens [180-182]. Jin *et al.* have presented a complete set of single-domain material properties for PZN-(0.06-0.07)PT [183]. Measurements for all studies were made with a technique that combined the resonance and ultrasonic methods [179]. In this work, the relative ratio between each component measured by Zhang *et al.* [177-179] was maintained while the magnitude was scaled using the material constants measured in this investigation. Material constants measured during quasi-static loading differ from measurements of the same constants with the resonance technique [74]. This is due to the rate-dependence of ferroelectric materials. Table 6-1 shows the material coefficients

used to describe the electromechanical response of each $\langle 111 \rangle$ oriented rhombohedral variant.

Table 6-1. Material coefficients of a rhombohedral variant for PMN-0.26PT, PMN-0.32PT, and PZN-0.045PT. Elastic compliance coefficients: s_{ij}^{E} (10^{-12} m^2/N); piezoelectric coefficients: d_{ij} (pm/V); dielectric coefficients: κ_{ij}^{σ} (nF/m); coercive field: E_C (kV/mm).

	PMN-0.26PT	PMN-0.32PT	PZN-0.045PT
s_{11}^{E}	9.3	10.9	11.7
s_{12}^{E}	-22.8	-9.5	-28.9
s_{13}^{E}	-0.8	-0.98	-1.1
s_{14}^{E}	-24.9	-29.2	-31.6
s_{33}^{E}	2.0	2.4	2.5
s_{44}^{E}	76.4	89.9	96.8
d_{31}	-44.7	-63.5	-35[a]
d_{33}	93	132	125[a]
d_{15}	2954	4200	3824[a]
d_{16}	-1238.9	-1761	-1902[a]
κ_{11}^{σ}	96.45	144.6	96.45
κ_{33}^{σ}	15.63	23.4	15.63
E_C	0.09	0.13[b]	0.17

[a]Liu and Lynch [184]
[b]Wan *et al*. [185]

6.2.1.2 Spontaneous Strain and Polarization

A $\langle 001 \rangle$ poled rhombohedral single crystal is in a four domain state with equal volume fractions of each variant. Because of the domain state the remanent strain is zero. The absence of remanent strain in the $\langle 001 \rangle$ poled crystal makes the determination of a remanent strain for the $\langle 111 \rangle$ poled single crystal from $\langle 001 \rangle$ experimental data not

possible. It can be reasonably assumed that the remanent strain in the single domain $\langle 111 \rangle$ poled rhombohedral crystal has the same value as the spontaneous strain of a single variant. The most accurate method for determining the remanent strain of a $\langle 111 \rangle$ poled single crystal would be to directly measure this orientation experimentally. However, there have been limited studies done in the $\langle 111 \rangle$ orientation. Due to their increased electromechanical response most experimental investigations of single crystal PMN-*x*PT and PZN-*x*PT have focused on the $\langle 001 \rangle$ and $\langle 011 \rangle$ crystal orientations. Liu and Lynch [66, 67] have measured the bipolar electromechanical response of PZN-0.045PT single crystals at various off-axis crystal cuts between the $\langle 001 \rangle$ and the $\langle 111 \rangle$ crystallographic orientations. The measured remanent strain values from this study were used to estimate the spontaneous polarization for a rhombohedral variant in a relaxor ferroelectric. It was assumed that the trend of the measured remanent strain values could be used to find the remanent strain for the $\langle 111 \rangle$ oriented single crystal, the spontaneous strain of each rhombohedral variant was the same and the spontaneous strain for PMN-*x*PT and PZN-*x*PT were approximately equal. Figure 6-2 shows the measured remanent strain values for each off-axis crystal cut. From initial inspection the experimental data looks quadratic. It was found, however, that the spontaneous strain estimated with a quadratic function did not match experimental results well in simulations. This indicates that the remanent strain values may saturate as the off-axis angle, α, increases due to the domain state. Equation (6-11) was used to simulate the remanent polarization saturation.

$$\varepsilon_{33}^{r} = \frac{\varepsilon^{s}}{2}\left[\tanh\left(\frac{2\pi\alpha}{\theta} - \pi\right) + 1\right] \tag{6-11}$$

where $\theta = \arccos\left(1/\sqrt{3}\right)$ is the angle between the $\hat{x}_3$ poling axes of the $\langle 111 \rangle$ and $\langle 001 \rangle$ coordinate systems. Figure 6-2 shows the measured remanent values compared to Equation (6-11).

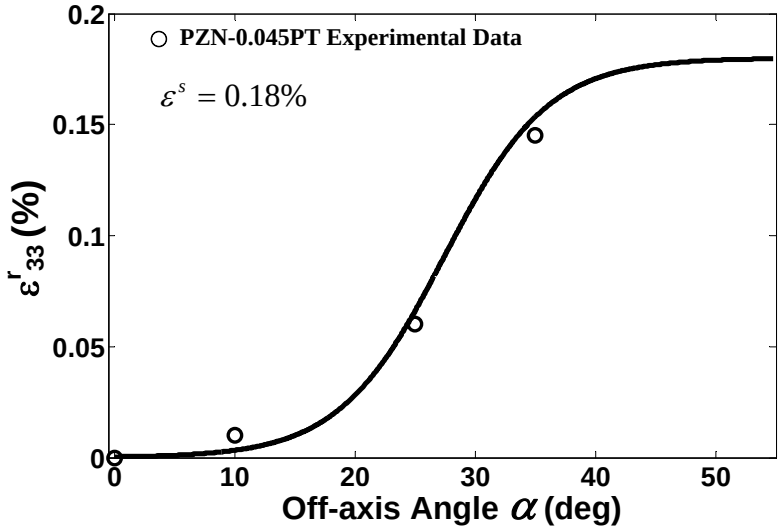

Figure 6-2. Measured remanent strain values of PZN-0.045PT single crystal specimens with the poling electric field oriented at various off-axis angles between the $\langle 001 \rangle$ and $\langle 111 \rangle$ crystallographic orientations.

Although the material used in the study by Liu and Lynch was a different single crystal material, it was a relaxor ferroelectric in the rhombohedral phase with similar electromechanical behavior. The spontaneous strain was estimated to be 0.18% for PMN-0.26PT and PZN-0.045PT. The spontaneous strain for PMN-0.32PT was estimated to be 0.2%. These values were used as the spontaneous strain of each variant in the rhombohedral crystal.

A similar analysis was not necessary for the spontaneous polarization of each variant. The $\langle 001 \rangle$ poled single crystal has a remanent polarization. Equation (6-12)

shows the relationship between the measured remanent strain in the $\langle 001 \rangle$ and $\langle 111 \rangle$ orientations.

$$\left(P_3^r\right)^{\langle 001 \rangle} = \frac{1}{\sqrt{3}}\left(P^s\right)^{\langle 111 \rangle} \tag{6-12}$$

Table 6-2 shows the estimated spontaneous strain and calculated spontaneous polarization for the rhombohedral variant.

Table 6-2. Spontaneous strain and polarization values for relaxor ferroelectric materials

	PMN-0.26PT	PMN-0.32PT	PZN-0.045PT
$P^s\,(C/m^2)$	0.42[a]	0.365[b]	0.47[c]
$\varepsilon^s\,(\%)$	0.18	0.2	0.18

[a]Webber *et al*. [60]
[b]McLaughlin *et al*. [68]
[c]Liu and Lynch [64]

6.2.2 Coordinate Systems for the Grain Scale

Three different coordinate systems were used. A global coordinate system defined the loading orientation, a crystal coordinate system defined the orientation of each grain relative to the global coordinate system and eight variant coordinate systems were used to define the material properties for each variant of each grain relative to each crystal coordinate system. Single crystal material properties were determined from previous measurements [60] as well as from other data presented in the literature [64, 68]. These data were used to deduce the single variant rhombohedral piezoelectric properties in the variant coordinate systems. Each variant was assumed to possess the same material properties relative to their individual coordinate system. Orthogonal

transformations were utilized to transform piezoelectric material properties, applied fields and material response between the global, crystal and variant coordinate systems. The elastic, piezoelectric and dielectric tensors were initially defined with respect to the variant coordinate system whereas the external fields were applied in the global reference frame. The resulting strain and electric displacement were calculated for each single crystal grain in the crystal coordinate system. Single crystal behavior was approximated by volume averaging the response of each variant and assuming negligible variant interaction. Equations (6-13) and (6-14) were used to determine the strain and electric displacement of each single crystal grain:

$$\varepsilon_{ij}^{C} = \sum_{\alpha=1}^{n} f^{\alpha}\left[a_{im}a_{jn}\varepsilon_{mn}^{\alpha}\right] \tag{6-13}$$

$$D_{i}^{C} = \sum_{\alpha=1}^{n} f^{\alpha}\left[a_{im}D_{m}^{\alpha}\right] \tag{6-14}$$

where C refers to the crystal coordinate system, α is the current variant under consideration, n is the total number of possible variants, f^{α} is the variant volume fraction of variant α and a_{ij} is the direction cosine matrix that defines the transformation between the crystal and variant coordinate systems. This system of equations is equally valid when transforming material properties between the crystal coordinate system and the global reference frame.

Simulation of polycrystalline material containing many randomly oriented single crystals required an additional transformation. It has been found that creating a system of transformation matrices through randomly generated Euler angles resulted in increased polarization around the north and south poles of the polycrystal. Figure 6-3 shows the

intersection of the x_1, x_2 and x_3 crystal axes of 10,000 single crystal grains with a sphere using one set of randomly oriented Euler angles. It can be seen that the x_1 and x_2 crystal axes have clustered around the equator, while the x_3 crystal axis is clustered about the north and south poles.

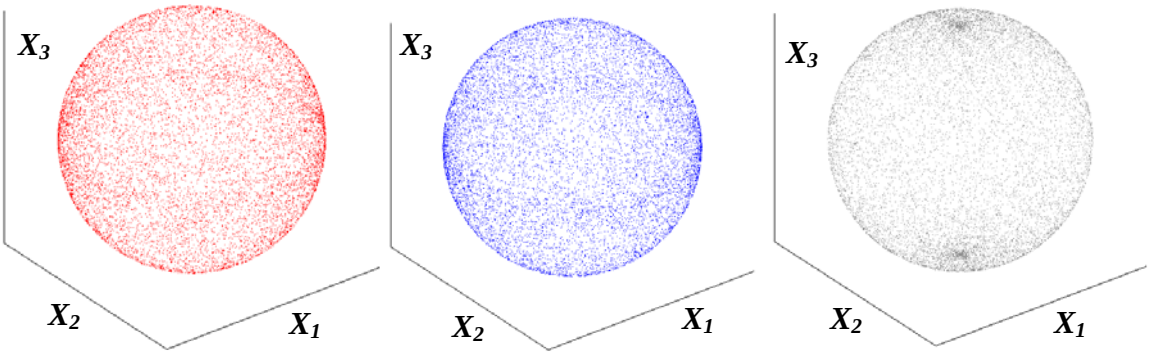

(a) (b) (c)

Figure 6-3. Intersection of the crystal axes x_1 (a), x_2 (b) and x_3 (c) with a sphere shown in the global coordinate system X_1-X_2-X_3 when one set of randomly selected Euler angles are used for transformation.

Clustering was reduced by randomly selecting two sets of Euler angles and performing two independent transformations for each grain. This process evenly distributed all three crystal axes. Equation (6-15) shows the final transformation matrix resulting from the matrix multiplication of two independent transformation matrices.

$$a_{ij} = a_{ip}^{(2)} a_{pj}^{(1)} \tag{6-15}$$

where summation is implied and the superscripts (1) and (2) refer to the first and second generated transformation matrix, respectively. Figure 6-4 shows the intersection of the x_1, x_2 and x_3 crystal axes of 10,000 single crystal grains with a sphere which have been

oriented according to Equation (6-15). It can be seen that there is no visible clustering and the distribution of single crystal orientation is very nearly uniform.

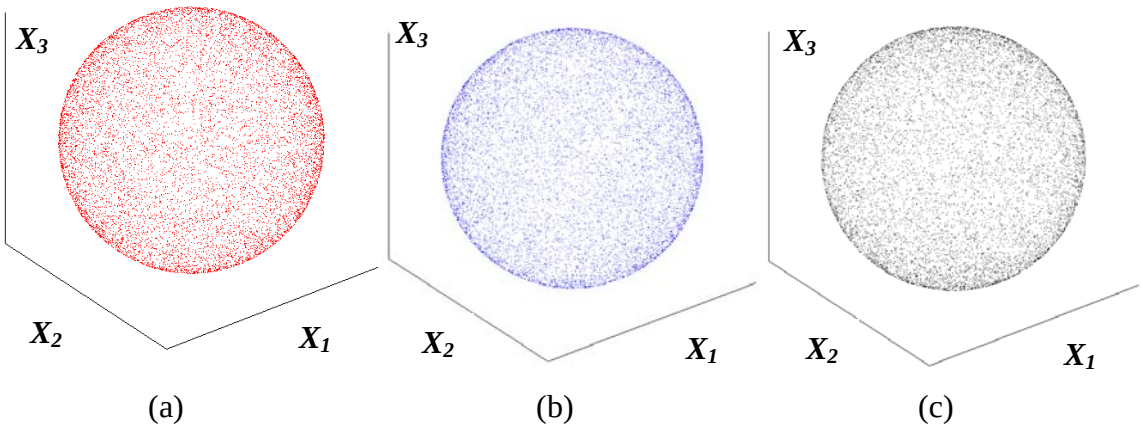

(a) (b) (c)

Figure 6-4. Intersection of the crystal axes x_1 (a), x_2 (b) and x_3 (c) with a sphere shown in the global coordinate system X_1-X_2-X_3.

When considering a polycrystalline material an additional volume average is performed on the effects of each grain. Equations (6-16) and (6-17) were used to determine the macroscopic strain and electric displacement of the polycrystal:

$$\varepsilon_{ij} = \sum_{C=1}^{m} f^{C}\left[a_{im}a_{jn}\varepsilon_{mn}^{C}\right] \tag{6-16}$$

$$D_{i} = \sum_{C=1}^{m} f^{C}\left[a_{im}D_{m}^{C}\right] \tag{6-17}$$

where C is the current grain under consideration, m is the total number of grains considered and f^{C} is the volume fraction of each grain which was assumed to be $1/m$.

6.2.3 Volume Fraction Evolution

The evolution of volume fractions of crystal variants is a non-linear process dependent on material composition, domain wall type and density, loading orientation and local defects. Domain walls which are responsible for much of the nonlinear behavior seen in relaxor ferroelectrics [6] can become pinned by intersection with other domain walls, distributed space charges that may diffuse under slow domain wall motion or other defects like grain boundaries. This suggests that a model that captures the effects of domain wall motion should have a threshold for breaking free of pinning sites. Once the wall has broken free of its pinning sites its mobility through the crystal structure will be higher. As the process nears completion there will be geometric constraints associated with compatibility conditions between the domain wall orientation and the grain boundary orientation as well as intergranular clamping. These constraints will hinder the final stages of the wall motion. It has been seen in experimental studies that the single domain state is unstable, possibly due to fringing fields that may be a strong function of boundary conditions [179]. The goal of this section is to introduce a model that captures these effects. This begins by again considering the work done per unit volume as a domain wall moves. The effect is illustrated schematically in Figure 6-5. As the compressive stress is increased in this simple qualitative two-variant model the volume fraction of variant β will increase at the expense of variant α when the domain wall between them translates. In the real ferroelectric material under consideration there are more than two possible variants. The following formulation will make use of two-variant model in Figure 6-5 for simplicity.

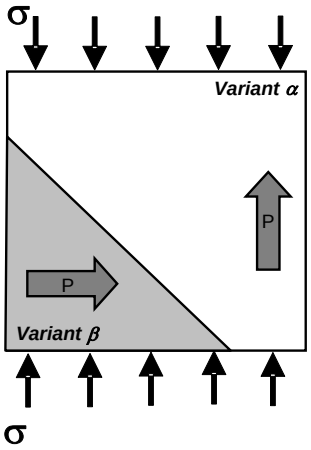

Figure 6-5. Qualitative schematic of the volume fraction evolution of crystal variants in a material with only two possible spontaneous polarization directions under an applied compressive stress.

When an external field is applied, work is done on the ferroelectric crystal. If the applied work is larger than a critical value then the ferroelectric material responds by reorienting the spontaneous polarization direction of some domains. This minimizes the energy of the system. The exact volume fraction of each domain that evolves is dependent on the magnitude and relative crystallographic orientation of the applied fields, the locally generated fields and the resistance of a domain to evolution. Local fields can be generated by inhomogeneities such as point charges or defects that can act as field concentrations. The resistance of a domain to evolution is affected by the energy threshold for initiation of domain wall motion, domain wall density and other local barriers such as grain boundaries and point charges. The effects on the driving force from the resistance of a domain to evolution is simulated by inclusion of kinematic hardening switching criterion which depends on the volume fractions of the two variants under consideration. Equation (6-18) shows the driving force necessary for volume fraction evolution.

$$G^{\alpha\to\beta} = G^{\alpha\to\beta}_{mech} + G^{\alpha\to\beta}_{elec} + G^{\alpha\to\beta}_{B} \geq G^{\alpha\to\beta}_{0} \tag{6-18}$$

where $G^{\alpha\to\beta}$ is the driving force and $G^{\alpha\to\beta}_{0}$ is the threshold for volume fraction evolution. The subscripts *mech* and *elec* denote the mechanical and electrical portion of the driving force. The total driving force is a function of the mechanical and electrical driving force due to applied fields and the back fields generated from the current volume fraction state of the α and β phases. This results in an expression for the driving force on a relaxor ferroelectric single crystal shown in Equation (6-19).

$$G^{\alpha\to\beta} = \sigma_{ij}\left(\Delta\varepsilon^{r}_{ij}\right)^{\alpha\to\beta} + E_i\left(\Delta D^{r}_{i}\right)^{\alpha\to\beta} + G^{\alpha\to\beta}_{B}\left(f^{\alpha}, f^{\beta}\right) \tag{6-19}$$

As external fields are applied the driving force computed in Equation (6-19) changes as a function of applied fields, the current volume fraction state and the material properties of each variant. If the driving force is lower than the critical threshold value governing domain switching then no evolution of the volume fraction between α and β is allowed. When the driving force is larger than the threshold value then evolution between α and β is allowed. As evolution between the α and β phase proceeds at fixed external applied fields there is a change in the back fields that decreases the driving force for further volume fraction evolution. When the back fields become large enough to neutralize the applied fields, evolution stops and the stable volume fraction state has been determined. Equation (6-20) shows the back field function that was used.

$$G^{\alpha\to\beta}_{B}\left(f^{\alpha}, f^{\beta}\right) = A\left(1 - f^{\alpha}\right)^{B} + C\left(f^{\beta}\right)^{D} \tag{6-20}$$

where *A, B, C* and *D* are material constants. Using the two-variant model presented in Figure 6-5 the back field can be determined as a function of the volume fraction of β. Figure 6-6 shows that when the volume fraction of β is zero, back fields are absent. As the volume fraction of α decreases at the expense of β it is assumed that more domain walls are present, causing barriers to volume fraction evolution. When the material is completely transformed to the β phase there is a negative back field that reduces the critical switching threshold for the one domain state. This is consistent with experimental investigations of $\langle 111 \rangle$ poled PZN crystals that appear to show that a depolarizing field, possibly generated by fringing fields dependent on boundary conditions, forces the one domain crystal into a multidomain state upon unloading of the electric field.

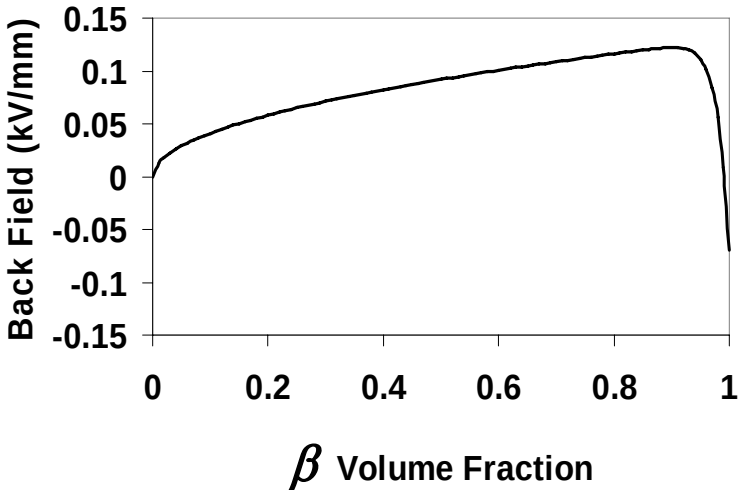

Figure 6-6. Simulated back field as a function of the volume fraction of β for a two-variant volume evolution model.

Combining Equations (6-18), (6-19), and (6-20) results in an expression for the driving force on a ferroelectric single crystal necessary to cause volume fraction evolution.

$$G^{\alpha\to\beta} = \sigma_{ij}\left(\Delta\varepsilon_{ij}^{r}\right)^{\alpha\to\beta} + E_i\left(\Delta D_i^{r}\right)^{\alpha\to\beta} + A\left(1-f^{\alpha}\right)^{B} + C\left(f^{\beta}\right)^{D} \geq G_0^{\alpha\to\beta} \tag{6-21}$$

When Equation (6-21) is satisfied, then volume fraction evolution proceeds.

6.2.4 Domain Wall Threshold Energy

A single crystal in the rhombohedral phase has eight possible domain types. The domain wall that separates any pair of domains is identified by the relative angle between the spontaneous polarization directions of the domains. In the rhombohedral phase there are three possible domain wall types: 180°, 109.47° and 70.53°. The exact method of motion for each domain wall during evolution is not known. It is possible that each domain wall type translates in a different manner. This would require an individual domain evolution model for each domain wall type. In the presented work, it was assumed that one evolution model was capable of simulating all domain wall types. However, it was also assumed that the energy threshold for switching was not the same. Equations (6-22a) and (6-22b) show the relative switching threshold ratios for 180° and 109.47° to 70.53° switches.

$$\frac{G_0^{180}}{G_0^{70}} = n_1 \tag{6-22a}$$

$$\frac{G_0^{109}}{G_0^{70}} = n_2 \tag{6-22b}$$

where G_0^{180}, G_0^{109} and G_0^{70} are the threshold driving force for switching for the 180°, 109.47° and 70.53° domain wall types and n_1 and n_2 are material constants.

This approach has been previously considered in the simulation of polycrystalline 8/65/35 PLZT experimental measurements [161]. It was found that the material had

sharp dips in butterfly shaped remanent strain as the applied field passed through the coercive field when subjected to a bipolar electric field with no applied compressive stress. As stress was increased the dips continually became more rounded. It was proposed that this was due to the differences in the switching thresholds between the three possible domain wall types. In measured experimental data of off-axis PZN-0.045PT single crystal specimens [67] between the $\langle 001 \rangle$ and the $\langle 111 \rangle$ orientations it was found that as the orientation angle was increased from the $\langle 001 \rangle$ direction the hysteresis loops developed deeper, sharper coercive field wells. The presented model is compared to the experimental measurements of Liu and Lynch [67] in a subsequent section of this chapter.

6.2.5 Phase Transformations

In Chapter 5, a model was presented that described the phase transformation behavior. The phase transformation model did not consider the evolution of phase boundaries; rather, it averaged the effects of discontinuous phase changes of nano-polar regions with compositional fluctuations. It has been shown that relaxor ferroelectric materials with different compositions show different phase transition behavior. Because of the assumed distribution of phase transformation initiation points, a continuous phase transformation is created.

6.2.5.1 Rhombohedral $\leftrightarrow$ Orthorhombic Phase Transformations

Experimental investigations from various researchers have shown the existence of field induced $R \leftrightarrow O$ phase transformations in relaxor ferroelectric single crystals [29, 42,

45, 60, 68]. This phenomenon is dependent on the magnitude and the relative crystallographic orientation of external loads, temperature and composition. The rhombohedral phase under consideration in the domain evolution model is stable at room temperature. This has allowed for many experimental measurements by various authors providing a complete set of anisotropic compliance, piezoelectric and dielectric material properties. This is not the case for the orthorhombic (Class *mm*2) phase which in the PMN-*x*PT and PZN-*x*PT compositions examined is only stable in the presence of bias fields. This raises an important difficulty: there exists very little experimental data to determine the full set of anisotropic material coefficients of the orthorhombic phase. Because the orthorhombic phase possesses no planes of symmetry many complex experimental measurements must be conducted that may be impossible to achieve. Due to these difficulties the compliance and dielectric material properties for the orthorhombic phase were modeled as linear isotropic such that

$$s_{ijkl}^{E} = \frac{1+\nu}{2Y}\left(\delta_{ik}\delta_{jl} + \delta_{il}\delta_{jk}\right) - \frac{\nu}{Y}\delta_{ij}\delta_{kl} \tag{6-23}$$

$$\kappa_{ij}^{\sigma} = \kappa\delta_{ij} \tag{6-24}$$

where Y is the Young's Modulus, ν is the Poisson's ratio, κ is the isotropic dielectric permittivity and δ_{ij} is the Kronecker delta. These idealized relationships represent the isotropic volume average compliance and permittivity. The orthorhombic piezoelectric tensor cannot be assumed linear isotropic. Direct measurements for the orthorhombic phase can be made from previous experimental data for the d_{32} piezoelectric coefficient of PMN-0.32PT [45]. The remaining constants (d_{33}, d_{31}, d_{24}, d_{15}) must be assumed so

that simulations matched experimental measurements. Equation (6-25) shows the matrix of piezoelectric constants for an orthorhombic crystal with *mm*2 symmetry.

$$d_{ij} = \begin{bmatrix} 0 & 0 & 0 & 0 & d_{15} & 0 \\ 0 & 0 & 0 & d_{24} & 0 & 0 \\ d_{31} & d_{32} & d_{33} & 0 & 0 & 0 \end{bmatrix} \tag{6-25}$$

Similar problems arise for the tetragonal phase (Class 4*mm*) which in the compositions considered is also only stable when a bias field is present. Various researchers have shown the existence of the field-induced tetragonal phase in relaxor ferroelectric single crystal specimens [29, 123, 186].

6.2.5.2 Spontaneous Strain and Polarization of the Orthorhombic Phase

From previous experimental measurements it is possible to estimate a component of the spontaneous strain tensor and the spontaneous polarization for the orthorhombic phase. Previous experimental characterizations of $[011]$ oriented PMN-0.32PT single crystals measured the electric displacement along the $[011]$ axis in response to an electric field in the $[011]$ direction and a stress in the $[100]$ direction [45]. Strain was measured in the direction of applied stress. Figure 6-7 shows a schematic of the single crystal orientation showing the cubic-referenced crystallographic axes and experimental data presented by McLaughlin *et al.* [45].

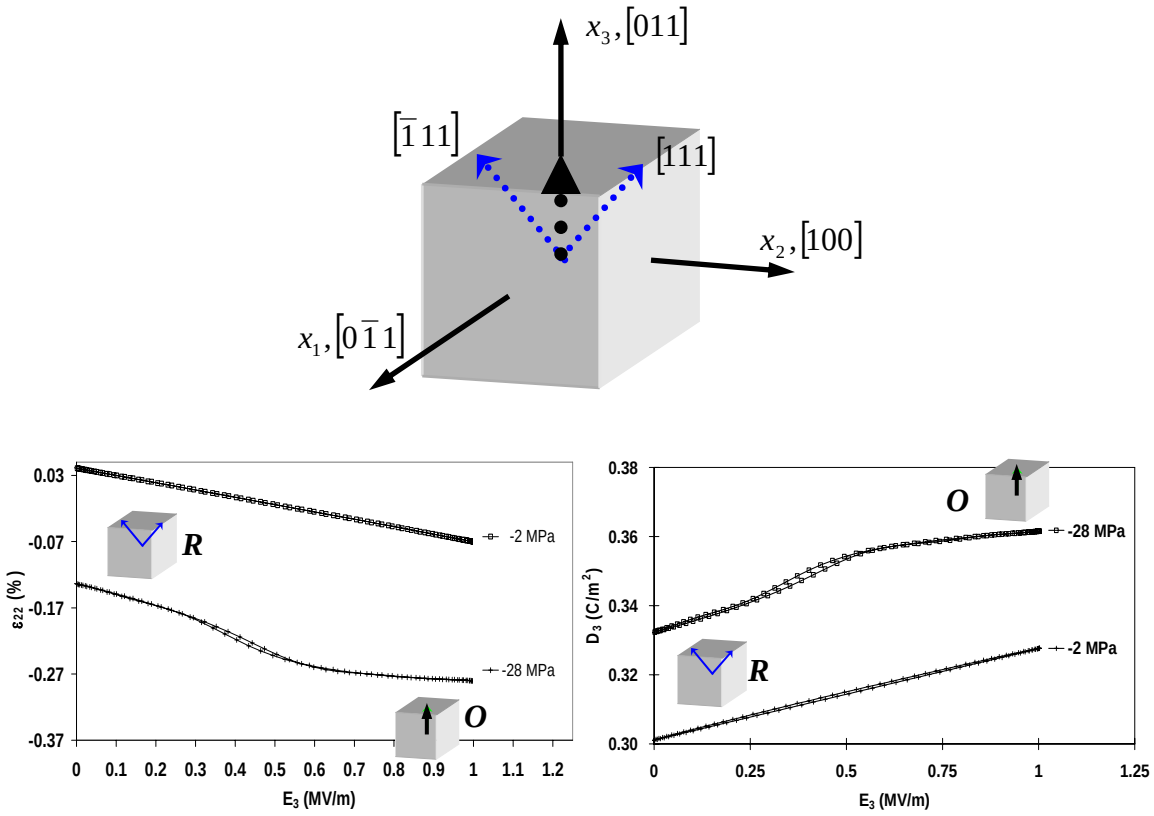

Figure 6-7. Experimental data for $[011]$ oriented PMN-0.32PT single crystal [45]. The blue dotted arrows represent the variants present in a rhombohedral single crystal poled along the $[011]$ axis and the thicker black dotted line represents an orthorhombic variant in a single crystal poled along the $[011]$ axis. Measured strain and electric displacement with inset figures showing the variant state are also shown.

From Figure 6-7 it can be seen that a phase transformation from R $\rightarrow$ O is caused by the application of stress and electric field doing sufficient work to overcome the phase transition threshold energy. Equation (6-26) represents the work per unit volume done to an isothermal ferroelectric material.

$$w = \sigma_{ij}\Delta\varepsilon_{ij} + E_m\Delta D_m \tag{6-26}$$

The phase transformation is assumed to be initiated when the measured material response deviates from linear by 5% of the slope. This point was determined for the measured data with a constant prestress value of -28MPa. Utilizing Equation (6-26) the work density required for the initiation of an $R \rightarrow O$ phase transformation in PMN-0.32PT was calculated to be $48 kJ/m^3$. Using this work density and the knowledge of the linear rhombohedral material properties, the initiation point for an $R \rightarrow O$ phase transformation can be estimated for electric field loading with no applied prestress. Using the dielectric permittivity measured from experimental data, the electric field required to cause a phase transition without applied prestress was determined to occur at $1.34 kV/mm$. Assuming that the same increase in electric displacement and strain during an $R \rightarrow O$ phase transition occurs for every prestress level, the spontaneous strain ε_{22}^{s} and polarization P_3^s can be estimated as -0.157 % and 0.337 C/m^2, respectively. This result is interesting because the spontaneous polarization of the rhombohedral phase for PMN-0.32PT was determined to be 0.365 C/m^2, making it larger than the orthorhombic phase. However, the component of the R phase along the $[011]$ axis is smaller than the spontaneous polarization of the orthorhombic phase, creating a positive phase transition driving force.

6.2.5.3 Determination of Material Properties and Phase Transition Behavior

Successful implementation of a phase transformation model into the micromechanical model through assumed spatial chemical and structural heterogeneities depends on determining complete material property tensors for the orthorhombic and tetragonal phases in addition to further experimental investigations into phase transformation behavior. For the PMN-*x*PT and PZN-*x*PT single crystal compositions

under consideration, both the orthorhombic and tetragonal phases are produced by the application of external load and are unstable in the unloaded condition.

The following discussion on the determination of material coefficients is based on quasi-static measurements of the load stable O and T phases, similar to those conducted in Chapter 3. Due to symmetry, there are 3 independent piezoelectric constants for the single-domain tetragonal phase $\left(d_{311}=d_{322}, d_{333}, d_{223}=d_{113}\right)$ and 5 independent piezoelectric constants for the single-domain orthorhombic phase $\left(d_{311}, d_{322}, d_{333}, d_{223}, d_{113}\right)$. Determination of the extensional components would require a single crystal specimen large enough to measure the longitudinal and transverse strain, simultaneously. There are various methods for measuring quasi-static strain, including strain gages and laser Doppler techniques. The shear coefficients for the O and T phases would be more difficult (potentially impossible) to experimentally determine. In order to measure the shear constants, an electric field must be applied perpendicular to the poling direction. For load stabilized phases an electric field larger than the coercive field would be required to transform the specimen into the new single-domain phase. This would repole the material in the measurement direction, thereby changing the measured material constant. Increasing the specimen temperature decreases the electric field and stress required to initiate a phase transformation in PMN-0.32PT single crystals [45, 68]. Experimental studies of $\langle 110 \rangle$ poled specimens show that with an ambient temperature of 60^{o}C in PMN-0.32PT the orthorhombic phase is present without an applied electrical of mechanical load. Although the material coefficients in a relaxor ferroelectric are temperature dependent, it can be assumed that the relative ratio between components of the piezoelectric tensor would remain constant. Measuring the material properties at an

elevated temperature could provide a complete set of piezoelectric coefficients that could be scaled by the extensional components measured at room temperature. Liu *et al.* [187] have measured the piezoelectric shear strain coefficients under a quasi-static electrical loading for $\langle 111 \rangle$ oriented PZN-0.045PT and PZN-0.08PT single crystals by a laser Doppler interferometer system using a heterodyne detection technique. This technique was able to measure shear strain at a dc bias field of approximately 14 *kV/cm*. Utilization a similar approach may allow for the measurement of shear coefficients in a heated specimen.

6.2.6 Program Flowchart

The previously developed model is represented visually by a flowchart. The interaction between each of the principle processes, calculations and decisions is shown in Figure 6-8.

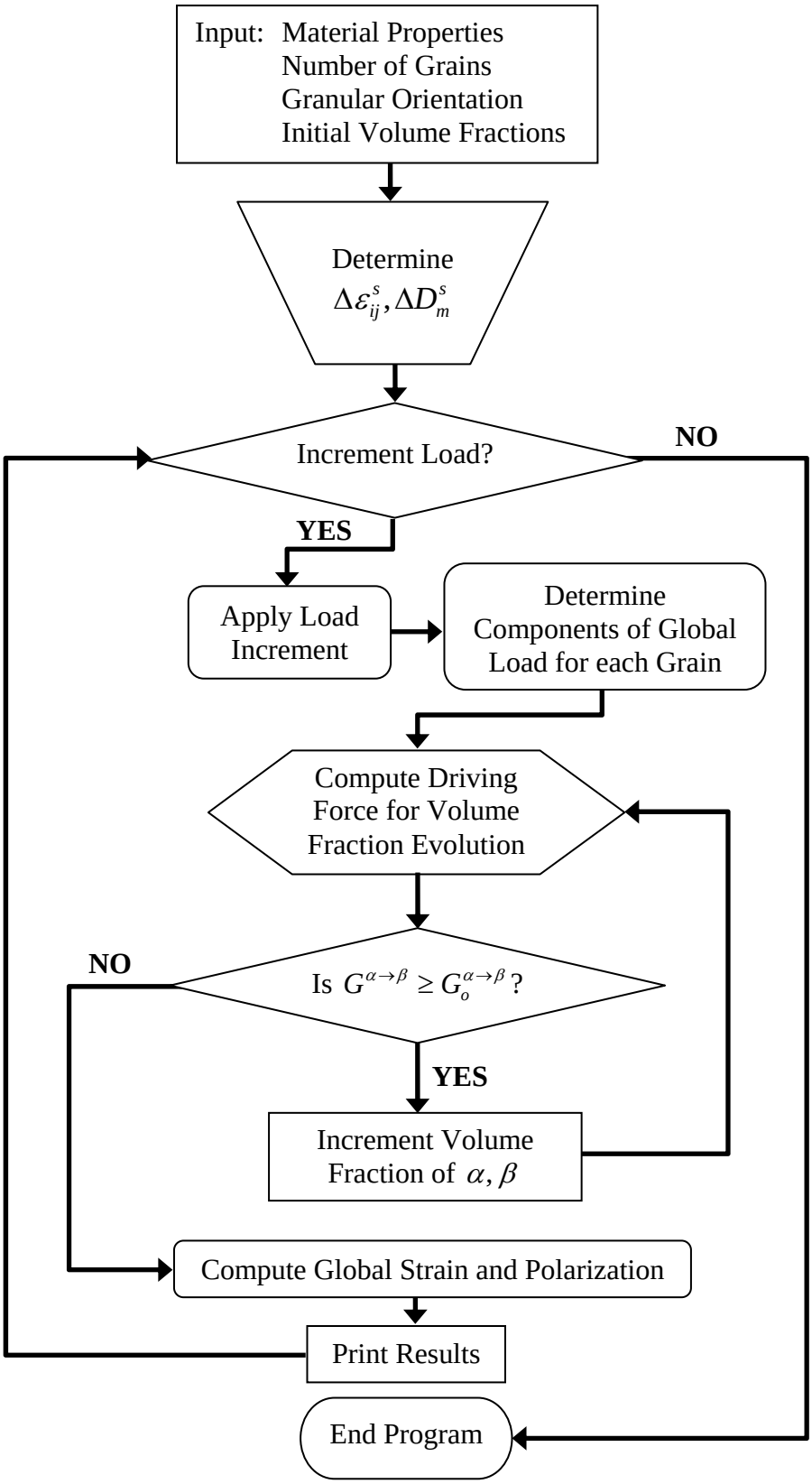

Figure 6-8. Flowchart of computational process in volume fraction evolution model utilized in the stand-alone micromechanical model program.

6.3 Single Crystal Model

The previously formulated model has been used to simulate the behavior of PMN-*x*PT and PZN-*x*PT single crystals. The simulation results are compared to experimental measurements at various orientation angles.

6.3.1 Orientation Dependence

The electromechanical response of relaxor ferroelectric single crystals such as PMN-*x*PT and PZN-*x*PT are orientation dependent. The domain states for identical single crystals with different orientations are not the same. This coupled with anisotropic material properties is the principal reason for the differences in the measured electromechanical behavior between $\langle 001 \rangle$, $\langle 011 \rangle$ and $\langle 111 \rangle$ oriented crystals. Although most experimental characterizations have focused on crystals aligned in one of those crystallographic directions (mostly $\langle 001 \rangle$ because of the larger electromechanical properties) several studies have been presented which show the measured behavior of single crystals at various off-axis orientation angles [45, 64, 66-68, 133, 134]. The presented model has been compared to the experimental measurements by Liu and Lynch [67] of PZN-0.045PT single crystals. Single crystal specimens in this study were oriented at off-axis angles of α = 0, 10, 25 and 35^{o} between the $\langle 001 \rangle$ and $\langle 111 \rangle$ orientations. Figure 6-9 shows a schematic illustrating α and x_3 which represents the poling direction.

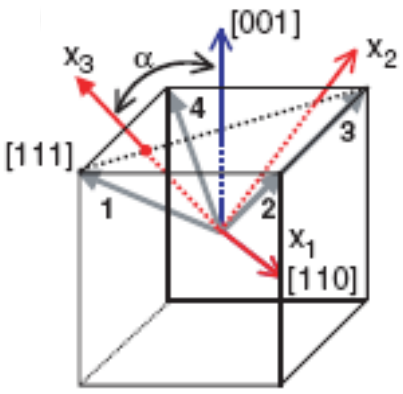

Figure 6-9. Schematic of a cubic unit cell showing how the off-axis angle was measured between the [001] and the [111] crystallographic orientations [67]. The x_3 vector represents the poling direction.

The same material properties and evolution parameters were used for all off-axis crystal simulations. The spontaneous polarization was calculated from [001] single crystal data and the spontaneous strain was assumed using the trend of measured remanent strain values from the various off-axis crystal specimens. Figure 6-10 shows the comparison of the experimental data to simulations. All simulations were compared to experimental measurements of PZN-0.045PT single crystals with a bias stress of -0.4 MPa at various crystallographic orientations. During simulations the material constants *A*, *B*, *C* and *D* were set to -0.2×10^6, 50, 0.15×10^6 and 1.0, respectively. The relative switching thresholds, n_1 and n_2, were assumed to be 10 and 1.5, respectively. The switching threshold of $n_1 = 10$ eliminated the possibility of 180^o switches. The material was found to evolve primarily through 70^o and 109^o switches.

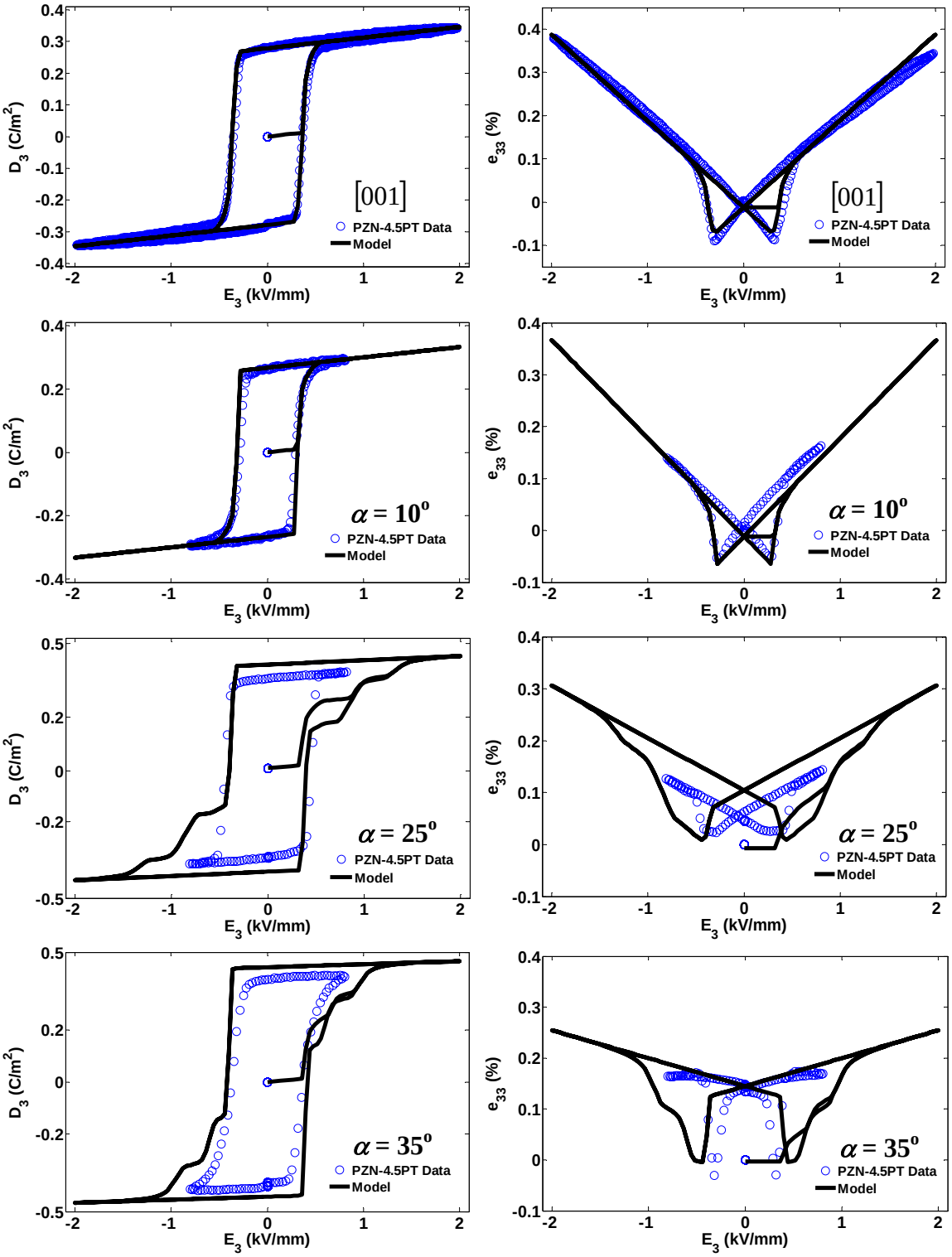

Figure 6-10. Comparison of simulations results to the measured electromechanical behavior of PZN-0.045PT single crystals. The orientation of the single crystal specimens was varied and is labeled in each plot. The blue circles are experimental data and the black line represents the simulation.

Simulations were also done for various off-axis crystal orientation of PZN-*x*PT to determine the remanent strain and linear piezoelectric properties determined by the model. Figure 6-11a shows the comparison between the experimental fit presented in Equation (6-11) to remanent strain measured in off-axis PZN-0.045PT characterizations and the model. Figure 6-11b shows contrasts the linear piezoelectric coefficient measured from experimental data and determined from simulations.

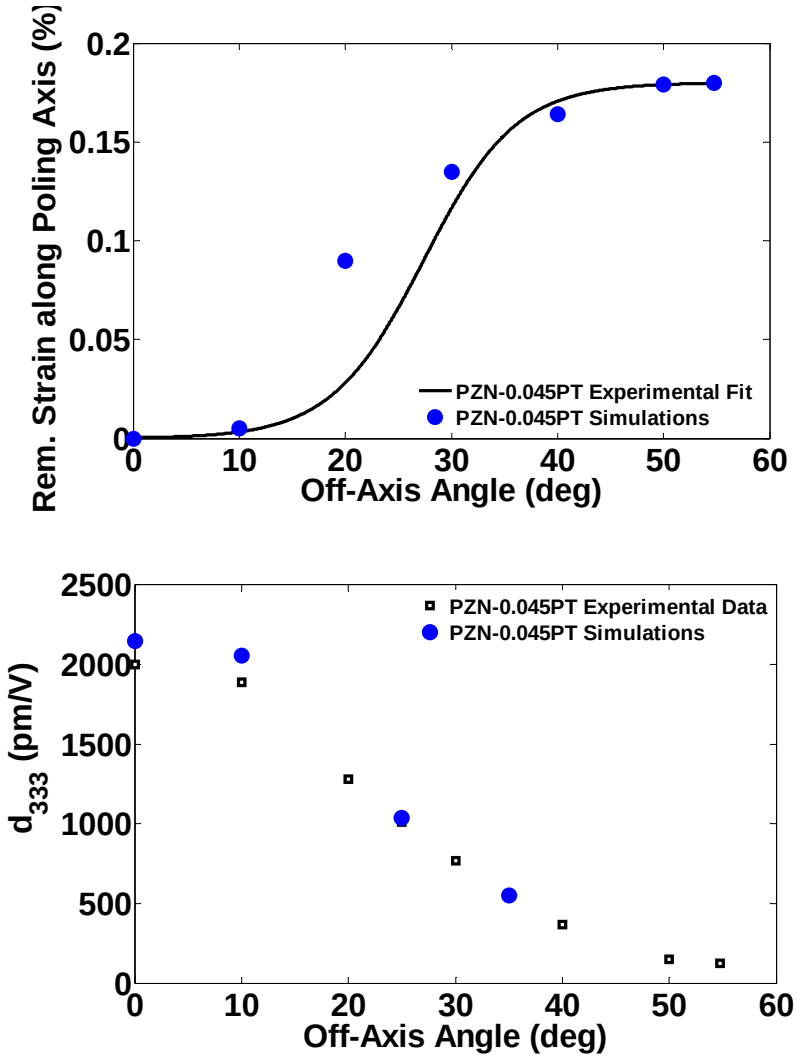

Figure 6-11. Comparison of off-axis simulations to the experimental fit of remanent strain and experimental data of linear piezoelectric coefficients.

6.3.2 Micromechanical Modeling of Phase Transformations

The phase transformation model previously presented was included in the micromechanical model to demonstrate that with further research a general, multiaxial phase transformations behavior can be implemented into a micromechanical model. The figures presented here are only possible because of the experimental measurements for domain engineered single crystal specimens by McLaughlin *et al*. [45]. These simulations represent an early effort at inclusion of the complex phenomenon of phase transitions in a micromechanical model. As previously stated, there have been no investigations that have determined a full set of material coefficients for the orthorhombic phase. In addition, the spontaneous strain and polarization must be deduced from a combination of experimental measurements and simulations. In spite of these shortcomings, the initial findings show interesting results. To tune the phase transformation portion of the micromechanical model the unipolar experiments of PMN-0.32PT were used because extensive test results of this composition are available [45, 68]. From these experimental findings, material constants for the orthorhombic phase can be assumed in addition to the initiation point of the $R \rightarrow O$ and $O \rightarrow R$ phase transitions. Figure 6-12 shows the simulation results of the bipolar electric field loading of an $[011]$ oriented PMN-0.32PT single crystal. This figure qualitatively shows that inclusion of phase transformation behavior in a micromechanical model is possible.

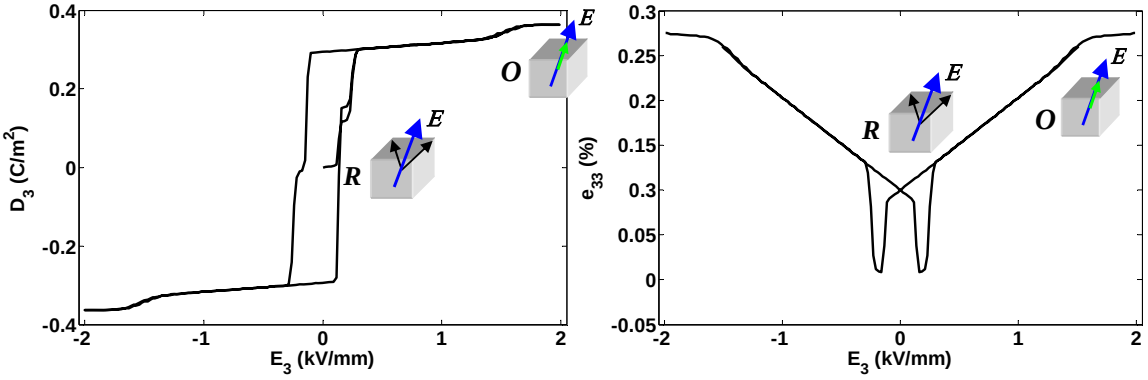

Figure 6-12. Simulation of PMN-0.32PT single crystal with $[011]$ oriented electrical loading at 0MPa prestress. Initial results show promise for further development of micromechanical model utilizing multiaxial phase transformations. Inset figures show the variants present for each phase.

The phase transformation model was able to capture the gradual diffuse phase transition behavior because domain engineered crystals were tested which enabled the direct experimental measurement of the material response in each phase. Inclusion of the phase transformation model would require the assumption of $R \leftrightarrow O$ and $R \leftrightarrow T$ phase transformations in a general, multiaxial case.

6.4 Polycrystalline Model

Extension of the single crystal model to polycrystalline materials is accomplished by modeling many individual single crystal grains. At the granular length scale a ferroelectric material is a complex network of grains, grain boundaries and inhomogeneities that cause an intricate system of interactions. In the following simulations intergranular interactions and field induced phase transformations were not assumed. In a real material, there is a complex network of local inhomogeneities that act as field concentrators. These generated local fields alter the phase transformation

behavior of each grain. An accurate representation of this behavior would require a microstructure-based finite element model that would utilize the developed micromechanical model with phase transformations along with a network of assumed inhomogeneities. Measurements of the types of inhomogeneities and their densities could potentially be obtained through electron backscatter diffraction measurements. This technique has already been used to study the thermal expansion induced microcracks in polycrystalline alumina [188]. Without the inclusion of phase transformations interesting conclusions can be drawn about the behavior of ferroelectric materials and the role of volume fraction evolution. Such simulations may help to determine the magnitude of the effect of phase transitions in a polycrystalline ferroelectric. 500 randomly oriented grains (4000 domains) were used during simulations because this was found to be greater than the minimum number of grains necessary to produce repeatable simulations of strain and electric displacement. It was found that more than approximately 300 grains produced convergence of the remanent strain and polarization values. Some elastic, piezoelectric and dielectric material properties of PMN-0.32PT single crystal specimens were previously measured [45]. These values were compared to the measured PMN-0.26PT single crystal material properties. The ratio between the material properties of PMN-0.32PT and the material parameters of the volume fraction evolution model were assumed to be the same as PMN-0.26PT single crystal specimens. During simulation of the polycrystalline material, a different threshold for switching was utilized for 70.53^{o}, 109.47^{o} and 180^{o} reorientations. It was found that assuming $n_1 = 10$ and $n_2 = 3$ to create a preference for 70.53^{o} evolution best fit experimental data.

6.4.1 Bipolar Electric Field Simulation of $[001]$ *Single Crystal PMN-0.26PT*

Simulations were completed for $[001]$ PMN-0.26PT single crystal and compared to experimental data. These simulations were done in order to determine appropriate material constants for volume fraction evolution of PMN-*x*PT single crystals of similar composition. During simulations the material constants *A*, *B*, *C* and *D* were set to -0.2 × 10^6, 50, 0.13 × 10^6 and 0.5, respectively. Figure 6-13 shows the simulations of single crystal experimental data.

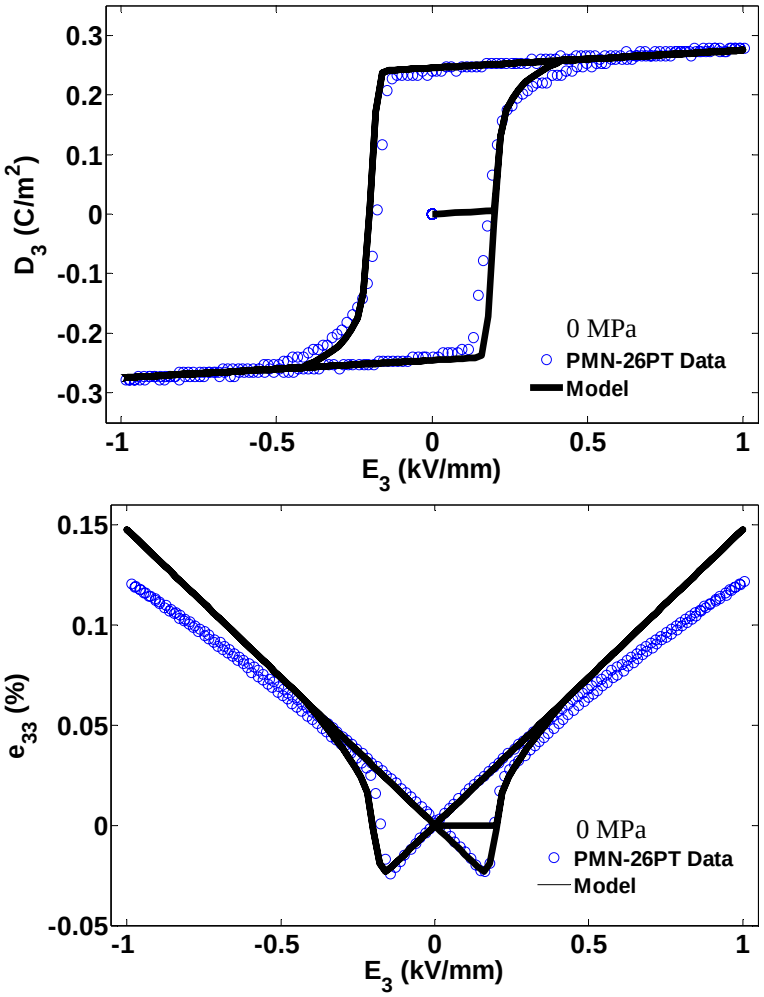

Figure 6-13. Comparison of simulations results to the measured electromechanical behavior of single crystal $[001]$ PMN-0.26PT.

6.4.2 Bipolar Electric Field Simulations of Polycrystalline PMN-0.32PT

The electromechanical response of simulated polycrystalline PMN-0.32PT to a bipolar electric field at constant bias stress were compared to experimental measurements [82]. It was found that the simulated strain and electric displacement hysteresis loops showed convergence at approximately 300 grains. During simulations 500 grains were used to ensure repeatable results. Figure 6-14 shows the comparison of the model results to experimental data.

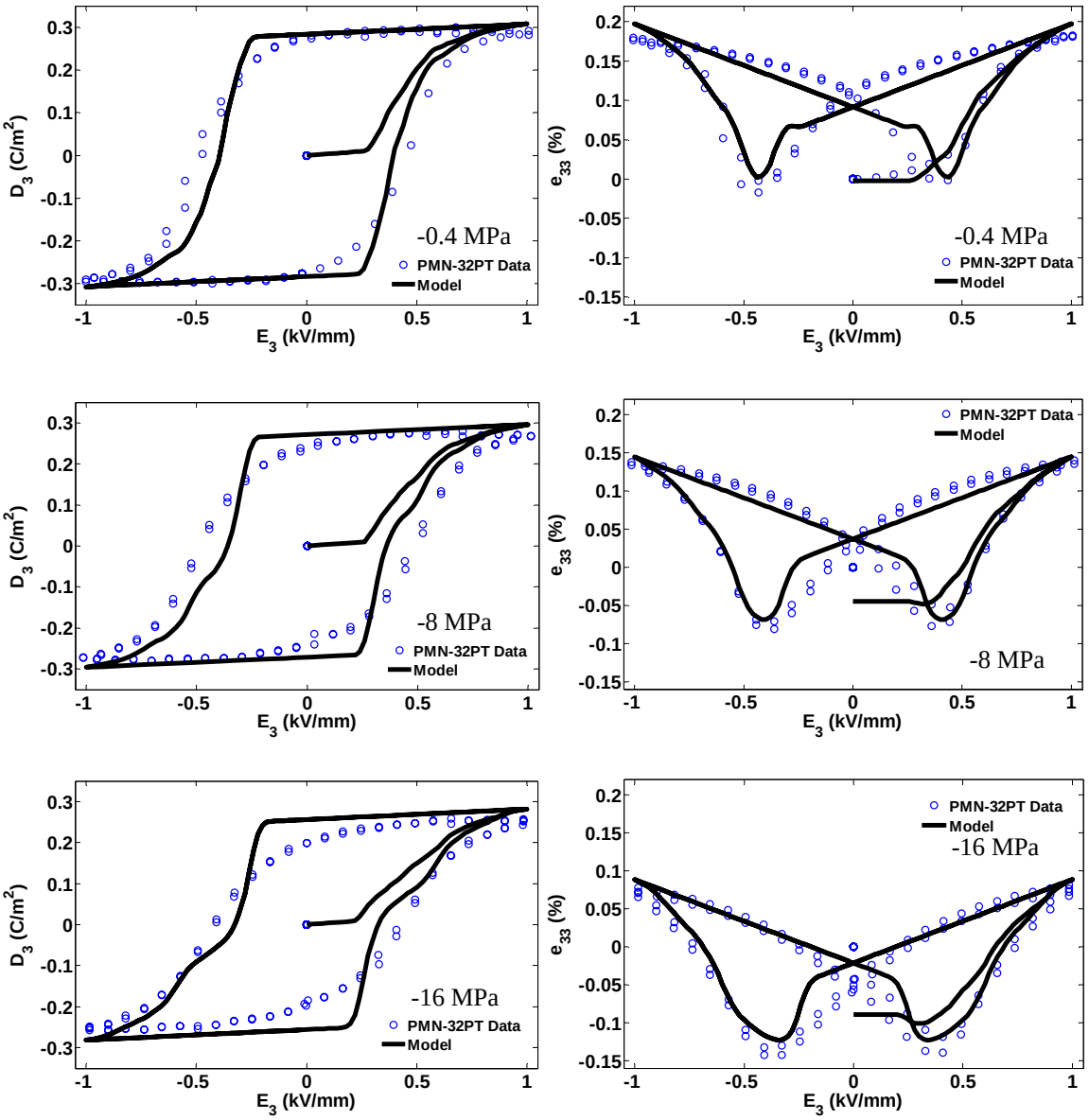

Figure 6-14. Comparison of the experimental data (blue circles) and model simulations (solid black line) for a bipolar electric field with a constant stress bias of 0 MPa (a), -8 MPa (b), and -16 MPa (c).

6.4.3 Unipolar Stress Simulations of Polycrystalline PMN-0.32PT

The electromechanical response of polycrystalline PMN-0.32PT to a unipolar compressive stress load at a constant electric field bias was simulated. During simulations electric field biases of 0, 1 and 2 times the coercive field value were applied.

The initially unpoled polycrystalline material modeled required the application of a simulated unipolar electric field to align the polar axes of each grain prior to simulated mechanical loading. If a simulated electric field was not applied prior to mechanical loading then no dielectric depoling was observed. This is a similar behavior to that observed in real ferroelectric materials. Figure 6-15 shows the simulation results. There are no experimental measurements of polycrystalline PMN-0.32PT specimens subjected to unipolar compressive stress loading for comparison to simulations.

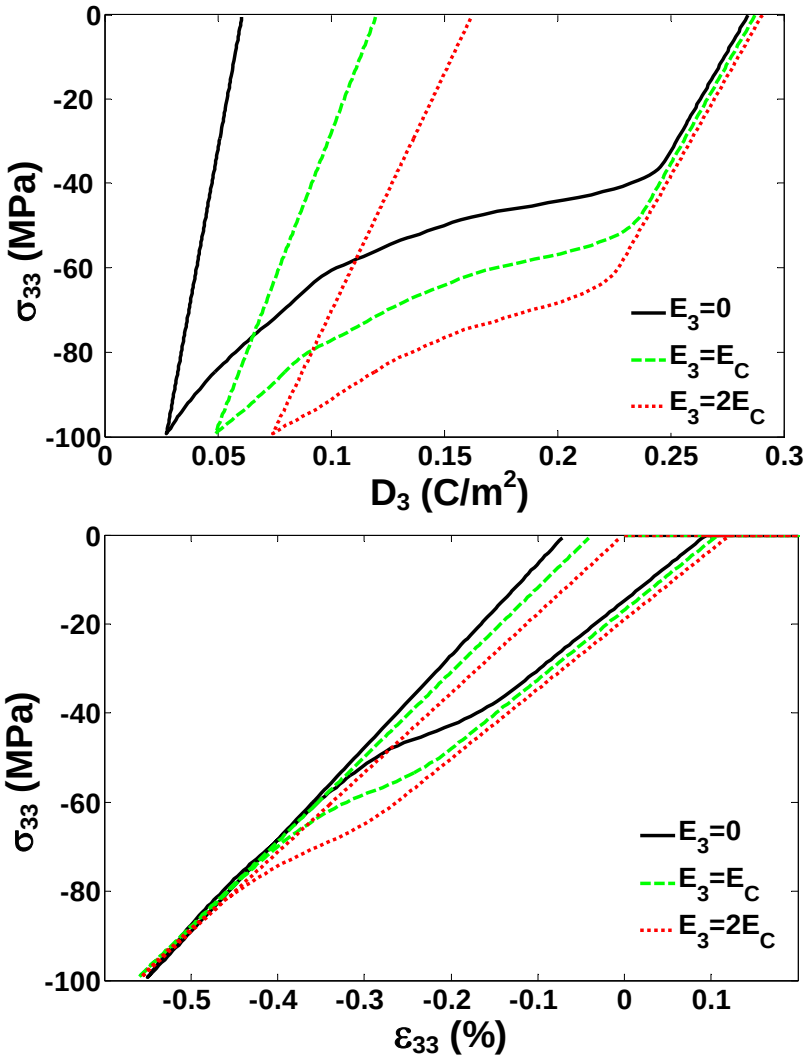

Figure 6-15. Simulations of unipolar compressive stress loading at constant electric field bias levels on the longitudinal strain (ε_{33}) and electric displacement (D_3) response of polycrystalline PMN-0.32PT.

6.5 Discussion

Volume fraction evolution in single crystal and polycrystalline ferroelectric materials is a complicated phenomenon that is dependent at multiple length scales on applied fields, local interactions, orientation and nonlinear material behaviors. The measured material coefficients of relaxor ferroelectrics have been shown to be dependent on loading orientation, load frequency and composition [45, 66-68, 133]. The proposed model utilizes a micromechanical model with volume fraction evolution scheme which makes the approximation that domains do not switch simultaneously. This model was set to accurately present experimentally measured single crystal behavior. Extension was made to polycrystalline material by volume averaging the effects of numerous randomly oriented single crystal grains. Simulations differed from experimental data; a discussion of the model follows.

Ferroelectric single crystal materials can have multiple domains simultaneously that evolve in response to applied fields and internal flaws and interactions. This is an extremely complex behavior where each domain wall type potentially moves in a different method and interactions between defects, specimen boundaries and other domains can affect the measurable response. Predicting these intricate networks of interactions is extremely difficult, if not impossible. Approximations are necessary to help account for this behavior. The presented model uses a single volume fraction evolution model that is tuned through material parameters semi-empirically fit to experimental data. The presented model is shown to be in excellent agreement with measured single crystal behavior without a complex volume fraction state. The simulations, however, only take into account the linear material properties and do not

account for interactions and lattice distortion effects which may cause some of the measured nonlinear strain response at higher electric field levels.

The single crystal model was compared to experimental measurements of electromechanical behavior PZN-0.045PT single crystals with an off-axis crystal cut. The model was shown to more correctly correspond to single crystal measurements in the $\langle 001 \rangle$ orientation. The model did not correctly predict the amount of hysteresis or the coercive field in the 25^o and 35^o crystal cuts. With reasonable accuracy, the simulated results matched the slope of the linear piezoelectric material behavior in each orientation, the remanent strain and the general shape of the hysteresis loops. The same material constants for volume fraction evolution were used in all simulations. By changing these factors, each off-axis loop could be accurately represented. This suggests that the volume fraction evolution model may be orientation dependent or a function of the current domain state. In the $\langle 001 \rangle$ orientation the domain state is stable and relatively simple as compared to the 25^o and 35^o off-axis orientations. Prediction of the current domain state for these orientations is more complicated. To account for the effects of a domain state phase field modeling would be required. An analysis of this type would be complex and computationally intensive.

Extending the single crystal model to polycrystalline materials added an additional length scale and its inherent additional interactions and nonlinear intergranular effects. Polycrystalline materials are comprised of many randomly oriented and sized single crystals that are arranged in a matrix interspersed with defects such as porosity and inclusions. In this study intergranular interactions were assumed negligible, although it was assumed that 180^o and 109.47^o switches required 10 and 3 times more work done

than 70.5^{o} switches, respectively. It can be seen from Figure 6-14 that the model accurately predicts the coercive field of the polycrystal from measured single crystal material properties. Through modeling, it has been found that by increasing the energy barriers for 180^{o} and 109.47^{o} switches the coercive field of the polycrystal is increased. This lends credence to 70.53^{o} switching dominating when each of the single crystal grains are constrained by grain boundaries and applied with local stress and electric fields created by intergranular interactions. In addition, the same domain evolution parameters used to model the single crystal specimen were used for the polycrystalline material simulations despite the compositional difference. This may have affected the domain evolution behavior and led to inaccuracies. During simulation there were no intergranular interactions or phase transformation effects included because these mechanisms are highly dependent on the local fields generated by inhomogeneities. To incorporate local inhomogeneities would obscure the domain wall motion effects and act as a curve fitting tool since the random system of interactions would be completely assumed to best fit experimental data.

It can be seen from Figure 6-14 that there was an abrupt change in electric displacement during bipolar loading as the reverse coercive field was reached. This is because the simulations utilized a single coercive field value. In real materials, even though a domain may be favorably aligned for reorientation to another spontaneous polarization direction, there is most likely a distribution of switching initiation points due to interactions at different length scales. This distribution of switching fields causes the material response to have a more gradual transition to the reverse polarization direction. There is also possibly a separate volume fraction evolution relationship for stress induced

switching. Figure 6-14 also shows a decrease in the required electric field to cause reverse polarization due to applied stress bias in the simulations. This effect is not as great as that seen in the experimental data. The unipolar stress cycle simulations in Figure 6-15 show that stress begins to cause reorientation at approximately -35 MPa. The stress bias used during experimentation was not large enough to cause stress induced depolarization. Real ferroelectric polycrystalline materials may also have local stress risers which could cause stress depoling at lower applied stress levels. The longitudinal strain experimental results show that there is a softening of the wells around the coercive field as the bias stress is increased. This region that was initially sharp becomes shallower and has less of an abrupt change as the material reverses polarization direction. The simulations also show this trend. At the highest presented bias stress level of -16 MPa the remnant strain value is slightly over-predicted. This may be due to the beginning of a phase transformation in the material. It has been previously shown that the phase transformation of $\langle 001 \rangle$ oriented PMN-0.32PT single crystals begins at approximately -15 MPa without electric field bias. It has also been shown that phase transformations can occur in various compositions of PMN-*x*PT specimens [29, 45, 68, 133, 134]. Single crystal specimens show phase transformations in response to applied fields more clearly than polycrystalline materials. This is because each grain can undergo a phase transformation at a different load level due to local interactions and random orientations. Because these effects are averaged it is possible that a phase transformation is not directly observed under low loads. Phase transformation behavior was not included in the simulation of polycrystalline or single crystal specimens.

The micromechanical model has been extended to the simulation of the longitudinal strain and electric displacement response of poled polycrystalline PMN-0.32PT to a unipolar compressive stress load with constant electric field bias levels. Simulations were done with the same volume fraction evolution model that was utilized to in bipolar electric field loading. It is possible that the reorientation behavior of domains is dependent on the type of loading applied. There are potentially internal interactions which may be affected differently by stress than electric field, changing the switching behavior. Experimental measurements of the velocity of domain walls in gadolinium molybdate [61] have shown that the ratio of stress driven domain wall mobility to the electric field driven domain wall mobility were equal to the ratio of the spontaneous strain to the spontaneous polarization, lending credibility to the previous statement. The simulations in Figure 6-15 show that when no electric field bias is present the specimen begins depoling at approximately -35 MPa. Complete depolarization occurred at approximately -130 MPa. The presence of an electric field however causes some of the domains to reorient upon the release of the mechanical load.

The presented model correlates well with experimental measurements of single crystal specimens. Utilization of the single crystal model to simulate polycrystalline behavior shows good predictive capabilities. The model was able to predict the behaviors of the polycrystal during electromechanical loading. This model is intended to further the understanding of domain volume fraction evolution and the effects on polycrystalline behavior.

6.6 Concluding Remarks

A micromechanical model has been presented which takes into account volume fraction evolution at the grain length scale in relaxor ferroelectric materials. Each grain was assumed to evolve independently and without interaction in order to show the volume fraction evolution of single crystal on polycrystalline materials. It was assumed that the evolution of one domain to each of the possible other domains progressed identically. This model has been shown to be in good agreement with single crystal and polycrystalline experimental data.

CHAPTER 7

MAJOR CONCLUSIONS

The development of relaxor ferroelectric single crystals exhibiting exceptional electromechanical properties has led to their utilization in many high-performance engineered structures. In addition to excellent material properties nonlinear, hysteric constitutive and phase transformation behavior has been observed. The complexity of the nonlinear behavior has motivated the presented research.

In Chapter 3 an improved experimental technique for measuring quasi-static constitutive behavior of ferroelectric materials was presented. This technique was able to reduce (or possibly eliminate) the clamping effects experienced during compressive stress loading by stacking three equally sized specimens and measuring strain only from the center specimen. Experimental measurements of the electromechanical behavior of single crystal $\langle 001 \rangle$ PMN-0.26PT and polycrystalline PMN-0.32PT were presented. These data showed that the polycrystalline materials exhibited increased hysteresis and lower electromechanical couplings. This difference was postulated to be due to the local network of inhomogeneities and random granular orientation not present in a single crystal. These experimental measurements served as the basis for modeling efforts.

In Chapter 4 the experimental measurements taken at NUWC for two compositions of single crystal $\langle 001 \rangle$ PMN-*x*PT were analyzed. These data provided three-dimensional surface plots of the constitutive and phase transition behavior. The compositional dependence of relaxor ferroelectric materials was shown. As the

composition of PT decreases in PMN-*x*PT single crystals phase transformations were shown to have an increased energy threshold and lower linear compliance, piezoelectric and dielectric material properties.

In Chapter 5 a model of the field driven continuous phase transformations observed in relaxor ferroelectric single crystals was presented. This model assumed that relaxor ferroelectric phase transition behavior was caused by spatial chemical and structural heterogeneity at the nanometer length scale. Through the inclusion of a work-energy analysis combined electromechanical loading was simulated. Knowledge of the complete single-domain material coefficients were not required as the material properties were measured directly from experimental data. This work simulated the observed continuous phase transitions exceptionally well and suggests that phase transformations are initiated when externally applied work reaches a critical value.

In Chapter 6 a volume fraction evolution micromechanical model was presented. Experimental results for single crystal specimens show non-instantaneous domain switching due to domain wall motion. This prompted the development of a volume fraction evolution model for single crystal materials. The model was developed from measured single-domain compliance, piezoelectric and dielectric material properties, not from material properties assumed from measurement of polycrystalline specimens. The single crystal experimental results from Chapter 3 were used to tune the evolution parameters. Utilizing this information, measured polycrystalline data from a similar composition were simulated. There was no inclusion of intergranular interactions, as this would have served as a fitting parameter and obscured the effects of the volume fraction

evolution. It was shown that the use of single-domain material properties could be used to accurately represent polycrystalline behavior.

The results presented from this research proved an improved understanding of the nonlinear polarization evolution and phase transformation behavior in relaxor ferroelectrics. The experimental measurements and subsequent analytical analysis furthered the understanding of the phase transition behavior and the effects of mechanisms in polycrystalline materials. The developed models gave theoretical insight into the mechanisms governing continuous phase changes and volume fraction evolution in relaxor ferroelectrics.

Open Issues

Although relaxor ferroelectric materials have been known of for over 50 years, there is still much yet to be understood about their behavior and the underlying mechanisms which cause it. There have been numerous experimental studies that have sought to understand the micro- and meso-scale structures through high resolution X-ray powder and neutron diffraction [189-195], piezoresponse force microscopy [196-202] and transmission electron microscopy [203, 204]. This experimental data is vital to unlocking the secrets of ferroelectric material behavior.

The presented dissertation has identified several important directions for future study. Firstly, the electric field and stress induced phase transformation behavior presented in Chapters 3 and 4 assumed the phase during mechanical and electrical loading from knowledge of the crystallographic orientation. These assumptions must be confirmed through diffraction studies of ferroelectric single crystals with external loads

in the same crystallographic orientations. Recent work has investigated the evolution of the domain structure and phases in poled and unpoled PZN-0.045PT during cooling from an increased temperature with neutron diffraction [194]. A similar study that considered the effects of external stress and electric field is needed.

Secondly, it has been shown that external fields can initiate orientation and composition dependent phase transitions in relaxor ferroelectric materials. However, the single-domain material properties of the load stable O and T phases have not been satisfactorily experimentally identified. At present there has been relatively few material coefficients experimentally determined for these load stable phases. Because of the low symmetry in the O phase, complex measurements will be likely be required during simultaneous multi-field loading. It has been shown in Chapter 6 that the presented phase transformation model can be implemented into the micromechanical model. Prediction of the multi-axial phase transformation behavior that would be required for a general micromechanical model would be complex and require comparison to phase field modeling.

Thirdly, the compositional dependence of relaxor ferroelectric PMN-*x*PT was illustrated in Chapter 4. Presently, this study is limited by the number of experimental data available. The model of the continuous field-driven phase transformations presented in Chapter 5 has shown excellent agreement with experimental data and predictive capabilities. Single crystal $\langle 001 \rangle$ oriented PMN-0.26PT data has been presented in Chapter 3. Utilizing previous single crystal PMN-0.32PT experimental data [68], it may be possible to extend this model to include compositional effects and could produce the

predictive ability to determine a map of the linear material coefficients through the $R \rightarrow O$ phase transformation as a function of composition and applied load.

Fourthly, much remains to be discovered about the complex phenomena of domain wall motion. There have been limited studies that measured the velocity of a domain wall in response to external fields. Flippen [61] qualitatively measured the velocity of a domain wall as a function of applied electric field and stress in gadolinium molybdate. It was shown that the ratio of stress driven domain wall mobility to the electric field driven domain wall mobility was equal to the ratio of the spontaneous strain to the spontaneous polarization. Lupascu *et al.* [205, 206] have studied ferroelectric/ferroelastic domain wall motion in gadolinium molybdate through the analysis of the discontinuities in the switching current, the ferroelectric Barkhausen pulses and in the acoustic emissions. Tikhomirov [207] was able to make optical measurements of an individual ferroelectric/ferroelastic domain wall oscillation due to a bipolar electric field in gadolinium molybdate. It was shown that oscillations were reduced to zero when the temperature was increased to the phase transition temperature. There have been promising phenomenological finite element-based domain wall motion models that have considered the effect of defects [115-117] and domain walls with finite thickness [208]. Further experimental work is required on the motion of domain walls in relaxor ferroelectric materials, especially in the vicinity of singularities, to expand these analytical studies. These measurements are crucial for creating an accurate constitutive model.

Finally, despite everything that is known about polycrystalline ferroelectric there is still more work needed to understand the effects of grain boundaries on switching and

phase transformations in ferroelectric polycrystalline materials. The micromechanical model developed from single crystal data presented in Chapter 6 showed good correlation with polycrystalline data of a similar composition. In this model, volume fraction evolution was included while phase transitions were excluded. Additional studies are required on the effects of constrained boundaries on phase transformations. It is possible that grain boundaries have a reduced effect on switching because of the presence of domains.

REFERENCES

1. Valasek, J., *Piezo-electric and Allied Phenomena in Rochelle Salt.* Phys. Rev., 1921. **17**: p. 475-481.

2. von Hippel, A., R.G. Breckenridge, F.G. Chesley, and L. Tisza, *High dielectric constant ceramics.* Ind. Eng. Chem., 1946. **38**(11): p. 1097-109.

3. Wul, B.M. and I.M. Goldman, *Dielectric constants of titanates of metals of the second group.* Dokl. Akad. Nauk SSSR, 1945. **46**: p. 154-57.

4. Jaffe, B., R.S. Roth, and S. Marzullo, *Properties of piezoelectric ceramics in solid-solution series lead titanate-lead zirconate-lead oxide: tin oxide and lead titanate-lead hafnate.* United States Bureau of Standards -- Journal of Research, 1955. **55**(5): p. 239-254.

5. Crawford, A.E., *Lead zirconate piezoelectric ceramics.* British Communications and Electronics, 1959. **6**(7): p. 516-519.

6. Jaffe, B., W.R. Cook, and H. Jaffe, *Piezoelectric Ceramics* 1971, London: New York, Academic Press.

7. Liu, X., E.F. McCandlish, L.E. McCandlish, K. Mikulka-Bolen, R. Ramesh, F. Cosandey, G.A. Rossetti Jr, and R.E. Riman, *Single-crystal-like materials by the self-assembly of cube-shaped lead zirconate titanate (PZT) microcrystals.* Langmuir, 2005. **21**(8): p. 3207-3212.

8. Smolenskii, G.A. and A.I. Agranovskii, *Dielectric polarization of number of complex compounds.* Soviet Physics -- Solid State, 1960. **1**(10): p. 1429-1437.

9. Smolenskii, G.A., V.A. Isupov, A.I. Agranovyskaya, and N.N. Krainik, *New ferroelectrics of complex composition, IV.* Soviet Physics - Solid State, 1961. **2**(11): p. 2651-2654.

10. Kamzina, L.S., N.N. Krainik, G.A. Smolensky, and V.A. Trepakov, *Photoinduced phenomena in lead magnesium niobate crystal at the diffuse phase transition.* Ferroelectrics, 1976. **18**(1-3): p. 113-116.

11. Bonner, W.A., E.F. Dearborn, J.E. Geusic, H.M. Marcos, and L.G. Van Uitert, *Dielectric and electro-optic properties of lead magnesium niobate.* Appl. Phys. Lett., 1967. **10**(5): p. 163-165.

12. Cross, L.E., S.J. Jang, R.E. Newnham, S. Nomura, and K. Uchino, *Large electrostrictive effects in relaxor ferroelectrics.* Ferroelectrics, 1980. **23**(3-4): p. 187-191.

13. Jang, S.J., K. Uchino, S. Nomura, and L.E. Cross, *Electrostrictive behavior of lead magnesium niobate based ceramics.* Ferroelectrics, 1979. **27**(1/4): p. 31-34.

14. Jang, S.J., K. Uchino, S. Nomura, and L.E. Cross, *Electrostrictive behavior of lead magnesium niobate based ceramic dielectrics.* Ferroelectrics, 1979. **27**(1/4): p. 31-34.

15. Pan, W.Y., W.Y. Gu, D.J. Taylor, and L.E. Cross, *Large piezoelectric effect induced by direct current bias in PMN:PT relaxor ferroelectric ceramics.* Japanese Journal of Applied Physics, Part 1: Regular Papers & Short Notes, 1989. **28**(4): p. 653-661.

16. Choi, S.W., T.R. Shrout, S.J. Jang, and A.S. Bhalla, *Morphotropic phase boundary in $Pb(Mg_{1/3}Nb_{2/3})O_3$-$PbTiO_3$ system.* Mater. Lett., 1989. **8**(6-7): p. 253-255.

17. Smolenskii, G.A. and A.I. Agranovskii, *Dielectric polarization of number of complex compounds.* Soviet Physics -- Solid State, 1960. **1**(10): p. 1429-1437.

18. Nomura, S., M. Yonezawa, K. Doi, S. Nanamatsu, N. Tsubouchi, and M. Takahashi, *Crystal structure and piezoelectric properties of $Pb(Zn_{1/3}Nb_{2/3})O_3$-$PbTiO_3$ solid solution.* NEC Research & Development, 1973(29): p. 15-21.

19. Yonezawa, M., K. Doi, S. Nanamatsu, N. Tsubouchi, M. Takahashi, and S. Nomura, *Crystal structure and piezoelectricity of the system $Pb(Zn_{1/3}Nb_{2/3})O_3$-$PbTiO_3$.* 1969. **16**(6): p. 253-8.

20. Kuwata, J., K. Uchino, and S. Nomura, *Phase transitions in the $Pb(Zn_{1/3}Nb_{2/3})O_3$-$PbTiO_3$ system.* Ferroelectrics, 1981. **37**(1-4 Pt 3): p. 579-582.

21. Kuwata, J., K. Uchino, and S. Nomura, *Dielectric and piezoelectric properties of $0.91Pb(Zn_{1/3}Nb_{2/3})O_3$-$0.09PbTiO_3$ single crystals.* Japanese Journal of Applied Physics, Part 1: Regular Papers & Short Notes, 1982. **21**(9): p. 1298-1302.

22. Park, S.-E. and T.R. Shrout, *Characteristics of relaxor-based piezoelectric single crystals for ultrasonic transducers.* IEEE Transactions on Ultrasonics, Ferroelectrics, and Frequency Control, 1997. **44**(5): p. 1140-1147.

23. Lopath, P.D., S.-E. Park, K.K. Shung, and T.R. Shrout. *Ultrasonic transducers using piezoelectric single crystal perovskite*. 1996. East Brunswick, NJ, USA: IEEE, Piscataway, NJ, USA.

24. Nye, J.F., *Physical properties of crystals: their representation by tensors and matrices*. 1967, London: Oxford University Press, Oxford.

25. *IEEE Standard Definitions of Primary Ferroelectric Terms.* ANSI/IEEE Std 180-1986.

26. Smolenskii, G.A., *Physical Phenomena in Ferroelectrics with Diffused Phase Transition.* J. Phys. Soc. Jpn., 1970. **28**: p. 26.

27. Nomura, S. and K. Uchino, *Recent Applications of PMN-Based Electrostrictors.* Ferroelectrics, 1983. **50**(1-4): p. 197-202.

28. Kuwata, J., K. Uchino, and S. Nomura, *Phase transitions in the $Pb(Zn_{1/3}Nb_{2/3})O_3$ -$PbTiO_3$ system* Ferroelectrics, 1981. **37**(1-4): p. 579-582.

29. Park, S.E. and T.R. Shrout, *Ultrahigh strain and piezoelectric behavior in relaxor based ferroelectric single crystals.* J. Appl. Phys., 1997. **82**(4): p. 1804-1811.

30. Haertling, G.H., *Ferroelectric ceramics: history and technology.* J. Am. Ceram. Soc., 1999. **82**(4): p. 797-818.

31. Harada, K., S. Shimanuki, T. Kobayashi, S. Saitoh, and Y. Yamashita, *Crystal growth and electrical properties of $Pb[(Zn_{1/3}Nb_{2/3})_{0.91}$-$Ti_{0.09}]O_3$ single crystals produced by solution Bridgman method.* J. Am. Ceram. Soc., 1998. **81**(11): p. 2785-2788.

32. Harada, K., S. Shimanuki, T. Kobayashi, S. Saitoh, and Y. Yamashita, *Growth of $Pb[(Zn_{1/3}Nb_{2/3})_{0.91}$-$Ti_{0.09}]O_3$ single crystal of ultrasonic transducer for medical application* J. Intell. Mater. Syst. Struct., 2000. **10**(6): p. 493-497.

33. Harada, K., S. Shimanuki, T. Kobayashi, Y. Yamashita, and S. Saitoh, *Growth of high-quality $Pb[(Zn_{1/3}Nb_{2/3})_{0.91}$-$Ti_{0.09}]O_3$ single crystals by excess ZnO addition.* J. Am. Ceram. Soc., 2002. **85**(1): p. 145-149.

34. Kobayashi, T., S. Saitoh, K. Harada, S. Shimanuki, and Y. Yamashita, *Growth of large and homogeneous PZN-PT single crystals for medical ultrasonic array transducers.* IEEE International Symposium on Applications of Ferroelectrics, 1998: p. 235-238.

35. Kobayashi, T., S. Shimanuki, S. Saitoh, and Y. Yamashita, *Improved Growth of Large Lead Zinc Niobate Titanate Piezoelectric Single Crystals for Medical Ultrasonic Transducers.* Jpn. J. Appl. Phys., 1997. **36**(9B): p. 4.

36. Kuwata, J., K. Uchino, and S. Nomura, *Dielectric and piezoelectric properties of $0.91Pb(Zn_{1/3}Nb_{2/3})O_3$ -$0.09PbTiO_3$ single crystals* Jpn. J. Appl. Phys., 1982. **21**(9): p. 1298-1302.

37. Bhaumik, I., G. Singh, S. Ganesamoorthy, A.K. Karnal, M.K. Tiwari, and V.S. Tiwari, *Compositional variation in 0.65 $PbMg_{2/3}Nb_{1/3}O_3$- $0.35PbTiO_3$ single crystals grown by high temperature solution growth technique.* Cryst. Res. Technol., 2007. **42**(4): p. 356-360.

38. Karaki, T., M. Adachi, Y. Hosono, and Y. Yamashita, *Distribution of piezoelectric properties in $Pb[(Mg_{1/3}Nb_{2/3})_{0.7}Ti_{0.3}]O_3$ single crystal.* Jpn. J. Appl. Phys., 2002. **41**(4 A): p. 402-404.

39. Ye, Z.G., *Crystal chemistry and domain structure of relaxor piezocrystals.* Curr. Opin. Solid State Mater. Sci., 2002. **6**(1): p. 35-44.

40. Oates, W.S., *Fracture of Ferroelectric Materials*. PhD Dissertation, 2004, The Georgia Institute of Technology.

41. La Orauttapong, D., B. Noheda, G. Ye, P.M. Gehring, J. Toulouse, D.E. Cox, and G. Shirane, *Phase diagram of the relaxor ferroelectric $(1-x)Pb(Zn_{1/3}Nb_{2/3})O_3$-$xPbTiO_3$* Phys. Rev. B: Condens. Matter, 2002. **65**: p. 144101.

42. Liu, T. and C. Lynch, *Characterization and Modeling of Relaxor Single Crystals.* Integ. Ferroelectr., 2005. **71**: p. 173.

43. Liu, T. and C.S. Lynch. *Phase field simulation of ferroelectric and antiferroelectric single crystals*. 2006. San Diego, CA, USA: Proc. SPIE Int. Soc. Opt. Eng.

44. Lines, M.E. and A.M. Glass, *Principles and Applications of Ferroelectric and Related Materials*. 1977, Oxford: Clarendon Press.

45. McLaughlin, E.A., T. Liu, and C.S. Lynch, *Relaxor ferroelectric PMN-32%PT crystals under stress and electric field loading: I-32 mode measurements.* Acta Mater., 2004. **52**(13): p. 3849-3857.

46. Liu, T., *Electromechanical Behavior of Relaxor Ferroelectric Crystals*. PhD Dissertation, 2004, The Georgia Institute of Technology.

47. Noheda, B., D.E. Cox, G. Shirane, Z.-G. Ye, and J. Gao, *Phase diagram of the ferroelectric relaxor $(1-x)PbMg_{1/3}Nb_{2/3}O_3$-$xPbTiO_3$.* Phys. Rev. B: Condens. Matter, 2002. **66**: p. 054104-1-10.

48. Singh, A.K. and D. Pandey, *Structure and the location of the morphotropic phase boundary region in $(1 - x)[Pb(Mg_{1/3}Nb_{2/3})O_3]$-$xPbTiO_3$.* J. Phys.: Condens. Matter, 2001. **13**(48): p. 931-936.

49. Singh, A.K. and D. Pandey, *Evidence for M_B and M_C phases in the morphotropic phase boundary region of $(1-x)[Pb(Mg_{1/3}Nb_{2/3})O_3]$-$xPbTiO_3$: A Rietveld study* Phys. Rev. B: Condens. Matter, 2003. **67**(6): p. 064102.

50. Bai, F., N. Wang, J. Li, D. Viehland, P.M. Gehring, G. Xu, and G. Shirane, *X-ray and neutron diffraction investigations of the structural phase transformation sequence under electric field in $0.7Pb(Mg_{1/3}Nb_{2/3})$-$0.3PbTiO_3$ crystal.* J. Appl. Phys., 2004. **96**(3): p. 1620-1627.

51. Cao, H., J.-F. Li, and D. Viehland, *Electric-field-induced orthorhombic to monoclinic MB phase transition in [111] electric field cooled Pb ($Mg_{1/3}Nb_{2/3}O_3$) - 30%PbTi O_3 crystals.* J. Appl. Phys., 2006. **100**(8): p. 084102.

52. Noheda, B., D.E. Cox, and G. Shirane, *Low symmetry phases in piezoelectric systems: PZN-xPT single crystal and powder.* Ferroelectrics, 2002. **267**: p. 147-155.

53. Noheda, B., D.E. Cox, G. Shirane, S.E. Park, L.E. Cross, and Z. Zhong, *Polarization rotation via a monoclinic phase in the piezoelectric 92%$PbZn_{1/3}Nb_{2/3}O_3$-8%$PbTiO_3$.* Phys. Rev. Lett., 2001. **86**(17): p. 3891-3894.

54. Lima-Silva, J.J., I. Guedes, J. Mendes Filho, A.P. Ayala, M.H. Lente, J.A. Eiras, and D. Garcia, *Phase diagram of the relaxor (1-x)Pb($Zn_{1/3}Nb_{2/3}$)O_3-x$PbTiO_3$ investigated by dielectric and Raman spectroscopies.* Solid State Commun., 2004. **131**: p. 111.

55. Zhang, S., S.-M. Lee, D.-H. Kim, H.-Y. Lee, and T.R. Shrout, *Electromechanical properties of PMN-PZT piezoelectric single crystals near morphotropic phase boundary compositions.* J. Am. Chem. Soc., 2007. **90**(12): p. 3859-3862.

56. Zhang, S., S.-M. Lee, D.-H. Kim, H.-Y. Lee, and T.R. Shrout, *Temperature dependence of the dielectric, piezoelectric, and elastic constants for Pb ($Mg_{1/3}Nb_{2/3}$)O_3 -$PbZrO_3$ -$PbTiO_3$ piezocrystals.* J. Appl. Phys., 2007. **102**(11): p. 114103.

57. Mauck, L.D., *The role of rate dependence and dissipation in the constitutive behavior of ferroelectric ceramics for high power applications*. PhD Dissertation, 2002, The Georgia Institute of Technology.

58. Eshelby, J.D., *The equation of motion of a dislocation.* Phys. Rev., 1953. **90**: p. 248-255.

59. Frank, F.C., *On the equations of motion of crystal dislocations.* Proc. Phys. Soc.: Sec. A, 1949. **62**: p. 131-135.

60. Webber, K.G., R. Zuo, and C.S. Lynch, *Ceramic and Single Crystal (1-x)PMN-xPT Constitutive Behavior under Combined Stress and Electric Field Loading.* Acta Mater., 2008. **56**(6): p. 1219-1227.

61. Flippen, R.B., *Domain wall dynamics in ferroelectric/ferroelastic molybdates.* J. Appl. Phys., 1975. **46**(3): p. 1068-1071.

62. Li, S., A.S. Bhalla, R.E. Newnham, and L.E. Cross, *90 deg domain reversal in Pb(Zr_xTi_{1+x})O_3 ceramics.* J. Mater. Sci., 1994. **29**(5): p. 1290-1294.

63. Ozgul, M., *Polarization switching and fatigue anisotropy in relaxor-lead titanate ferroelectric single crystals*. PhD Dissertation, 2003, The Pennsylvania State University

64. Liu, T. and C.S. Lynch, *Ferroelectric properties of [110], [001] and [111] poled relaxor single crystals: measurements and modeling.* Acta Mater., 2003. **51**(2): p. 407-416.

65. Liu, S.F., S.E. Park, T.R. Shrout, and L.E. Cross, *Electric field dependence of piezoelectric properties for rhombohedral 0.955Pb($Zn_{1/3}Nb_{2/3}$)O_3- 0.045$PbTiO_3$ single crystals.* J. Appl. Phys., 1999. **85**(5): p. 2810.

66. Liu, T. and C.S. Lynch, *Orientation dependence of nonlinearity and hysteresis in PZN-4.5%PT single crystals I: Unipolar response.* J. Intell. Mater. Syst. Struct., 2006. **17**(11): p. 953-957.

67. Liu, T. and C.S. Lynch, *Orientation dependence of nonlinearity and hysteresis in PZN-4.5%PT single crystals II: Bipolar electromechanical response.* J. Intell. Mater. Syst. Struct., 2006. **17**(10): p. 931-937.

68. McLaughlin, E.A., T. Liu, and C.S. Lynch, *Relaxor ferroelectric PMN-32%PT crystals under stress, electric field and temperature loading: II-33 mode measurements.* Acta Mater., 2005. **53**(14): p. 4001-4008.

69. Ujiie, R. and K. Uchino. *Dynamical domain observation in relaxor ferroelectrics*. 1990. Honolulu, HI, USA: Ultrasonics Symposium Proceedings.

70. Berlincourt, D. and H.H.A. Krueger, *Domain processes in lead titanate zirconate and barium titanate ceramics* J. Appl. Phys., 1959. **30**(11): p. 1804-1810.

71. Cao, H. and A.G. Evans, *Nonlinear deformation of ferroelectric ceramics.* J. Am. Chem. Soc., 1993. **76**(4): p. 890-896.

72. Chen, W. and C.S. Lynch, *Multiaxial constitutive behavior of ferroelectric materials.* J. Eng. Mater. Technol., 2001. **123**(2): p. 169-175.

73. Huber, J.E., J. Shieh, and N.A. Fleck. *Multiaxial response of hard and soft ferroelectrics under stress and electric field*. 2002. San Diego, CA, United States: Proc. SPIE Int. Soc. Opt. Eng.

74. Lynch, C.S., *The effect of uniaxial stress on the electro-mechanical response of 8/65/35 PLZT.* Acta Mater., 1996. **44**(10): p. 4137-4148.

75. Zhou, D., M. Kamlah, and B. Laskewitz. *Multi-axial non-proportional polarization rotation tests of soft PZT piezoceramics under electric field loading*. 2006. San Diego, CA, USA: Proc. SPIE Int. Soc. Opt. Eng.

76. Fett, T., D. Munz, and G. Thun, *Stress-strain behaviour of a soft PZT ceramic under tensile and compression loading and a transverse electric field.* Ferroelectrics, 2003. **297**: p. 83-90.

77. Fett, T., D. Munz, and G. Thun, *Multiaxial deformation behavior of PZT from torsion tests.* J. Am. Chem. Soc., 2003. **86**(8): p. 1427-1429.

78. Zhou, D., M. Kamlah, and D. Munz, *Effects of uniaxial prestress on the ferroelectric hysteretic response of soft PZT.* J. Eur. Ceram. Soc., 2005. **25**(4): p. 425-432.

79. Zhou, D., M. Kamlah, and D. Munz, *Effects of bias electric fields on the non-linear ferroelastic behavior of soft lead zirconate titanate piezoceramics.* J. Am. Chem. Soc., 2005. **88**(4): p. 867-874.

80. Huber, J.E. and N.A. Fleck. *Multiaxial models and experiments with ferroelectrics*. 2000. Newport Beach, CA, USA: Proc. SPIE Int. Soc. Opt. Eng.

81. Bogoroditskii, N.P. and V.V. Pasynkov, *Properties of Electronic Materials*, ed. R.C. Glass. 1967, Cambridge: Boston Technical Publishers, Inc.

82. Webber, K.G., R. Zuo, and C.S. Lynch. *Micromechanical modeling of PMN-32%PT ceramic based on single crystal properties.* 2006. San Diego, CA, USA: Proc. SPIE Int. Soc. Opt. Eng.

83. Chen, I.W. and Y. Wang, *Domain wall model for relaxor ferroelectrics.* Ferroelectrics, 1998. **206-207**(1-4; 1-2): p. 245-263.

84. Jin, L., Z. Xi, Z. Xu, and X. Yao, *Study of ferroelectric domain morphology in PMN-32% PT single crystals.* Ceram. Int., 2004. **30**(7): p. 1695-1698.

85. Liu, T. and C.S. Lynch. *Phase field simulation of ferroelectric single crystals.* 2005. Orlando, FL, USA: Proc. ASME.

86. Oates, W.S., A. Malbec, S. Herdic, and C.S. Lynch. *Phase field modeling of domain structures in ferroelectric materials*. 2004. San Diego, CA, USA: Proc. SPIE Int. Soc. Opt. Eng.

87. Okino, H., J. Sakamoto, and T. Yamamoto, *Cooling-rate-dependence of dielectric constant and domain structures in (1-x)Pb($Mg_{1/3}Nb_{2/3}$)O_3-x$PbTiO_3$ single crystals.* Jpn J. Appl. Phys., Part 1, 2005. **44**(9 B): p. 7160-7164.

88. Park, B.M., S.W. Ha, S.K. Yun, and G.S. Lee. *Piezoelectric actuation and micro-domain behaviors in the monolithically patterned PMN-PT single crystal*. 2005. Gyeongju, South Korea: Integ. Ferroelectr.

89. Yasuda, N., M. Sakaguchi, Y. Itoh, H. Ohwa, Y. Yamashita, M. Iwata, and Y. Ishibashi, *Effect of electric fields on domain structure and dielectric properties of*

$Pb(In_{1/2}Nb_{1/2})O_3$-$PbTiO_3$ near morphotropic phase boundary. Japanese Journal of Applied Physics, Part 1: Regular Papers, Short Notes and Review Papers, 2003. **42**(9 B): p. 6205-6208.

90. Huber, J.E., N.A. Fleck, C.M. Landis, and R.M. McMeeking, *Constitutive model for ferroelectric polycrystals.* J. Mech. Phys. Solids, 1999. **47**(8): p. 1663-1697.

91. McMeeking, R.M. and C.M. Landis, *A phenomenological multi-axial constitutive law for switching in polycrystalline ferroelectric ceramics.* Int. J. Eng. Sci., 2002. **40**(14): p. 1553-1577.

92. Hwang, S.C., C.S. Lynch, and R.M. McMeeking, *Ferroelectric/ferroelastic interactions and a polarization switching model.* Acta Metall. Mater., 1995. **43**(5): p. 2073-2084.

93. Yang, W. and L.Q. Chen, *Computer simulation of the dynamics of 180° ferroelectric domains.* J. Am. Chem. Soc., 1995. **78**(9): p. 2554-6.

94. Landis, C.M., *Fully coupled, mult-axial, symmetric constitutive laws for polycrystalline ferroelectric ceramics.* J. Mech. Phys. Solids, 2002. **50**: p. 127-152.

95. Cavalheiro, A.A., J.C. Bruno, M.A. Zaghete, and J.A. Varela, *(1-x)PMN-xPT ceramics prepared by conventional and modified columbite route: Effect on electrical properties.* Ferroelectrics, 2006. **331**: p. 121-128.

96. Li, J.B., G. Rao, G. Liu, J. Chen, L. Lu, X. Jing, S. Li, and J. Liang, *Structural transition in unpoled (1-x)PMN-xPT ceramics near the morphotropic boundary.* J. Alloys Compd., 2006. **425**(1-2): p. 373-378.

97. Roy, S. and P. Sarah, *Dielectric properties of chemically synthesized PLZT and PZT: Diffused phase transition and effect of lead non-stoichiometry.* J. Phys. D: Appl. Phys., 2007. **40**(15): p. 4668-4673.

98. Cross, L.E., *Relaxor ferroelectrics: An overview.* Ferroelectrics, 1994. **151**(1-4 pt 1): p. 305-320.

99. Fu, H. and R.E. Cohen, *Polarization rotation mechanism for ultrahigh electromechanical response in single-crystal piezoelectrics.* Nature, 2000. **403**(6767): p. 281-283.

100. Noheda, B., D.E. Cox, G. Shirane, R. Guo, B. Jones, and L.E. Cross, *Stability of the monoclinic phase in the ferroelectric perovskite $PbZr_{(1-x)}Ti_xO_3$* Phys. Rev. B: Condens. Matter, 2001. **63**(014103): p. 1-6.

101. Schmidt, V.H., R. Chien, I.C. Shih, and C.-S. Tu, *Polarization rotation and monoclinic phase in relaxor ferroelectric PMN-PT crystal.* AIP Conference Proceedings, 2003. **677**(1): p. 160-167.

102. Vanderbilt, D. and M.H. Cohen, *Monoclinic and triclinic phases in higher-order Devonshire theory.* Phys. Rev. B: Condens. Matter, 2001. **63**(094108): p. 1-9.

103. Devonshire, A.F., *Theory of barium titanate.* Philos. Mag., 1949. **40**(309): p. 1040-1063.

104. Hu, H.L. and L.Q. Chen, *Three-dimensional computer simulation of ferroelectric domain formation.* J. Am. Chem. Soc., 1998. **81**(3): p. 492-500.

105. Li, Y.L., S.Y. Hu, Z.K. Liu, and L.Q. Chen. *Phase-field simulation of domain structure evolution in ferroelectric thin films*. in *Proceedings of the Materials Research Society Symposium*. 2001.

106. Zuo, R., T. Granzow, D.C. Lupascu, and J. Rodel, *PMN-PT ceramics prepared by spark plasma sintering.* J. Am. Chem. Soc., 2007. **90**(4): p. 1101-1106.

107. Eshelby, J.D., *The force on an elastic singularity.* Philos. Trans., 1951. **A244**: p. 87-112.

108. Eshelby, J.D., *Energy relations and the energy-momentum tensor in continuum mechanics.* In: M. F. Kanninen *et al*., editor, Inelastic Behaviour of Solids, 1970.

109. Gross, D., S. Kolling, R. Mueller, and I. Schmidt, *Configurational forces and their application in solid mechanics.* Eur. J. Mech.: Solids, 2003. **22**: p. 669-692.

110. Rice, J.R., *Path independent integral and approximate analysis of strain concentration by notches and cracks.* J. Appl. Mech., 1968. **35**: p. 379-386.

111. Pak, Y.E., *Crack extension force in a piezoelectric material.* J. Appl. Mech., 1990. **57**(3): p. 647-653.

112. Sosa, H.A. and Y.E. Pak, *Three-dimensional eigenfunction analysis of a crack in a piezoelectric material.* Int. J. Solids Struct., 1990. **26**(1): p. 1-15.

113. Mueller, R., D. Gross, and D.C. Lupascu, *Driving forces on domain walls in ferroelectric materials and interaction with defects.* Comput. Mater. Sci., 2006. **35**(1): p. 42-52.

114. Mueller, R., D. Gross, and G.A. Maugin, *Use of material forces in adaptive finite element methods.* Computat. Mech., 2004. **33**(6): p. 421-434.

115. Schrade, D., R. Mueller, D. Gross, T. Utschig, V.Y. Shur, and D.C. Lupascu, *Interaction of domain walls with defects in ferroelectric materials.* Mech. Mater., 2007. **39**(2): p. 161-174.

116. Schrade, D., R. Mueller, B.X. Xu, and D. Gross. *Domain wall pinning by point defects in ferroelectric materials*. 2007. San Diego, CA, USA: Proc. SPIE Int. Soc. Opt. Eng.

117. Schrade, D., R. Mueller, B.X. Xu, and D. Gross, *Domain evolution in ferroelectric materials: A continuum phase field model and finite element implementation.* Comput. Methods Appl. Mech. Eng., 2007. **196**(41-44): p. 4365-4374.

118. Chen, W. and C.S. Lynch, *Model for simulating polarization switching and AF-F phase changes in ferroelectric ceramics.* J. Intell. Mater. Syst. Struct., 1998. **9**(6): p. 427-431.

119. Fan, J., *A Meso-electro-mechanical Model for PMN-PT-BT Ceramics Behavior.* J. Intell. Mater. Syst. Struct., 2004. **15**(3): p. 203-207.

120. Viehland, D. and J.F. Li, *Anhysteretic field-induced rhombhohedral to orthorhombic transformation in <110>-oriented 0.7Pb($Mg_{1/3}Nb_{2/3}$)O_3-0.3$PbTiO_3$ crystals* J. Appl. Phys., 2002. **92**(12): p. 7690-7692.

121. Zhao, X., J. Wang, H. Luo, H.L.W. Chan, and C.L. Choy, *Effect of a bias field on the dielectric properties of 0.69Pb($Mg_{1/3}Nb_{2/3}$)O_3-0.31$PbTiO_3$ single crystals with different orientations.* J. Phys.: Condens. Matter, 2003. **15**(40): p. 6899-6908.

122. Ren, W., S.F. Liu, and B.K. Mukherjee, *Piezoelectric properties and phase transitions of <001>-oriented Pb($Zn_{1/3}Nb_{2/3}$)O_3 -$PbTiO_3$ single crystals.* Appl. Phys. Lett., 2002. **80**(17): p. 3174.

123. Davis, M., D. Damjanovic, and N. Setter, *Electric field-, temperature-, and stress-induced phase transitions in relaxor ferroelectric single crystals.* Phys. Rev. B: Condens. Matter, 2006. **73**: p. 014115.

124. Eshelby, J.D., *The elastic field outside an ellipsoidal inclusion.* Proc. R. Soc. London, Ser. A, 1959. **252**: p. 561.

125. Huber, J.E. and N.A. Fleck, *Multi-axial electrical switching of a ferroelectric: theory versus experiment.* J. Mech. Phys. Solids, 2001. **49**: p. 785.

126. Cao, H., J. Li, and D. Viehland, *Structural origin of the relaxor-to-normal ferroelectric transition in Pb($Mg_{1/3}Nb_{2/3}O_3$)-x$PbTiO_3$.* J. Appl. Phys., 2006. **100**(3): p. 034110.

127. Durbin, M.K., J.C. Hicks, E. Park, and T.R. Shrout, *X-ray diffraction and phenomenological studies of the engineered monoclinic crystal domains in single crystal relaxor ferroelectrics.* J. Appl. Phys., 2000. **87**(11): p. 8159-8164.

128. Han, J. and W. Cao, *Electric field effects on the phase transitions in [001]-oriented (1-x)Pb($Mg_{1/3}Nb_{2/3}$)O_3 -x$PbTiO_3$ single crystals with compositions near the morphotropic phase boundary* Phys. Rev. B: Condens. Matter, 2003. **68**(13): p. 134102-134106.

129. Viehland, D. and J. Powers, *Electromechanical coupling coefficient of <001>-oriented $Pb(Mg_{1/3}Nb_{2/3})O_3$ -$PbTiO_3$ crystals: Stress and temperature independence* Appl. Phys. Lett., 2001. **78**(20): p. 3112-3114.

130. Viehland, D. and J. Powers, *Effect of uniaxial stress on the electromechanical properties of 0.7$Pb(Mg_{1/3}Nb_{2/3})O_3$ -0.3$PbTiO_3$ crystals and ceramics* J. Appl. Phys., 2001. **89**(3): p. 1820-1825.

131. Viehland, D., K. Uchino, and S. Priya, *Importance of structural irregularity on dielectric loss in (1-x)$Pb(Mg_{1/3}Nb_{2/3})O_3$-x$PbTiO_3$ crystals.* Appl. Phys. Lett., 2002. **80**(22): p. 4217.

132. Ziebinska, A., K. Roleder, Z. Ujma, A. Winiarski, and M. Pawelczyk, *Piezoelectric activity and phase transitions in $(PMN)_{0.69}$-$(PT)_{0.31}$ single crystal.* Phase Transitions, 2005. **78**(7-8): p. 647-654.

133. Feng, Z., H. Luo, Y. Guo, T. He, and H. Xu, *Dependence of high electric-field-induced strain on the composition and orientation of $Pb(Mg_{1/3}Nb_{2/3})O_3$ -$PbTiO_3$ crystals.* Solid State Commun., 2003. **126**(6): p. 5.

134. Wan, Q., C. Chen, and Y.P. Shen, *Electromechanical coupling properties of [001], [011] and [111] poled $Pb(Mg_{1/3}Nb_{2/3})O_3$-0.32$PbTiO_3$ single crystals.* J. Mater. Sci., 2006. **41**(10): p. 2993-3000.

135. Rajan, K.K., M.J. Zhang, and L.-C. Lim, *Optimum compositions for $Pb(Zn_{1/3}Nb_{2/3})O_3$-$PbTiO_3$ single crystal for high-performance applications.* Jpn. J. Appl. Phys., 2005. **44**(1A): p. 264-266.

136. Liu, T. and C.S. Lynch. *Crystal Variant Based Modeling of Relaxor Single Crystals*. 2003. San Diego, CA, USA: Proc. SPIE Int. Soc. Opt. Eng.

137. Webber, K.G., H.C. Robinson, G.A. Rossetti Jr, and C.S. Lynch, *A Distributed Step-Like Switching Model of the Continuous Field Driven Phase Transformations Observed in PMN-xPT Relaxor Ferroelectric Single Crystals.* Accepted to Acta Mater., Feb 2008.

138. Bokov, A.A. and Z.G. Ye, *Recent progress in relaxor ferroelectrics with perovskite structure.* J. Mater. Sci., 2006. **41**(1): p. 31-52.

139. Garcia, O., A. Pelaiz, F. Calderon, and H. Amorin, *Dielectric behavior of PLZT x/80/20 ferroelectric ceramics.* Ferroelectrics, 2003. **294**: p. 203-210.

140. Singh, A.K., D. Pandey, and O. Zaharko, *Powder neutron diffraction study of phase transitions in and a phase diagram of (1–x)[$Pb(Mg_{1/3}Nb_{2/3})O_3$]-x$PbTiO_3$.* Phys. Rev. B: Condens. Matter, 2006. **74**: p. 024101.

141. Bai, F., J. Li, and D. Viehland, *Domain engineered states over various length scales in (001)-oriented $Pb(Mg_{1/3}Nb_{2/3})O_3$-x%$PbTiO_3$ crystals: Electrical history dependence of hierarchal domains.* J. Appl. Phys., 2005. **97**(5): p. 054103.

142. Davis, M., *Picturing the elephant: Giant piezoelectric activity and the monoclinic phases of relaxor-ferroelectric single crystals.* J. Electroceram., 2007. **19**(1): p. 23-45.

143. Noheda, B., *Structure and high-piezoelectricity in lead oxide solid solutions.* Curr. Opin. Solid State Mater. Sci., 2002. **6**: p. 27.

144. Noheda, B. and D.E. Cox, *Bridging phases at the morphotropic boundaries of lead oxide solid solutions.* Phase Transitions, 2006. **79**(1-2): p. 5-20.

145. Jin, Y.M., Y.U. Wang, A.G. Khachaturyan, J.F. Li, and D. Viehland, *Conformal miniaturization of domains with low domain-wall energy: Monoclinic ferroelectric states near the morphotropic phase boundaries.* Phys. Rev. Lett., 2003. **91**(19): p. 197601-1.

146. Jin, Y.M., Y.U. Wang, A.G. Khachaturyan, J.F. Li, and D. Viehland, *Adaptive ferroelectric states in systems with low domain wall energy: Tetragonal microdomains.* J. Appl. Phys., 2003. **94**(5): p. 3629-3640.

147. Rao, W.-F. and Y.U. Wang, *Domain wall broadening mechanism for domain size effect of enhanced piezoelectricity in crystallographically engineered ferroelectric single crystals.* Phys. Rev. Lett., 2007. **90**(4): p. 041915.

148. Wang, H., J. Zhu, N. Lu, A.A. Bokov, Z.G. Ye, and X.W. Zhang, *Hierarchical micro-nanoscale domain structure in M_c phase of (1-x)$Pb(Mg_{1/3}Nb_{2/3})O_3$-x$PbTiO_3$ single crystal.* Appl. Phys. Lett., 2006. **89**(4): p. 042908.

149. Cao, H. and D. Viehland, *Fragile phase stability in (1-x)$Pb(Mg_{1/3}Nb_{2/3})O_3$-x$PbTiO_3$ crystals: A comparison of [001] and [110] field-cooled phase diagrams.* Phys. Rev. B: Condens. Matter, 2006. **73**: p. 184110.

150. Rossetti Jr, G.A. and A.G. Khachaturyan, *Inherent nanoscale structural instabilities near morphotropic boundaries in ferroelectric solid solutions.* Appl. Phys. Lett., 2007. **91**(7): p. 072909.

151. Landis, C.M., J. Wang, and J. Sheng. *Micro-electromechanically Informed Phenomenological Constitutive Models for Ferroelectrics*. San Diego, CA, USA: Proc. SPIE Int. Soc. Opt. Eng.

152. Chan, K.H. and N.W. Hagood. *Modeling of nonlinear piezoceramics for structural actuation* 1994. Orlando, FL, USA: Proc. SPIE Int. Soc. Opt. Eng.

153. Chen, X., D.N. Fang, and K.C. Hwang, *Micromechanics simulation of ferroelectric polarization switching.* Acta Mater., 1997. **45**(8): p. 3181-3189.

154. Delibas, B., A. Arockiarajan, and W. Seemann, *A nonlinear model of piezoelectric polycrystalline ceramics under quasi-static electromechanical loading.* J. Mater. Sci. - Mater. Electron., 2005. **16**(8): p. 507-515.

155. Hwang, S.C. and R.M. McMeeking, *Finite element model of ferroelectric polycrystals.* Ferroelectrics, 1998. **211**(1-4): p. 177-194.

156. Hwang, S.C. and R.M. McMeeking, *Prediction of switching in polycrystalline ferroelectric ceramics.* Ferroelectrics, 1998. **207**(3-4): p. 465-495.

157. Hwang, S.C. and R.M. McMeeking, *Finite element model of ferroelastic polycrystals.* Int. J. Solids Struct., 1999. **36**(10): p. 1541-1556.

158. Lynch, C.S., S.C. Hwang, and R.M. McMeeking. *Micromechanical theory of the nonlinear behavior of ferroelectric ceramics*. 1995. Coll. Station, TX, USA: Proc. SPIE Int. Soc. Opt. Eng.

159. McMeeking, R.M. and S.C. Hwang, *On the potential energy of a piezoelectric inclusion and the criterion for ferroelectric switching.* Ferroelectrics, 1997. **200**(1-4): p. 151-173.

160. Michelitsch, T. and W.S. Kreher, *Simple model for the nonlinear material behavior of ferroelectrics.* Acta Mater., 1998. **46**(14): p. 5085-5094.

161. Chen, W. and C.S. Lynch, *A micro-electro-mechanical model for polarization switching of ferroelectric materials.* Acta Mater., 1998. **46**(15): p. 5303-5311.

162. Huber, J.E., N.A. Fleck, and R.M. McMeeking, *Crystal plasticity model for ferroelectrics.* Ferroelectrics, 1999. **228**(1-4): p. 39-52.

163. Landis, C.M. and R.M. McMeeking, *A self-consistent constitutive model for switching in polycrystalline barium titanate.* Ferroelectrics, 2001. **255**(1): p. 13.

164. Lynch, C.S., C. Wei, and L. Teiqi. *Multiaxial constitutive behavior of ferroelectric materials*. 2000. Newport Beach, CA, USA: Proc. SPIE Int. Soc. Opt. Eng.

165. Mauck, L.D. and C.S. Lynch. *A micro-electromechanical model of ferroelectric materials with thermal and rate effects*. 2003. San Diego, CA, USA: Proc. SPIE Int. Soc. Opt. Eng.

166. Mauck, L.D. and C.S. Lynch, *Thermo-electro-mechanical behavior of ferroelectric materials. Part 1: A computational micromechanical model versus experimental results.* J. Intell. Mater. Syst. Struct., 2003. **14**(9): p. 587-602.

167. Rodel, J. and W.S. Kreher, *Self-consistent modelling of non-linear effective properties of polycrystalline ferroelectric ceramics.* Comput. Mater. Sci., 2000. **19**(1-4): p. 123-132.

168. Rodel, J. and W.S. Kreher. *Modeling of domain wall contribution to the effective properties of polycrystalline ferroelectric ceramics*. 2000. Newport Beach, CA, USA: SPIE-Int. Soc. Opt. Eng.

169. Landis, C.M. and R.M. McMeeking. *Self consistent model for switching in polycrystalline ferroelectrics electrical polarization only*. 1999. Newport Beach, CA, USA: Proc. SPIE Int. Soc. Opt. Eng.

170. Lu, W., D.N. Fang, and K.C. Hwang, *Nonlinear evolution of ferroelectric domains.* Commun. Nonlinear Sci. Numer. Simul., 1997. **2**(1): p. 30-35.

171. Lu, W., D.N. Fang, and K.C. Hwang, *Micromechanics of ferroelectric domain switching behavior. Part II: Constitutive relations and hysteresis.* Theor. Appl. Fract. Mech., 2001. **37**(1-3): p. 39-47.

172. Lu, W., D.N. Fang, and K.C. Hwang, *Micromechanics of ferroelectric domain switching behavior. Part I: Coupled electromechanical field of domain inclusions.* Theor. Appl. Fract. Mech., 2001. **37**(1-3): p. 29-38.

173. Fan, J., W.A. Stoll, and C.S. Lynch, *Nonlinear constitutive behavior of soft and hard PZT: experiments and modeling.* Acta Mater., 1999. **47**(17): p. 4415-4425.

174. Duine, R.A., A.S. Nunez, and A.H. MacDonald, *Thermally assisted current-driven domain-wall motion.* Phys. Rev. Lett., 2007. **98**(5): p. 056605.

175. Gordon, A. and L. Bakaleinikov, *Sideways dynamics of ferroelectric domain walls.* Physica B, 2007. **388**(1-2): p. 359-69.

176. Cady, W.G., *Piezoelectricity; an introduction to the theory and applications of electromechanical phenomena in crystals*. 1946, New York: McGraw-Hill. 806.

177. Zhang, R., B. Jiang, and W. Cao, *Erratum: "Orientation dependence of piezoelectric properties of single domain 0.67Pb($Mn_{1/3}Nb_{2/3}$)O_3-0.33$PbTiO_3$ crystals" (Appl. Phys. Lett. (2003) 82 (3737)).* Appl. Phys. Lett., 2003. **83**(1): p. 204.

178. Zhang, R., B. Jiang, and W. Cao, *Orientation dependence of piezoelectric properties of single domain 0.67Pb($Mg_{1/3}Nb_{2/3}$)O_3-0.33$PbTiO_3$ crystals.* Appl. Phys. Lett., 2003. **82**(21): p. 3.

179. Zhang, R., B. Jiang, and W. Cao, *Single-domain properties of 0.67Pb($Mg_{1/3}Nb_{2/3}$)O_3-0.33$PbTiO_3$ single crystals under electric field bias.* Appl. Phys. Lett., 2003. **82**(5): p. 787-789.

180. Yin, J., B. Jiang, and W. Cao, *Elastic, piezoelectric, and dielectric properties of 0.955Pb($Zn_{1/3}Nb_{2/3}$)O_3 -0.045$PbTiO_3$ single crystal with designed multidomains* IEEE Transactions on Ultrasonics, Ferroelectrics and Frequency Control, 2000. **47**(1): p. 285-291.

181. Zhang, R., B. Jiang, W. Cao, and A. Amin, *Complete set of material constants of $0.93Pb(Zn_{1/3}Nb_{2/3})O_3$-$0.07PbTiO_3$ domain engineered single crystal.* J. Mater. Sci. Lett., 2002. **21**(23): p. 1877-1879.

182. Zhang, R., B. Jiang, W. Jiang, and W. Cao, *Complete set of properties of $0.92Pb(Zn_{1/3}Nb_{2/3})O_3$ -$0.08PbTiO_3$ single crystal with engineered domains* Mater. Lett., 2003. **57**(7): p. 1305-1308.

183. Jin, J., K.K. Rajan, and L.C. Lim, *Properties of single domain $Pb(Zn_{1/3}Nb_{2/3})O_3$-(6-7)%$PbTiO_3$ single crystal.* Jpn. J. Appl. Phys., Part 1, 2006. **45**(11): p. 8744-8747.

184. Liu, T. and C.S. Lynch, *Domain engineered relaxor ferroelectric single crystals.* Continuum Mech. Thermodyn., 2006. **18**(1-2): p. 119-135.

185. Wan, Q., C. Chen, and Y.P. Shen, *Effects of stress and electric field on the electromechanical properties of $Pb(Mg_{1/3}Nb_{2/3})O_3$-$0.32PbTiO_3$ single crystals.* J. Appl. Phys., 2005. **98**(2): p. 024103.

186. Paik, D.S., S.E. Park, S. Wada, S.F. Liu, and T.R. Shrout, *E-field induced phase transition in <001>-oriented rhombohedral $0.92Pb(Zn_{1/3}Nb_{2/3})O_3$-$0.08PbTiO_3$ crystals.* J. Appl. Phys., 1999. **85**(2): p. 1080-1083.

187. Liu, S.F., W. Ren, B.K. Mukherjee, S.J. Zhang, T.R. Shrout, P.W. Rehrig, and W.S. Hackenberger, *The piezoelectric shear strain coefficient of <111> -oriented Pb $(Zn_{1/3}Nb_{2/3})O_3$-$PbTiO_3$ piezocrystals.* Appl. Phys. Lett., 2003. **83**(14): p. 2886-2888.

188. Yousef, S.G., J. Rödel, E.R. Fuller Jr., A. Zimmermann, and B.S. El-Dasher, *Microcrack evolution in alumina ceramics: experiment and simulation.* J. Am. Ceram. Soc., 2005. **88**(10): p. 8.

189. Li, J.-B., G. Rao, G. Liu, J. Chen, L. Lu, X. Jing, S. Li, and J. Liang, *Structural transition in unpoled (1 - x)PMN-xPT ceramics near the morphotropic boundary.* Journal of Alloys and Compounds, 2006. **425**(1-2): p. 373-378.

190. Li, J.B., G.H. Rao, G.Y. Liu, J.R. Chen, and J.K. Liang, *Effect of Ti on the stability of phases in the (1 - x)$Pb(Mg_{1/3}Nb_{2/3})O_3$-$xPbTiO_3$ solid solution.* Ferroelectrics, 2005. **313**: p. 71-80.

191. Yang, Y., C. Feng, W. Yao, and Y. Yu, *Effects of different dopants on diffuse phase transition and ordering degree in lead magnesium niobate.* Japanese Journal of Applied Physics, Part 1: Regular Papers and Short Notes and Review Papers, 2001. **40**(12): p. 6884-6887.

192. Yu, S., K. Yao, and F.E.H. Tay, *Observations and analyses on the thermal stability of (1 - x)$Pb(Zn_{1/3}Nb_{2/3})O_3$-$xPbTiO_3$ thin films.* Chemistry of Materials, 2007. **19**(17): p. 4373-4377.

193. Janolin, P.-E., B. Dkhil, M. Davis, D. Damjanovic, and N. Setter, *Uniaxial-stress induced phase transitions in [001]c-poled 0.955Pb($Zn_{1/3}Nb_{2/3}$)O_3-0.045$PbTiO_3$.* Appl. Phys. Lett., 2007. **90**(15): p. 152907.

194. Piltz, R.O., *Neutron diffraction study of domain structures in poled and unpoled PZN-4.5%PT.* Physica B: Condensed Matter, 2006. **385-386 I**: p. 169-172.

195. Vittayakorn, N., C. Puchmark, G. Rujijanagul, X. Tan, and D.P. Cann, *Piezoelectric properties of (1 - x)Pb($Zr_{1/2}Ti_{1/2}$)O_3-xPb($Zn_{1/3}Nb_{2/3}$)O_3 ceramics prepared by the columbite-(wolframite) precursor method.* Current Applied Physics, 2006. **6**(3): p. 303-306.

196. Zeng, H.R., H.F. Yu, R.Q. Chu, G.R. Li, H.S. Luo, and Q.R. Yin, *Spatial inhomogeneity of ferroelectric domain structure in Pb($Mg_{1/3}Nb_{2/3}$)O_3-30%$PbTiO_3$ single crystals.* Materials Letters, 2005. **59**(2-3): p. 238-240.

197. Abplanalp, M., D. Barosova, P. Bridenbaugh, J. Erhart, J. Fousek, P. Gunter, J. Nosek, and M. Sulc, *Ferroelectric domain structures in PZN-8%PT single crystals studied by scanning force microscopy.* Solid State Communications, 2001. **119**(1): p. 7-12.

198. Okino, H., T. Ida, H. Ebihara, and T. Yamamoto, *Visualization of the domain orientation in relaxor ferroelectric single crystals by piezoresponse force microscopy.* Ferroelectrics, 2002. **268**: p. 119-124.

199. Zeng, H.R., K. Shimamura, E.A.G. Villora, S. Takekawa, K. Kitamura, J.Y. Xu, and Q.R. Yin, *Piezoresponse imaging and local characterization of ferroelectric domains in Pb($Zn_{1/3}Nb_{2/3}$)O3-7%$PbTiO_3$ single crystals.* Physica Status Solidi - Rapid Research Letetrs, 2007. **1**(2): p. 62-64.

200. Lee, J.H., Y.J. Oh, T.Y. Kim, M.R. Choi, and W. Jo, *Piezoelectric and electromechanical properties of relaxor ferroelectric Pb($Mg_{1/3}Nb_{2/3}$)O_3(65%)-$PbTiO_3$(35%) thin films observed by scanning force microscopy.* Ultramicroscopy, 2007. **107**(10-11): p. 954-957.

201. Su, W.-S., Y.-F. Chen, W.Y. Shih, H. Luo, and W.-H. Shih, *Domain switching in lead magnesium niobate-lead titanate polycrystalline sheets at single grain level.* Applied Physics Letters, 2007. **91**(11): p. 112903.

202. Wong, K.S., X. Zhao, J.Y. Dai, C.L. Choy, X.Y. Zhao, and H.S. Luo, *Study of domain boundary polarization in (111)-cut [Pb($Mg_{1/3}Nb_{2/3}$)O_3]0.7($PbTiO_3$)0.3 single crystal by piezoresponse force microscopy.* Applied Physics Letters, 2006. **89**(9): p. 092906.

203. Tai, C.W. and K.Z. Baba-Kishi, *Relationship between dielectric properties and structural long-range order in (x)Pb($In_{1/2}Nb_{1/2}$)O_3:(1 - x)Pb($Mg_{1/3}Nb_{2/3}$)O_3 relaxor ceramics.* Acta Materialia, 2006. **54**(20): p. 5631-5640.

204. Purice, A., G. Dinescu, N. Scarisoreanu, P. Verardi, F. Craciun, C. Galassi, and M. Dinescu, *Ferroelectric thin films obtained by pulsed laser deposition.* Journal of the European Ceramic Society, 2006. **26**(14): p. 2937-2943.

205. Lupascu, D.C., V.Y. Shur, and A.G. Shur, *Dynamics of a single-planar domain wall in ferroelectric-ferroelastic $Gd_2(MoO_4)_3$.* Applied Physics Letters, 2002. **80**(13): p. 2359.

206. Lupascu, D.C., T. Utschig, V.Y. Shur, and A.G. Shur, *The dynamics of domain walls determined from acoustic emission measurements.* Ferroelectrics, 2003. **290**: p. 207-215.

207. Tikhomirov, O.A., *Anomalies of ferroelectric domain wall motion near the transition point.* Journal of Applied Physics, 1996. **80**(4): p. 2358.

208. Su, Y. and C.M. Landis, *Continuum thermodynamics of ferroelectric domain evolution: Theory, finite element implementation, and application to domain wall pinning.* Journal of the Mechanics and Physics of Solids, 2007. **55**(2): p. 280-305.